NOAA Technical Report NESDIS 148 Report for Dedicated JPSS VIIRS Ocean Color Calibration/Validation Cruise December 2015

Technical Report · October 2016

DOI: 10.7289/V5/TR-NESDIS-148

33 authors, including:

Michael Ondrusek
Southwest Fisheries Science Center
64 PUBLICATIONS **4,724** CITATIONS

SEE PROFILE

Veronica Lance
National Oceanic and Atmospheric Administration
37 PUBLICATIONS **942** CITATIONS

SEE PROFILE

Robert Arnone
University of Southern Mississippi
277 PUBLICATIONS **5,899** CITATIONS

SEE PROFILE

Sherwin Ladner
United States Naval Research Laboratory
74 PUBLICATIONS **387** CITATIONS

SEE PROFILE

NOAA Technical Report NESDIS 148

doi:10.7289/V5/TR-NESDIS-148

Report for Dedicated JPSS VIIRS Ocean Color Calibration/Validation Cruise December 2015

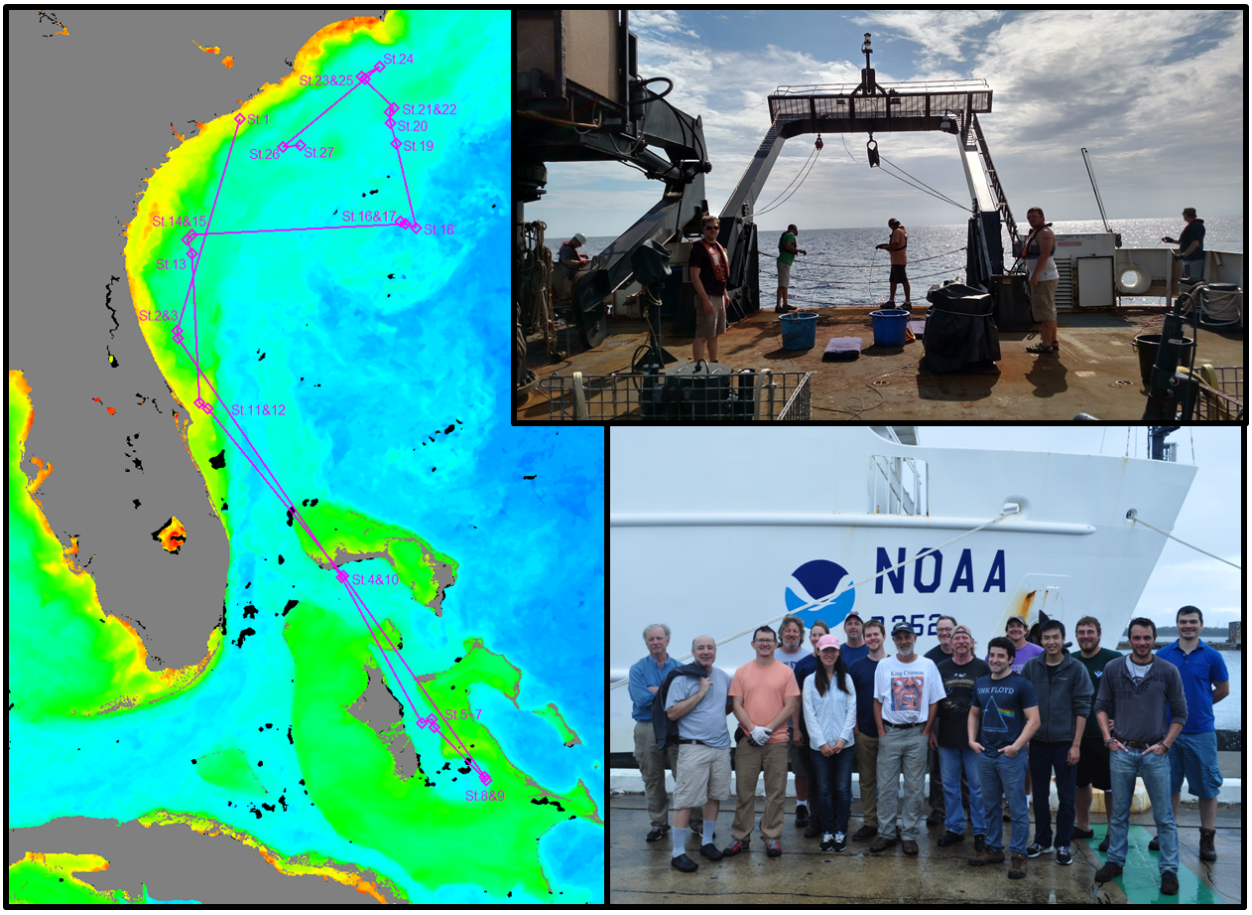

Washington, D.C.
October 2016

US DEPARTMENT OF COMMERCE
National Oceanic and Atmospheric Administration
National Environmental Satellite, Data, and Information Service

NOAA TECHNICAL REPORTS
National Environmental Satellite, Data, and Information Service

The National Environmental Satellite, Data, and Information Service (NESDIS) manages the Nation's civil Earth-observing satellite systems, as well as global national data bases for meteorology, oceanography, geophysics, and solar-terrestrial sciences. From these sources, it develops and disseminates environmental data and information products critical to the protection of life and property, national defense, the national economy, energy development and distribution, global food supplies, and the development of natural resources.

Publication in the NOAA Technical Report series does not preclude later publication in scientific journals in expanded or modified form. The NESDIS series of NOAA Technical Reports is a continuation of the former NESS and EDIS series of NOAA Technical Reports and the NESC and EDS series of Environmental Science Services Administration (ESSA) Technical Reports.

Copies of earlier reports may be available by contacting NESDIS Chief of Staff, NOAA/ NESDIS, 1335 East-West Highway, SSMC1, Silver Spring, MD 20910, (301) 713-3578.

*Cover image: (Left) December 2015 dedicated VIIRS Cal/Val cruise track with stations plotted overlaid onto a VIIRS-SNPP MSL12 science quality Level-3 chlorophyll image time-binned for the extent of the cruise, 2 December 2015 to 15 December 2015. Chlorophyll color is log scale from 0 mg m^{-3} (blue) to 64 mg m^{-3} (red). (Top Right) Science crew simultaneously deploying four profiling hyperspectral radiometers from the back deck of the NOAA Ship *Nancy Foster*. (Bottom Right) Science crew in port.

NOAA Technical Report NESDIS 148

doi:10.7289/V5/TR-NESDIS-148

Report for Dedicated JPSS VIIRS Ocean Color December 2015 Calibration/Validation Cruise

Edited by Veronica P. Lance[1,2*]
NOAA/NESDIS Center for Satellite Applications and Research (STAR), 5830 University Research Court, College Park, MD 20740, USA
[2]Global Science and Technology, Inc., 7855 Walker Drive, Suite 200, Greenbelt, MD 20770, USA

*Corresponding author: veronica.lance@noaa.gov

Contributing authors:

Michael Ondrusek[1]*, Veronica P. Lance[1,2], Eric Stengel[1] and Menghua Wang[1],
[1]NOAA/NESDIS Center for Satellite Applications and Research (STAR), 5830 University Research Court, College Park, MD 20740, USA
[2]Global Science and Technology, Inc., 7855 Walker Drive, Suite 200, Greenbelt, MD 20770, USA
*michael.ondrusek@noaa.gov

And (alphabetical by group lead last name):

Robert Arnone[3]*, Sherwin Ladner[4], Wesley Goode[4] and Ryan Vandermeulen[3,5,6]
[3]University of Southern Mississippi, Stennis Space Center, MS 39529, USA
[4]Naval Research laboratory, Stennis Space Center, MS 39529, USA
[5]NASA Goddard Space Flight Center 8800 Greenbelt Rd, Greenbelt, MD 20770, USA
[6]Science Systems and Applications, Inc, 10210 Greenbelt Road, Suite 600, Lanham, MD 20706, USA
*robert.arnone@usm.edu

Scott Freeman[7,8]*, Joaquin E. Chaves[7,8] and Antonio Mannino[7]
[5]NASA Goddard Space Flight Center 8800 Greenbelt Rd, Greenbelt, MD 20770, USA
[6]Science Systems and Applications, Inc, 10210 Greenbelt Road, Suite 600, Lanham, MD 20706, USA
*scott.a.freeman@nasa.gov

Alex Gilerson*, Sam Ahmed, Carlos Carrizo, Ahmed El-Habashi, Robert Foster and Matteo Ottaviani
City College of the City University of New York, 160 Convent Ave, New York, NY 10031, USA
*gilerson@ccny.cuny.edu

Joaquim I. Goes*, Helga do Rosario Gomes and Kali McKee
Lamont Doherty Earth Observatory at Columbia University, 61 Route 9W, Palisades, NY, 10964, USA
*jig@ldeo.columbia.edu

Chuanmin Hu*, Charles Kovach, David English and Jennifer Cannizzaro
College of Marine Science, University of South Florida, 140 7th Avenue South, St. Petersburg, FL 33701, USA
*huc@usf.edu

B. Carol Johnson
National Institute of Standards and Technology, Physical Measurement Laboratory,100 Bureau Drive, Stop 8441, Gaithersburg, MD 20899-8441, USA
*carol.johnson@nist.gov

Zhongping Lee*, Jianwei Wei, Quoqing Wang and Junfang Lin
School for the Environment, University of Massachusetts Boston, 100 Morrissey Blvd, Boston, MA 02125, USA
*zhongping.lee@umb.edu

Nicholas Tufillaro*, Jasmine Nahorniak, and Curtiss O. Davis
[5]College of Earth, Ocean and Atmospheric Sciences, Oregon State University, Corvallis, OR 97331, USA
*nbt@coas.oregonstate.edu

Kenneth J. Voss
Department of Physics, University of Miami, Knight Physics Building, Coral Gables, FL 33124, USA
*voss@physics.miami.edu

*Group corresponding contact

Washington, DC
October 2016

US DEPARTMENT OF COMMERCE
Penny Pritzker, Secretary

National Oceanic and Atmospheric Administration
Dr. Kathryn Sullivan, Under Secretary of Commerce for Oceans and Atmosphere and NOAA Administrator

National Environmental Satellite, Data, and Information Service
Dr. Stephen Volz, Assistant Administrator

Contents

List of Figures

List of Tables

List of Equations

Preface

The Ocean Color Team at the National Oceanic and Atmospheric Administration (NOAA) Center for Satellite Applications and Research (STAR) is focused on "end-to-end" production of high quality satellite ocean color products. In situ validation of satellite data is essential to produce the high quality, fit-for-purpose remotely sensed ocean color products that are required and expected by all NOAA line offices, as well as by external (both applied and research) users. In addition to serving the needs of its diverse users within the US, NOAA has an ever increasing role in supporting the international ocean color community and is actively engaged in the International Ocean-Colour Coordinating Group (IOCCG). The IOCCG, along with the Committee on Earth Observation Satellites (CEOS) Ocean Colour Radiometry Virtual Constellation (OCR-VC), is developing the International Network for Sensor Inter-comparison and Uncertainty assessment for Ocean Color Radiometry (INSITU-OCR). The INSITU-OCR has identified, amongst other issues, the crucial need for sustained in situ observations for product validation, with long-term measurement programs established and maintained beyond any individual mission.

NOAA/STAR scientists have been collecting in situ data throughout all the ocean color satellite missions. Since the launch in fall 2011 of the Visible Infrared Imaging Radiometer Suite (VIIRS) aboard the Suomi National Polar-orbiting Partnership (SNPP) platform, part of the US Joint Polar Satellite System (JPSS) program, the NOAA/STAR Ocean Color Team has been making in situ measurements continually in support of validation and algorithm development activities. The first dedicated VIIRS Ocean Color Calibration/Validation (Cal/Val) cruise supported by NOAA Office of Marine and Air Operations (OMAO) was successfully conducted in November 2014. Objectives and activities of that field campaign are detailed in the National Environmental Satellite, Data, and Information Service (NESDIS) Technical Report #146 [*Ondrusek et al.*, 2015].

Building upon the success of the November 2014 field campaign, the second dedicated VIIRS Cal/Val cruise took place during December 2015, again off the US East Coast aboard the NOAA Ship *Nancy Foster*. This cruise was made possible by: 1) OMAO for ship time, 2) the JPSS program for funding many of the participating groups and 3) NOAA/NESDIS/STAR. This report documents details in activities for the December 2015 dedicated Cal/Val cruise. We at NOAA/STAR look forward to continuing these dedicated ocean color validation campaigns on NOAA vessels annually. These activities provide in situ measurements needed to produce the best quality, fit-for-purpose ocean color remote sensing data and data products for NOAA applications and for users beyond NOAA. These observations support validation activities for the current JPSS VIIRS sensor on SNPP, which is now the primary source for NOAA operational remotely sensed ocean color data products. Future campaigns will support VIIRS on JPSS-1, planned for launch in 2017 and future JPSS missions (i.e., JPSS-2 and beyond) as well as non-NOAA US (e.g., National Aeronautics and Space Administration (NASA) and United States Geological Survey (USGS)) and international (e.g., the Ocean and Land Colour Instrument (OLCI) aboard Sentinel-3 of the European Union's Copernicus mission and the Second Generation Global Imager (SGLI) aboard Global Climate Observation Mission-Climate (GCOM-C) mission from the Japan Aerospace Exploration Agency) ocean color related satellite missions. In collaboration with the US and the international ocean community, we endeavor to improve our understanding of global and coastal ocean optical, biological, and biogeochemical properties which leads to applications and products that support the NOAA mission of science, service and stewardship.

Menghua Wang
Chief, Marine Ecosystems & Climate Branch; VIIRS Ocean Color Cal/Val Team Lead
Paul DiGiacomo
Chief, Satellite Oceanography & Climatology Division; NOAA Rep. to the IOCCG; OCR-VC Co-Chair

NOAA Technical Report NESDIS 148
Report for
December 2015 Dedicated JPSS VIIRS Ocean Color Calibration/Validation Cruise

1. Overview and Summary of Purpose, Project, Principal Investigators and Participants

The overall aim of this NOAA VIIRS 2015 Ocean Color Calibration/Validation (Cal/Val) Cruise aboard the NOAA Ship *Nancy Foster* (NF-15-13) was the collection of high quality in situ optical and related biogeochemical data for purpose of validating of satellite ocean color radiometry and derived products from VIIRS-SNPP, part of the JPSS program [*Wang et al.*, 2013; *Wang et al.*, 2014]. A second aim was to make measurements in support of science and applied studies that seek to characterize the optical signatures of the variety of water masses encountered (i.e., coastal, near-shore, cross-shelf, eddies, fronts, filaments, blue water, etc.). Thirdly, the design of the sampling strategies will lead to quantifying the confidence intervals of these measurements. Together, the validation of radiometry, the optical signatures of water types and the quantification of uncertainties, will lead to improvements in the extent and accuracy of satellite derived observations of the near surface ocean environment.

The original project plan allowed for 13 days at sea. Actual executed cruise days were 2 to 13 December 2015, a total of 12 days at sea. Ship time aboard the NOAA Ship *Nancy Foster* (http://www.moc.noaa.gov/nf/) was funded through an allocation by the NOAA Office of Marine and Aviation Operations (OMAO). Ten investigator groups from 11 institutions participated in the cruise. Some of these investigators are funded partly through JPSS program. Table 1 lists the principal investigators of the research groups, their institutions and the abbreviation used for each research group throughout this report. Fifteen scientists (maximum berthing allowance; see Table 2) sailed and conducted measurements with the support of officers and crew of the *Nancy Foster*. The cruise departed from and returned to Charleston, SC, US, the *Foster's* home port. The primary area of operations was the Western Atlantic along the US Southeastern Coast and into Bahamian waters, including cross-shelf, Gulf Stream, blue waters and the Tongue of the Ocean, which is a deep-water canyon of relatively clear, blue, oligotrophic warm water in the Caribbean. The cruise track was optimized to accommodate sampling transient features present in the region while respecting weather conditions during the time of the cruise. The cruise transited over 3700 km and occupied 27 stations for collection of underway and profile ocean color and related measurements during the 12 days. As expected in December in the Gulf Stream region, the weather conditions changed daily representing a wide variety of atmospheric conditions, from cloudy to clear days. On several days, in situ measurements coincided with cloud free VIIRS-SNPP satellite overpasses, enabling "match-ups" for the purpose of ocean color validation. In addition, laboratory calibrations of optical instruments were conducted in collaboration with NIST at the NOAA/STAR facility in College Park, MD both before and after the cruise. The laboratory calibrations used NIST traceable lamps. NIST also provided a reference plaque (known as the "blue tile") currently in development to be used on board for instrument inter-comparison exercises.

To date, not all of the data processing and sample analysis from the cruise has been completed. Sample processing is on-going and follow-up results and analyses are expected to be published as peer-reviewed literature in scientific journals in the future as work is completed. The cruise data collection will be deposited at NOAA CoastWatch/OceanWatch and made available for convenient access to the ocean community. Data will be formally archived through NOAA/NESDIS National Centers for Environmental Information (NCEI) as required by NOAA.

Table 1. Principal investigators (PIs), participating institutions and institution abbreviations.

PI Name (Last, First)	Participating Institutions	Research Group Abbreviation
Ondrusek, Michael*	NOAA/NESDIS Center for Satellite Applications and Research	NOAA/STAR
Arnone, Robert	University of Southern Mississippi (USM) and Naval Research Center (NRL)	Stennis
Davis, Curtiss	Oregon State University	OSU
Gilerson, Alex and Ahmed, Sam	City College of New York	CCNY
Goes, Joaquim	Lamont-Doherty Earth Observatory at Columbia University	LDEO
Hu, Chuanmin	University of South Florida	USF
Johnson, B. Carol	National Institute of Standards and Technology	NIST
Lee, ZhongPing	University of Massachusetts, Boston	UMB
Mannino, Antonio	NASA Goddard Space Flight Center	NASA/GSFC
Voss, Kenneth	University of Miami	U. Miami

*Chief Scientist

Table 2. List of science party personnel aboard the NOAA Ship *Nancy Foster* (alphabetical order).

Name (Last, First)	Title	Research Group/Home Institution*
Arnone, Robert	Research Professor	Stennis/USM
Carrizo, Carlos	PhD Student	CCNY
Chaves, Joaquin	Staff Research Scientist	NASA/GSFC
Freeman, Scott	Staff Research Scientist	NASA/GSFC
el Habashi, Ahmed	PhD Student	CCNY
Kovach, Charles	Researcher	USF
Lin, Junfang	Postdoctoral Researcher	UMB
Ladner, Sherwin	Researcher	Stennis/NRL
Ondrusek, Michael	Chief Scientist	NOAA/STAR
Goode, Wesley	Researcher	Stennis/NRL
Ottaviani, Matteo	Researcher	CCNY
Stengel, Eric	Researcher	NOAA/STAR
Tufillaro, Nicholas	Researcher	OSU
Vandermeulen, Ryan	Remote Sensing Analyst	Stennis/USM
Wang, Guoqiang	PhD Student	UMB

*See Table 1 for institution abbreviations.

2. Introduction

NOAA has been providing ocean color validation and calibration support since the launch of the Coastal Zone Color Scanner (CZCS) [*Gordon et al.*, 1980; *Hovis et al.*, 1980] in the late 1970's. This includes cruises for the validation of satellite data and the development of the Marine Optical BuoY (MOBY) [*Clark et al.*, 1997] in the Sea-viewing Wide Field-of-view Sensor (SeaWiFS) era [*Gordon*, 2010]. Today, MOBY has become the primary vicarious calibration reference standard for all satellite ocean color sensors and is supported by NOAA.

The JPSS VIIRS-SNPP satellite ocean color program Cal/Val science plan calls for in situ observations for the purpose of developing and validating ocean color Environmental Data Records (EDRs) for both global and coastal regions. To this aim, the NESDIS/STAR ocean color group has conducted dedicated NOAA VIIRS Cal/Val Cruises to validate VIIRS satellite ocean color data [*Wang et al.*, 2013; *Wang et al.*, 2014] with the best in situ sensor radiances and derived products in multiple types of water masses. Additional goals of these dedicated cruises include investigating uncertainties of in situ validation measurements and analyzing the capability of the VIIRS sensor to observe and study oceanic processes. The first dedicated NOAA VIIRS Ocean Color Cal/Val cruise aboard a NOAA ship (the NOAA Ship *Nancy Foster*, project NF-14-09) was conducted successfully in November 2014. That cruise was staged from the *Foster's* home port of Charleston, SC and took place along the US Mid-Atlantic Coast, crossing the Gulf Stream several times [*Ondrusek et al.*, 2015]. The 2015 cruise (the subject of this report) is the second in the series of dedicated ocean color Cal/Val cruises anticipated annually.

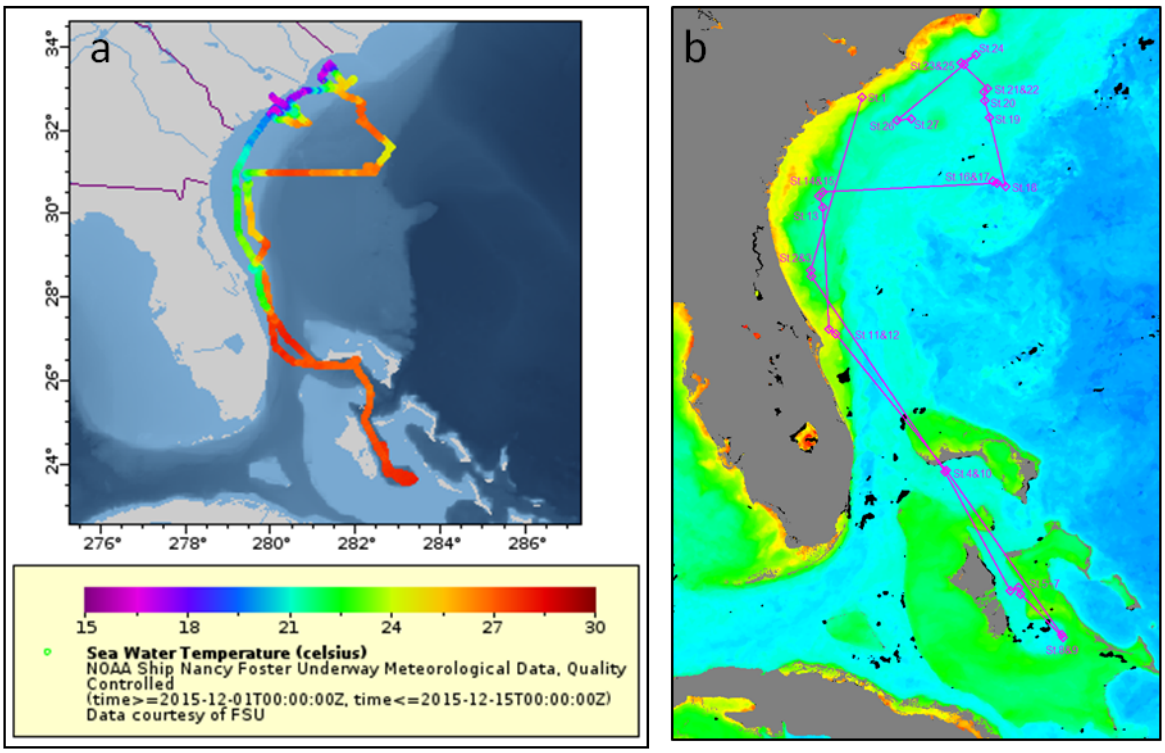

Figure 1. a) Overall cruise track of December 2015 shown with ship's quality controlled underway sea surface temperature data (http://coastwatch.pfeg.noaa.gov/erddap/tabledap/fsuNoaaShipWTER.graph?longitude%2Clatitude%2CseaTemperature&time%3E=2015-12-01T00%3A00%3A00Z&time%3C=2015-12-15T00%3A00%3A00Z&.draw=markers&.marker=6%7C3&.color=0xFFFFFF&.colorBar=%7CC%7CLinear%7C15%7C30%7C&.bgColor=0xffccccff)) and b) stations labeled overlaid onto a VIIRS-SNPP MSL12 science quality Level-3 chlorophyll image time-binned for the extent of the cruise, 2 December 2015 to 15 December 2015. Chlorophyll color is log scale from 0 mg m^{-3} (blue) to 64 mg m^{-3} (red).

The 2015 cruise concentrated on Western Atlantic waters along the South East US Coast and into Bahamian waters, crossing the Gulf Stream multiple times (Fig. 1). Twenty-seven stations were occupied over 12 days. The stations were designed to enable investigators to make in situ measurements in a variety of environmental conditions for the purpose of validating the VIIRS performance. Station locations were modified in real time during the cruise to attempt to optimize the number of clear sky days, and hence, the number of match-ups between the VIIRS satellite data and in situ observations.

At each station, simultaneous measurements were made with a suite of radiometric instruments to enable comparisons of the most widely utilized validation measurement techniques using in-water profiling radiometers and hand-held above water radiometers. Optical properties were also surveyed continuously while underway by instrumentation plumbed into the ship's flow-through sea water system and mounted on masts at the bow of the ship. Additionally, water samples were collected at stations and from the flow-through sea water system for chemical analyses of several environmental properties. More details regarding measurements follow in Section 5 and in the reports on each group's activities in Section 7.

3. Cruise Objectives

Similar to the 2014 cruise, this 2015 cruise made shipboard observations of apparent optical properties (AOPs) and inherent optical properties (IOPs) such as absorption and scattering by constituent materials in the water as well as biogeochemical and biological measurements in support of the three primary objectives: 1) validation of the VIIRS-SNPP ocean color satellite observations; 2) characterization of the differences in the uncertainties associated with measurements by a variety of instruments and protocols; and 3) spectral characterization of ocean variability (i.e., coastal, near-shore, cross-shelf, eddies, fronts, filaments, blue water) toward the future aim of using remotely sensed satellite ocean color data to monitor and study oceanographic processes. These three objectives are discussed further below.

1) Validate VIIRS ocean color satellite remote sensing

Satellite sensor performance is evaluated, or validated, by matching up satellite observations with in situ observations, which are considered the "true" values for this purpose. The primary properties derived from ocean color satellite observations are AOPs including spectral remote sensing reflectance ($R_{rs}(\lambda)$) and spectral normalized water-leaving radiance ($nL_w(\lambda)$) where λ represents a specified nominal wavelength or band. Other satellite ocean color remote sensing products are estimated by applying algorithms to $nL_w(\lambda)$s. The NOAA Multi-Sensor Level-1 to Level-2 (MSL12) ocean color data processing system is currently generating eight standard VIIRS-SNPP products including nL_ws at the 5 VIIRS ocean color bands (410 nm, 443 nm, 486 nm, 551 nm and 671 nm) [*Gordon and Wang*, 1994; *Wang*, 2007], chlorophyll concentration (Chl-*a*) [*O'Reilly et al.*, 1998; *Hu et al.*, 2012] and the water diffuse attenuation coefficient at 490 nm ($K_d(490)$) [*Wang et al.*, 2009] and also integrated across the so-called photosynthetically active radiation (PAR) wavelengths 400 nm to 700 nm (K_d(PAR)) [*Son and Wang*, 2015]. Therefore, in situ measurements for satellite validation are focused primarily on these AOP radiometric properties and also on determining Chl-*a* and other properties contributing to light attenuation. Several types of instruments and methods were deployed for radiometric observations including in-water, above water seaward and above water skyward approaches discussed later. Uncertainties associated with these in situ observations are discussed in the second objective below.

2) Determine uncertainties associated with in situ ocean color measurements

The second cruise objective was to quantify uncertainties of the in situ measurements that are used for the validation of VIIRS ocean color products (see Objective 1) and characterize the differences observed under measurement conditions of repeatability and reproducibility [*GUM*, 1995]. For a recent description of how to apply uncertainty estimates to ocean color, see the review article by Johnson et al. [2014]. Uncertainties in products such as remote sensing reflectance that are derived from satellite ocean color data are associated with the determination of atmospheric correction [*Gordon and Wang*, 1994; *Wang*, 2007; *IOCCG*, 2010] and the bidirectional reflectance distribution function (BRDF) of the seawater. Products derived from $nL_w(\lambda)$s are uncertain due to spatial and temporal variability of the natural environment as well as the veracity of the underlying model algorithms. The in situ measurements used in VIIRS product validation and measured in this cruise include both in-water and atmospheric parameters. The data sets assembled from this cruise will be analyzed to determine uncertainties, using the observed differences under conditions of repeatability and reproducibility, and will be used in

estimations of the uncertainty in the match-ups of VIIRS and in situ data. The following approaches, which represent conditions of reproducibility, were used to quantify measurement differences associated with: a) replicate observations from multiple identical (same model) instruments deployed in parallel; b) observations of the same in situ parameters but using different types of instruments (i.e., profiling in–water versus above-water versus hybrid floating instruments); c) different deployment protocols for sample collection; d) different post-processing methods for the in situ data; and e) spatial and temporal variability of the ocean waters.

a) *Differences associated with identical instruments and protocols* — Many investigators simultaneously deployed multiple instruments of the same or similar make and model using identical collection protocols for in-water and above-water validation measurements.

b) *Differences from instrumentation* — Investigators deployed multiple instruments of different makes or models in parallel to measure the same in situ ocean color parameters but using collection protocols and processing that are instrument-specific.

c) *Differences from sampling protocols* — Sampling protocols may differ among investigators and also among different types of instruments. Some investigators experimented with different sampling protocols using the same instrument. Where possible, the differences associated with collection protocols will be assessed (whether from the same or different types of instruments).

d) *Differences from post-processing methods* — Data sets from identical instruments and collection protocols (as discussed in Section 2a above) will be processed in multiple ways. First, data sets will be processed by individual investigators using their own preferred post-processing methods. Second, all data sets will be processed by one or more common post-processing methods.

e) *Differences in match-ups due to natural environmental variability (i.e., spatial and temporal variability of the ocean waters)* — From observation data collected at stations and from the underway seawater flow-through system, the spatial and temporal variability of the bio-optical properties of water masses will be analyzed and compared with the nominal 750 m resolution of the VIIRS satellite-derived ocean color data. Our objective is to determine the coherent scales of these spatial and temporal changes for match-ups between VIIRS and in situ measurements.

3) Characterize the optical properties of dynamic ocean processes

The third objective of this cruise is to optically characterize ocean variability related to dynamic processes in open and coastal waters for the purpose of exploring the utility of VIIRS ocean color products in identifying and monitoring oceanographic processes from space. The Gulf Stream region represents a major ocean circulation structure, which is characterized by significant variability in optical and physical properties resulting from biological and physical processes as continental shelf waters interact with open waters to produce upwelling and downwelling regions, coastal fronts, advection and dispersion [*Arnone et al.*, 1990; *Dickey*, 1991]. The cruise data will be used to evaluate and demonstrate the ability of VIIRS ocean color products to differentiate the variations of spectral features produced by these physical and biological processes. For example, the optical properties of spectral absorption and backscattering coefficients may be associated with different phytoplankton functional groups. These phytoplankton functional groups could then be retrievable from VIIRS satellite data.

4. Cruise Track, Sampling Strategies and Overall Conditions

The project investigators along with the crew of the *Nancy Foster* loaded and secured instrumentation on 30 November and 1 December 2015. The ship departed Charleston, SC on 2 December 2015 and proceeded southward along the coast stopping at stations along the way. When approximately offshore of

Miami, the ship turned eastward and headed to the Bahamas. Many stations were occupied over the several days spent investigating Bahamian waters and the Tongue of the Ocean. Plans for small boat operations to sample in shallow optical depth waters were abandoned due to poor and cloudy weather conditions (i.e., no clear-sky satellite overpasses). The return track stayed relatively near shore up the Florida Coast to approximately Savannah. The track then made an excursion offshore across the Gulf Stream to the edge of the slope, turned northward and then returned westward back across the Gulf Stream. Off the coast near Charleston, a passive drifter was released and followed in an effort to follow and sample a particular water mass in a Lagrangian fashion before a couple of final stations and heading to port on 13 December 2015.

Data collection was performed continuously throughout the cruise. Instruments were installed on the bow of the ship for making continuous observations from above water. Other instruments were installed on the ship's underway, surface sea water, flow-through system and were in operation continuously (day and night). Various profiling and floating optical instrument packages and the ship's Conductivity (salinity), Temperature and pressure (Depth) Rosette package including Niskin bottles for water collection at discreet depths (CTD/Rosette) were deployed at stations (nominally at one location while the ship was not making substantial headway, i.e., "on station"). Sometimes, water samples were collected from the flow-through system either to supplement discrete station sampling or in the place of Niskin bottle sampling at select stations where the CTD/Rosette package was not deployed. On station and underway activities are summarized below. For a measurement-based discussion of observations and instrument types, see Section 5. Also see individual group sub-sections in Section 7 for details and see also Tables A1 to A5 in Appendix A.

Station Activities

Discrete stations were conducted daily, weather conditions permitting, during daylight hours between ~0800 EST and ~1730 EST local time (between ~1300 UTC and ~2230 UTC). Stations were planned to optimize cloud free conditions when they were available. A total of 27 stations were occupied over the course of the 12 days at sea. Ten of those 27 stations covering 4 days (on 8 December 2015 and between 10 December 2015 to 12 December 2015) resulted in good quality match-ups with VIIRS satellite observations. Generally, several activities took place at each station, including:

- AOPs (i.e., radiometry) from several perspectives: profiling, floating and above sea surface
- IOPs (e.g., absorption, backscatter, fluorescence, etc.); profiling, floating
- CTD/Rosette instrument profiles
    - Temperature, salinity, depth, dissolved O_2, chlorophyll fluorescence
- CTD/Rosette water collection from two discreet depths, nominally 1) near surface and 2) mixed layer within the first optical depth (ranging from 12 m to 35 m)
    - Extracted Chl-*a*
    - Suspended particulate material (SPM)
    - Particle absorption by filter pad technique (FPT)
    - Phytoplankton pigments by high performance liquid chromatography (HPLC)
    - Dissolved and particulate organic carbon (DOC, POC)
    - Chromophoric dissolved organic matter (CDOM)
    - Nutrients; N (nitrate and nitrite), P and Si
    - Preserved phytoplankton samples for microscopy and automated imagery
- Secchi depth
- Aerosol optical thickness

Underway flow-through activities

The ship's sea water flow-through system was equipped with a series of bio-optical and hydrographic instruments for continuous underway sampling. The intake point at the sea chest was at a depth of 3 m.

Observational data were synchronized with time and location and were monitored in real time for determining station locations across Gulf Stream fronts and other features. The flow-through data will also be used for spatial variability analyses.

- IOPs (e.g., absorption, backscatter, etc.)
- Phytoplankton imagery
- Temperature, salinity
- Chlorophyll and ultraviolet (UV) fluorescence

Above water – on deck observations
AOPs were collected continuously from instruments mounted on the bow of the ship.

5. Overview of Observations

5.1 Introduction to Observations

Multiple optical instruments were assembled for this cruise to address the overall objectives and specific questions discussed earlier. As summarized in Section 4, in situ observations were made on station and also while underway. On station, a large suite of measurements was made of water column and above water characteristics from various instruments and water samples were collected at discrete depths for later chemical analyses. Underway sampling was conducted continuously for a more limited suite of measurements of the near-surface water and above sea surface conditions. Following is a measurement-based accounting of the various observation types. Further details of deployment and instruments are provided in individual group sub-sections in Section 7 and consolidated in Tables A1 to A5 in Appendix A. Note that commercial equipment, instruments, or materials are identified in this report to foster understanding. Such identification does not imply recommendation or endorsement by the National Institute of Standards and Technology (NIST) or any of the participating institutions, nor does it imply that the materials or equipment identified are necessarily the best available for the purpose.

5.2 AOPs (Radiometry)

Radiometers measure AOPs, including downwelling irradiance (E_d), upwelling radiance (L_u) and incoming solar irradiance (E_s) spectrally (λ) across a range of wavelengths (e.g., ~300 nm to 900 nm). These properties are used to determine in situ $nL_w(\lambda)$ (which are then in turn are comparable with the satellite $nL_w(\lambda)$ products).

Water Column (on station)
- $nL_w(\lambda)$, R_{rs}, and constituents
    - At stations, 4 free-falling AOP profiling packages
        - Three hyperspectral profilers (NOAA/STAR, OSU and USF)
        - One multispectral profiler (NASA/GSFC)
- Secchi depth (UMB)

Sea Surface: Floating (on station)
- $nL_w(\lambda)$, R_{rs}, and constituents - Three instrument packages with hyperspectral radiometric sensors and configured to float at the sea surface were also deployed on station (1 by UMB; 2 by the Stennis group)
- Spectral upwelling radiance distribution (U. Miami)

Above Surface (on station and continuous)
- $nL_w(\lambda)$, R_{rs}, and constituents

    - Seven handheld radiometers were deployed at stations with effort to make observations simultaneously under identical conditions (4x ASDs: NOAA, Stennis, USF, CCNY; 2x Spectral Evolution: OSU, CCNY; and 1x GER: CCNY).
    - Additionally, on-board experiments were conducted with subsets of handheld instruments, testing different locations on the ship, protocols and reference tiles (see the NIST Section 7.10 for further descriptions of NIST blue tile and the Stennis group Section 0 for more descriptions of these experiments).
    - Two instrument packages were mounted on poles in the bow of the ship and collected above water AOP measurements continuously (NASA/GSFC and CCNY). The NASA/GSFC package made standard unpolarized observations while the CCNY package was highly modified to measure both polarized and unpolarized AOPs.
- Aerosol optical thickness (a component of atmospheric correction algorithms); Five handheld sun photometers were deployed at stations (NOAA, Stennis, USF, CCNY and UMB).
- Daily solar irradiance integrated from 400 nm to 700 nm (i.e., daily PAR)

5.3 IOPs (e.g., absorption, backscatter, fluorescence, etc.)

Several instrument packages measured IOPs during the cruise. On station, water column data were collected at discreet points in time and geographic location (latitude and longitude) but with high depth resolution (i.e., continuous profile) using specialized IOP profiling packages, IOP instruments on the ship's CTD/Rosette package, and IOP sensors mounted on the AOP packages discussed earlier (Section 5.2). IOP instruments were also plumbed into the ship's near surface sea water flow-through system providing data more or less continuously in time but only for the near surface water. Generally, the IOP observations made relate to chlorophyll fluorescence, CDOM absorption, light attenuation and optics relating to particles. Instrument packages had unique combinations of sensors and are described in more detail within the specific group's sub section in Section 7.

<u>Water Column – profiling (on station)</u>

- Measurements from dedicated IOP packages
    - Hyperspectral total absorption ($a(\lambda)$; UMB, NASA/GSFC)
    - Hyperspectral CDOM absorption (a_{CDOM}; NASA/GSFC)
    - Multispectral a_{CDOM} (UMB)
    - Backscatter (b_b; at 7 channels, UMB; at 9 channels, NASA/GSFC)
    - Fluorescence (at 2 channels, UMB)
    - Volume scattering function (VSF; at 9 channels, NASA/GSFC)
- IOPs included on AOP packages
    - Chlorophyll fluorescence (NOAA/STAR and USF)
    - CDOM fluorescence (NOAA/STAR and USF)
    - Phycoerythrin fluorescence (NOAA/STAR)
    - Scattering (b; at 443 nm, 550 nm and 860 nm by NOAA/STAR and at 660 nm by USF).
- IOP on Ships CTD/Rosette package:
    - Chlorophyll fluorescence (ship)

<u>Continuous – near surface (underway flow-through)</u>

- Hyperspectral $a(\lambda)$ and a_{CDOM} (Stennis)
- b_b at 470 nm, 572 nm and 670 nm (Stennis)
- Beam attenuation *(c)*
- Chlorophyll and UV fluorescence (ship)

5.4 Non-optical measurements

These parameters were determined from analyses of discreet water samples collected from Niskin bottles on the CTD/Rosette or from the underway flow-through system:

- Extracted fluorometric Chl-*a* (fluorometry; USF)
- Suspended Particulate Material (SPM; mass; NOAA/STAR)
- FPT absorption (spectrophotometry; USF)
- Phytoplankton pigments (HPLC; NASA/GSFC)
- DOC (combustion catalytic oxidation and infrared gas analyzer, NASA/GSFC)
- POC and PON (C H N combustion elemental analyzer; NASA/GSFC)
- CDOM (spectrophotometry; NASA/GSFC)
- N, P and Si (colorimetry; LDEO)
- Phytoplankton assemblage characterization (microscopy; LDEO and automated imagery; UMB)

These parameters were observed by the standard instrumentation on the ship's CTD-rosette package.

- Salinity
- Temperature
- Dissolved O_2

These parameters were observed by other onboard instrumentation maintained by the ship.

- Acoustic Doppler Current Profiler (ADCP)
- Meteorology
    - Wind speed
    - Wind direction
    - Sea state
    - Air temperature

6. Laboratory Calibration of Radiometers

Pre- and/or post-cruise calibrations of several radiometers used in this cruise were conducted at the NOAA/STAR Optical Characterization Experiment Laboratory in College Park, Maryland using a NIST traceable type FEL 1000 W standard irradiance lamp #667 and an Optronic Laboratories OL-455-18 integrating sphere for radiance with values traceable to NIST. A discussion of the theoretical basis for radiometric instrument calibration was included in the 2014 cruise Technical Report [*Ondrusek et al.*, 2015] as based on primary research by Zibordi and Voss [2014] and by Johnson et al. [2014] and others. Before the cruise, on 19 November 2015, and then again directly after the cruise, on 27 to 28 January 2016, the NOAA/STAR HyperPro (Satlantic), USF HyperPro (Satlantic), NASA/GSFC C-OPS (Biospherical), UMB RISBA (Satlantic, modified by UMB), and the Stennis/NRL HyperTSRB (Satlantic) radiometers were all calibrated. Figure 2 shows an example of the pre- and post-cruise calibration results for the NOAA/STAR L_u 206 irradiance sensor and E_d 233 irradiance sensor along with expected values for the lamp. Figure 3 shows the percent difference between the expected lamp values and those measured by the radiometers.

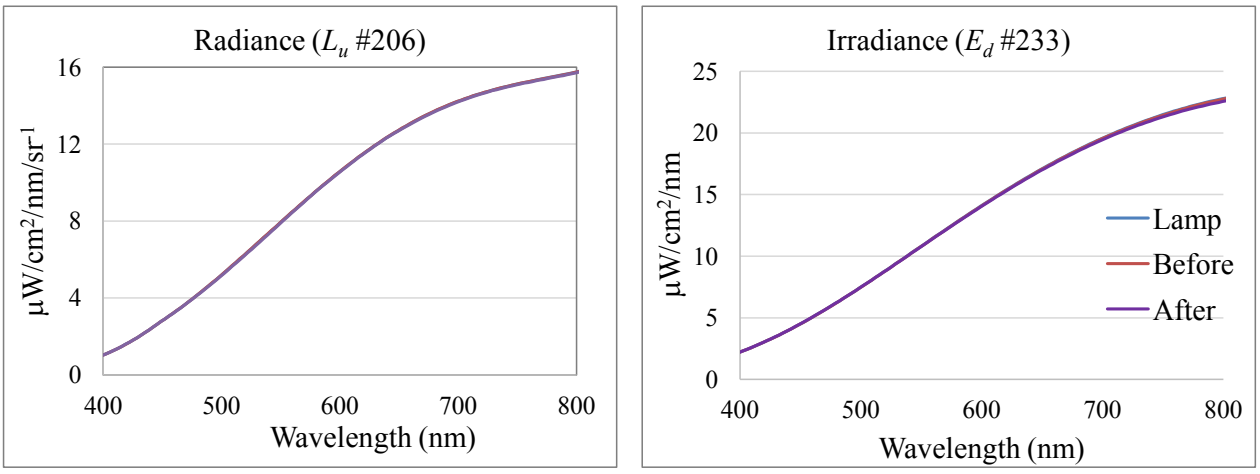

Figure 2. Example of the pre- (red lines, before) and post- (purple lines, after) cruise calibration of the NOAA/STAR radiance sensor (L_u 206; left) and irradiance sensor (E_d 233; right) used in the December 2015 Cal/Val cruise shown with the NIST traceable FEL-557 lamp reference values (blue lines).

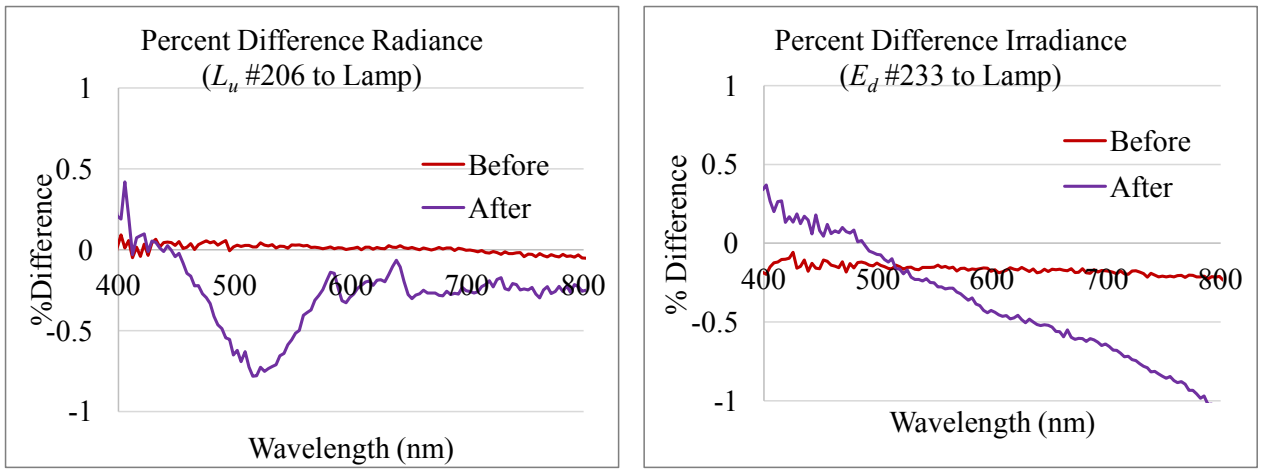

Figure 3. Percent difference between the sensor measurements (radiance, left and irradiance, right) and the expected values of the lamp before (red lines) and after (purple lines) the cruise..

7. Participating Science Groups' Activities, Methods and Protocols

7.1 NOAA/STAR – Michael Ondrusek and Eric Stengel

HyperPro in-water radiometry

One of the primary tools used by NOAA/STAR for in situ ocean color radiance validations is a Satlantic HyperPro Profiler II (specifications and manuals for the HyperPro can be found at http://www.satlantic.com). The HyperPro system has a downward looking HyperOCR radiometer that measures upwelling radiance ($L_u(\lambda)$) and an upward looking HyperOCI irradiance sensor to measure downwelling irradiance ($E_d(\lambda)$) in the water column. In addition, there is an above-water upward looking HyperOCI irradiance sensor to measure downwelling irradiance ($E_s(\lambda)$) used as a reference. The E_s sensor was mounted on a telescoping tower pictured in Fig. 4. These measurements are used to calculate $nL_w(\lambda)$ spectra observed by ocean color satellites. $nL_w(\lambda)$ spectra can be used to validate satellite ocean color

radiances and develop ocean color derived products such as Chl-*a* or SPM concentrations used in ecological studies [*Ondrusek et al.*, 2012].

Figure 4. Telescoping tower with E_s reference sensors.

The HyperPro Profiler II is deployed in a free falling mode where it is lowered and raised in the water column while taking care to keep it away from the ship and avoid ship shadowing. The weight is adjusted on the profiler to allow a descent rate of 0.1 m s^{-1} to 0.3 m s^{-1}. Each HyperOCR or HyperOCI has a 256 channel silicon photodiode array detector with 10 nm spectral resolution and spectral sampling of 3.3 nm $pixel^{-1}$. The instruments are calibrated from 350 nm to 900 nm. The HyperOCRs have dark signal corrections performed using shutter dark measurements collected every 5th scan. The radiometers were calibrated before and after the cruise as described in Section 6. The profiler is equipped with depth, temperature, tilt and two WET Labs ECO-Puck Triplet sensors. One ECO-Puck sensor measures fluorescence estimates of Chl-*a*, CDOM and phycoerythrin. The second ECO-Puck sensor measures backscattering b_b at 443 nm, 550 nm, and 860 nm. The operation of the HyperPro Profiler II instrument is described at: http://satlantic.com/sites/default/files/documents/ProfilerII-RevK-Manual.pdf.

The system was deployed by hand simultaneously with the USF HyperPro Profiler II (Section 7.4), the OSU HyperPro Profiler II (Section 7.7) and the NASA C-OPS Profiler (Section 7.9). For each station, the sun was positioned directly off the stern and the 4 profiling instruments were positioned evenly spaced at the stern (Fig. 5). All four instruments were lowered to the sea surface, together with the ship maintaining approximately 1 knot speed to get the profilers at least 20 m off the stern. After that, the ship maintained just enough speed to prevent the profilers from closing in on the ship and to prevent them from crossing cables while profiling. For each station, 3 to 5 multicast measurement sets were conducted (section D of Profiler II manual). For each set, all four profilers were lowered to 10 m and raised together 3 to 5 times. If sky conditions changed significantly during the cast, the set was stopped and restarted when the conditions were favorable again. Examples of match-ups between the NOAA HyperPro R_{rs} data and VIIRS ocean color satellite data are shown in Fig. 6. The VIIRS data was processed using NOAA's MSL12 (http://www.star.nesdis.noaa.gov/jpss/documents/AMM/VIIRS_OCC_Val.pdf).

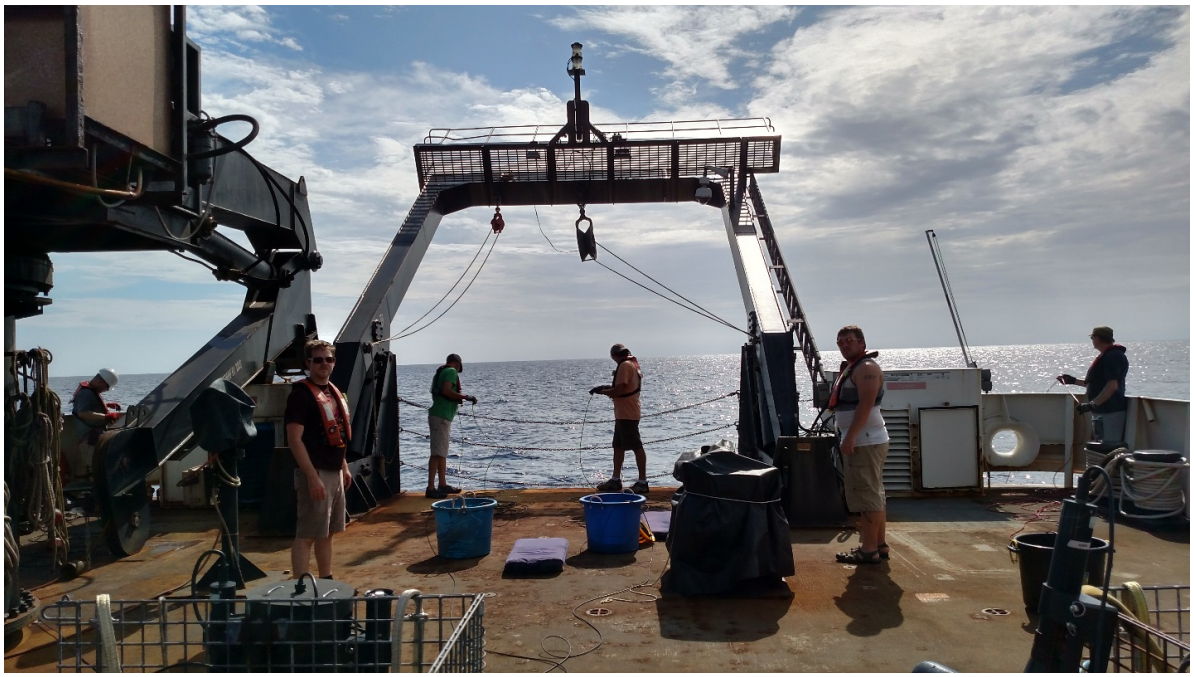

Figure 5. Four profiling radiometers were deployed simultaneously off the stern at each station.

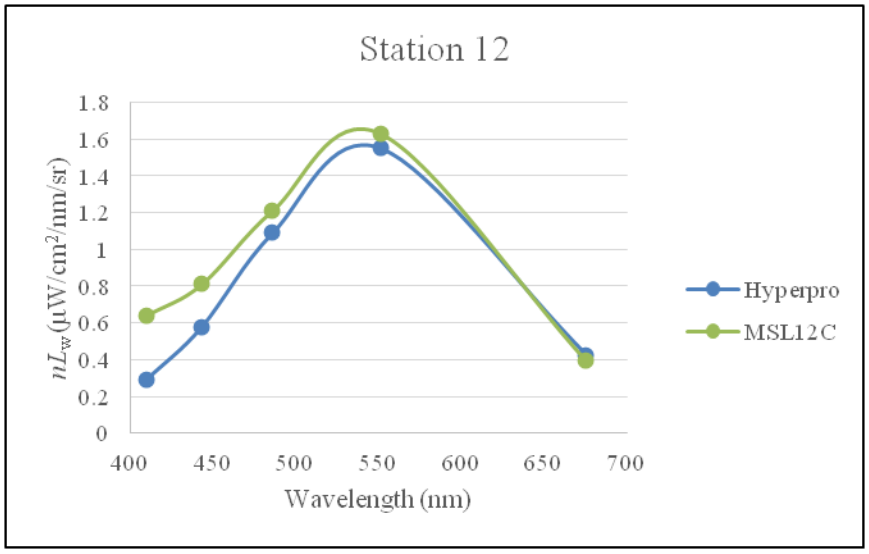

Figure 6. Preliminary NOAA VIIRS *vs*. NOAA HyperPro comparisons from 8 December 2015, Station 12. NOAA VIIRS data are averaged over 5 x 5 pixels.

The data were processed using Satlantic Prosoft processing software version 8.1.2. The $nL_w(\lambda)$ spectra are calculated using the equation:

$$nL_w(\lambda) = L_w(0^+, \lambda) * F_0(\lambda)/E_s(\lambda) \quad (1)$$

where F_0 is the mean extraterrestrial solar irradiance [*Neckel and Labs*, 1984] and $E_s(\lambda)$ is the downwelling spectral irradiance just above the surface and is measured with the above water HyperOCR irradiance reference sensor. $L_w(\lambda)$ is the water-leaving radiance calculated just above the surface by:

$$L_w(0^+, \lambda) = L_u(0^-, \lambda) * [(1-\rho(\lambda, \theta))/n_w(\lambda)^2] \quad (2)$$

where, $\rho(\lambda, \theta)$ is the sea surface Fresnel reflectance and is set as 0.021, and $n_w(\lambda)$ is the Fresnel refractive index of seawater and is set here as 1.345. $L_u(0^-, \lambda)$ is the calculated upwelling radiance just below the surface and is determined by using the diffuse attenuation coefficient (KL_u) calculated using a least squares regression fit from log transformed measured $L_u(\lambda)$ values and the intercept just below the surface.

ASD above-water radiometry

Above-water radiometry measurements were conducted using an ASD HandHeld2 radiometer (http://www.asdi.com/products/fieldspec-spectroradiometers/handheld-2-portable-spectroradiometer). Remote sensing reflectance, $R_{rs}(\lambda)$, measurements were conducted at seventeen stations and the NIST blue tile comparison was conducted at 4 stations. For each observation, Stennis/NRL protocols were followed. This includes utilizing optics which provided a 10° field of view (FOV) and sampling rate of five scans each time the trigger is activated. The instrument was optimized before each set of five scans to adjust the integration time. Five scans were collected of the sky at an azimuth of 135° from the sun and 50° from the horizon with an unobstructed view of the sky. The next five scans were collected again with an azimuth of 135° from the sun and 50° from the horizon of a "gray plaque". This gray plaque is a10% gray standard reference plaque with a known bi-directional reflectance function (BRDF), and assumed to have a semi-Lambertian surface. Finally, five scans of the water are conducted using the same scan angles and using care to provide an unobstructed view. Processing is being conducted using NRL-developed processing software that follows the guidelines of *Mueller et al*. [2003] and utilizes 5 different processing models including: R_{rs}_sfc (no near infrared (NIR) reflectance correction), R_{rs}_fresnel (Fresnel correction omitted), R_{rs}_*Carder and Steward* [1985], R_{rs}_*Lee et al.* [*Lee et al.*, 1997], and R_{rs}_*Gould et al.* [*Gould et al.*, 2001].

Extracted fluorometric Chl-*a*

Chl-*a* concentrations were measured using a Turner 10 AU Fluorometer [*Welschmeyer*, 1994]. Surface samples were collected in duplicate at each station from the CTD or flow-through system, and 100 mL to 400 mL of seawater were filtered onto a 25 mm diameter, 0.7 µm glass microfiber filter (GF/F; Whatman). The filters were extracted in 90% acetone in a freezer for at least 48 h. The samples were vortexed then centrifuged for 5 min before being measured on the Turner 10 AU.

Suspended Particulate Material (SPM)

SPM samples were collected in duplicate from the surface waters for each station. Up to 2 L of water were collected for each sample and processed according to techniques outlined by Hunter [*Hunter*, 2006]. Water samples were filtered on pre-weighed 47 mm diameter GF/F filters. The samples were filtered under positive pressure until the filtration stopped. The volume of filtrate was then measured with a graduated cylinder and recorded. Filters were placed in 47 mm diameter Petri dishes and oven dried at 60 °C for 12 h then stored in a desiccator until analysis.

Filters were weighed on a Sartorius CPA 2250 balance (with a precision of 0.01 μg) and weighed at least three times until consecutive readings were less than 0.055% variable [*EPA*, 1971].

7.2 U. Miami – Kenneth J. Voss

New Upwelling Radiance Distribution camera System (NURADS) measurements of the BRDF or Radiance Distribution

NURADS measures the spectral upwelling radiance distribution [*Voss and Chapin*, 2005]. The upwelling light field from the same water type in the ocean varies with illumination geometry and viewing geometry. Almost all measurements of the upwelling radiance used for satellite validation/calibration are made in the nadir direction (instrument looking straight down, light coming straight up), however the satellite views the ocean at different angles, depending on where the specific pixel is in the satellite scan line. To relate the measurement made on the ground to what the satellite is viewing requires information on the variation of the radiance with direction, which is the radiance distribution. The shape of the radiance distribution also changes spectrally, so this spectral variation of the radiance distribution must also be determined. This is exactly the parameter that NURADS measures.

The model used to correct for the oceanic BRDF in the data reduction process of satellite data is provided in Morel et al. [2002]. This model has been validated several times [*Voss and Morel*, 2005; *Voss et al.*, 2007; *Gleason et al.*, 2012], but the model is aimed at Case I waters (water parameters determined by a statistical relationship with Chl-*a*), and breaks down in coastal waters. While we have taken a considerable amount of open ocean radiance distribution data, and some coastal radiance distribution data, because of the variability of the water properties in the coastal area it is reasonable to expand the data set and to take radiance distribution data along with other validation data when doing experiments such as this.

The NURADS instrument was calibrated following previously published protocols [*Voss and Zibordi*, 1989; *Voss and Chapin*, 2005]. Mike Ondrusek (NOAA/STAR) deployed the instrument at stations in conjunction with other instruments as described elsewhere (Sections 5.2, 7.1 and Table A5). Floats were attached to the instrument to allow it to measure at the surface, 20 m to 50 m away from the ship (measurement depth is 0.75 m). When deployed, the instrument measures the upwelling radiance continuously, cycling through the 6 different wavelengths and associated dark measurements. NURADS measurements were made at 8 stations (12, 18, 20, 21 and 23 to 26). The data are currently being reduced and quality controlled.

7.3 UMB – Zhongping Lee, Jianwei Wei, Guoqing Wang and Junfang Lin

In situ observations of the remote sensing reflectance and inherent optical properties in the Northwest Atlantic Ocean

Our objectives for this cruise included: 1) to obtain R_{rs} through direct measurements using the skylight-blocked approach for instrumental inter-comparison and validation of the VIIRS ocean color data; 2) to measure the inherent optical properties including the total absorption and total attenuation coefficients (a_{pg} and c_{pg}) to assess the measurement uncertainty and evaluate VIIRS ocean color products; and 3) to measure phytoplankton assemblage using an imaging flow cytometry system in order to understand the primary contributors to photosynthesis.

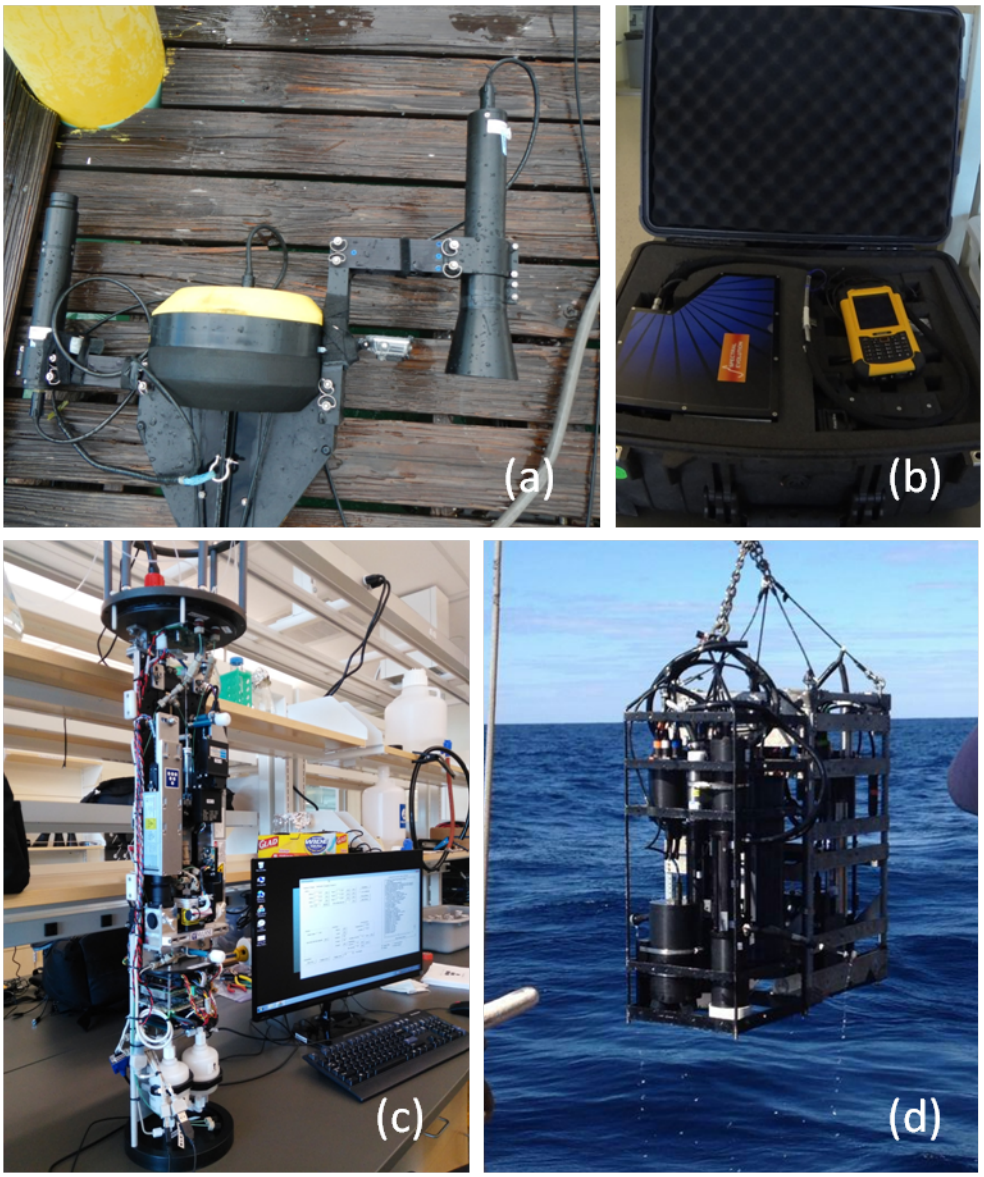

Figure 7. Instruments deployed in NOAA VIIRS cruise: (a) Radiometer Incorporating the Skylight-Blocked Apparatus (RISBA), (b) Spectral Revolution spectral radiometer, (c) IFCB, (d) IOP measuring package.

Instruments and Deployments

Radiometer Incorporating the Skylight-Blocked Apparatus (RISBA)

To characterize the water optical properties, we measured the water-leaving radiance (L_w) with a hyperspectral radiometer incorporating the skylight-blocked apparatus [*Lee et al.*, 2013]. The RISBA system is equipped with one hyperspectral irradiance sensor (HyperOCI, Satlantic Inc.) measuring the above-water downwelling plane irradiance (E_s) and one hyperspectral radiance sensor (HyperOCR, Satlantic Inc.) which simultaneously records the water-leaving radiance $L_w(0^+)$ by blocking off the surface-reflected skylight (Fig. 7a).

The Satlantic's hyperspectral radiometers are fully digital optical packages. HyperOCR has an FOV of 11.5° in air (8.5° in water). The radiance can be measured at about 3 nm increments from ultraviolet (~350 nm) to near-infrared (~800 nm) wavelengths with a wavelength accuracy of ±0.1 nm. And each spectral band is approximately 10 nm wide. HyperOCI has a cosine response collector and measures irradiance with a standard uncertainty of ±3% for sun angles 0° to 60° and ±10% for sun angles 60° to 85°.

Both radiometers were calibrated by the manufacturer and further validated at the NOAA STAR radiometric calibration facilities. During deployment, the instrument package was always kept >20 m away from the ship to avoid shadows or reflections of the ship hull. For the measured E_s and $L_w(0^+)$ data pairs, only those with inclination less than 5° were used for further analysis. The E_s was interpolated spectrally so as to match-up with the wavelengths of the L_w sensor. The instantaneous remote sensing reflectance was first determined as the ratio of instantaneous $L_w(0^+)$ to the corresponding E_s

$$R_{rs}(\lambda,t) = \frac{L_w(0^+,\lambda,t)}{E_s(\lambda,t)} \tag{3}$$

The first mode of the $R_{rs}(698, t)$ data sequence was then located from its probability density function. Further, all those measurements of $R_{rs}(698,t)$ beyond ±15% of the mode were filtered out. This procedure was designed to eliminate those potentially contaminated measurements by sea surface reflection and/or immersed sensor head at high sea conditions. The remaining $R_{rs}(\lambda,t)$ spectra were used to derive the median $R_{rs}(\lambda)$ spectrum at each station.

Above-water Radiometer

The SR-1900 spectroradiometer (Spectral Evolution, Inc; Fig. 7b) measured the sky radiance (L_{sky}) and the total of surface-reflected sky radiance and water-leaving radiance ($L_{ref}+ L_w$), and the downwelling plane irradiance (E_s). The measurements were recorded at 768 spectral bands (350 nm to1900 nm). The spectral resolution is 4 nm between 350 nm to1000 nm and 10 nm between 1000 nm and 1900 nm. When measuring L_{sky} and $L_{ref}+ L_w$, the radiometer was pointed to the target at 90 deg azimuth direction relative to the sun and 45° zenith/nadir angle.

IOP instruments

Two ac-s meters (Wetlabs Inc; Fig. 7d) were integrated with one backscattering meter (BB7FL2, WetLabs Inc) to measure the IOPs. The ac-s meter measures the absorption and attenuation coefficients at 80 plus wavelengths from 400 nm to 732 nm. Two ac-s meters were used to simultaneously measure the total absorption and attenuation coefficients, a_{pg} and c_{pg}, to evaluate the measurement uncertainty and data processing methods. Pure water calibration was carried out before and in the middle of the cruise using nano-pure water.

The BB7FL2 meter measured the backscattering coefficient at seven wavelengths (412 nm, 440 nm, 488 nm, 532 nm, 595 nm, 695 nm and 715 nm) and the CDOM and chlorophyll fluorescence at two wavelengths. Dark currents were measured in situ by covering the sensor heads with black electric tape. A new instrument calibration was performed immediately after the cruise by WetLabs Inc.

Imaging FlowCytoBot (IFCB)

The IFCB (Fig. 7c) uses a combination of video and flow cytometric technology to capture images of organisms for identification and measure chlorophyll fluorescence associated with each image. The IFCB has sufficient resolution (~1 μm) to image nano- and microplankton (~10 μm to >100 μm). Phytoplankton in this size range can be especially important in coastal phytoplankton blooms, and microzooplankton are critical to the diets of many grazers.

The images can be automatically processed and classified following the approach described by Sosik and Olson [2007]. The approach relies on a supervised machine learning algorithm where the training will be based on example images collected in situ and categorized by manual inspection. Samples were measured in the instrument during the cruise but post-processing is required for a complete analysis.

Some preliminary Results

Satellite and in situ data match-ups

A total of 19 stations were covered with measurements of remote sensing reflectance and 5 match-up stations obtained between VIIRS and in situ measurements. Figure 8 compares VIIRS R_{rs} with in situ R_{rs}. It is noted that the VIIRS R_{rs} data were retrieved over an area of 3×3 pixels. No consideration was taken of the ocean color quality flags or masks. According to the match-up comparisons, strong agreement was observed at Station 23. For other stations, the VIIRS measurements of $R_{rs}(488)$, $R_{rs}(555)$ and $R_{rs}(670)$ were generally slightly lower than in situ measuements. An exception is observed at Station 25, where the VIIRS measurements are consistently higher than in situ measurements. One likely reason is the difference in the observation time (~1.5 h) between VIIRS overpass and in situ measurement, which could be significant for the optical properites of dynamic waters in these offshore regions.

IOP measurement uncertainties

Hyperspectral absorption and scattering coefficients are commonly measured with the ac-s system (Wetlabs, Inc.). The data from the a-tube requires a critical correction to remove the scattering contribution of the water components. Various scattering correction schemes have been developed and used for this process, but no consistent agreement has been reached on their performance. During the NOAA VIIRS Cal/Val cruise, we integrated two ac-s meters with the same data handler (DH-4, Wetlabs Inc) for simultaneous measurements of total absorption and attenuations. These two ac-s meters (s/n: acs-105 and acs-180) were calibrated with nano-pure water following the benchtop funnel method of Sullivan et al. [2006]. All the nano-pure water calibration and in situ measurements were calibrated to the same temperature. Salinity corrections were also made based on CTD measurements. For the scattering correction, we tested four different schemes: baseline method [*Zaneveld et al.*, 1994], proportional method [*Zaneveld et al.*, 1994], baseline^{+} method [*Röttgers et al.*, 2013] and proportional^{+} method [*Röttgers et al.*, 2013]. The same reference wavelength for the correction was set to an NIR band at 715 nm.

Inter-instrument uncertainty

To assess the inter-instrument measurement uncertainty, we estimated the symmetric absolute percentage difference as

$$\delta = \frac{2}{N}\sum_{i=1}^{N}\frac{|x_i - y_i|}{|x_i + y_i|} \qquad (4)$$

where x and y refer to the measurements of a_{dg} by two ac-s meters. This δ is taken as the measurement uncertainty per scattering correction scheme. Figure 9 compares the measurements of non-water absorption coefficient, $a_{pg}(\lambda)$, retrieved by two ac-s meters. These data were averaged for first 15 m of the upper water column. Two sets of $a_{pg}(\lambda)$ measurements have shown significant discrepancies, which are to some degree dependent on the scattering correction schemes. In general, the best agreement with the smallest difference is found for the $a_{pg}(\lambda)$ processed by the baseline+ scheme, at least for these relatively clear waters.

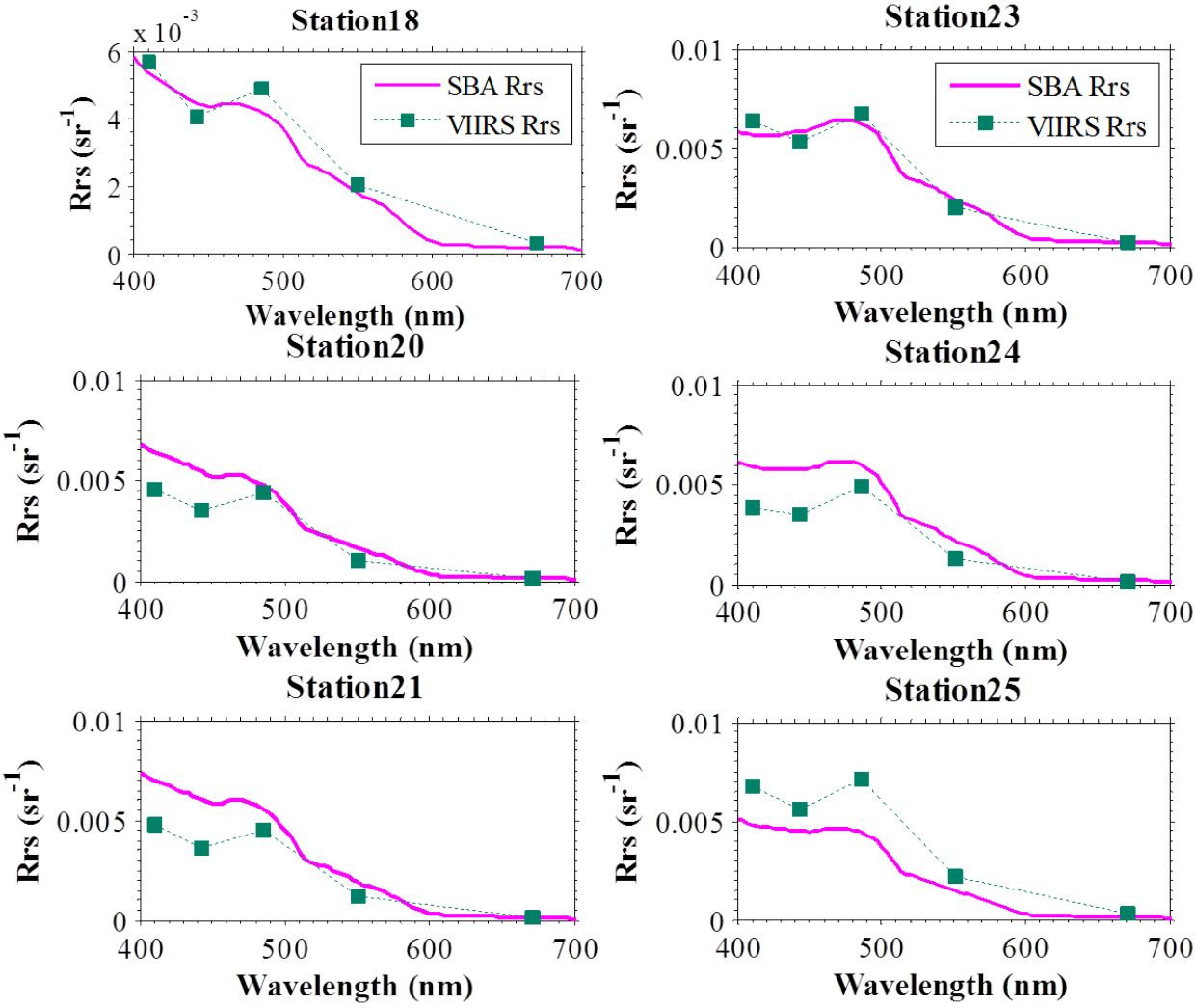

Figure 8. Comparison of NOAA VIIRS ocean color and in situ measurement match-ups.

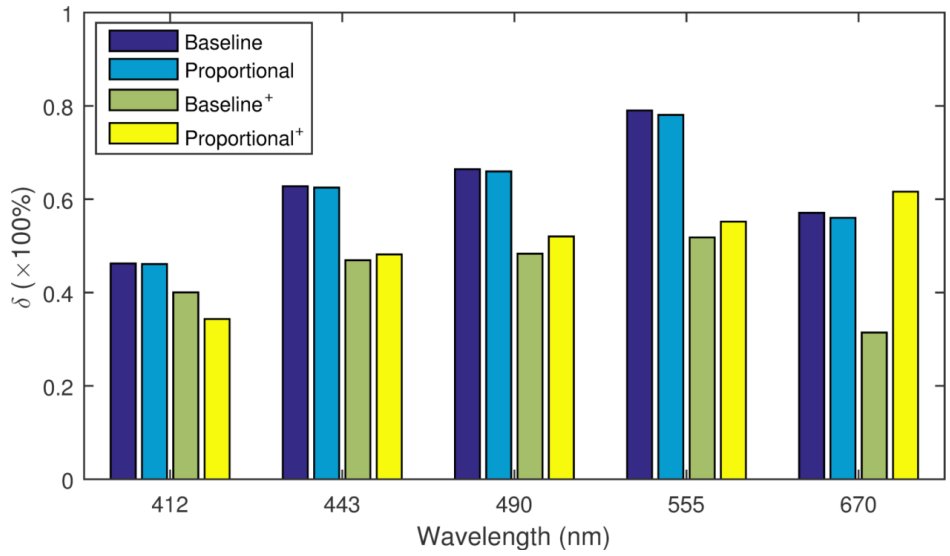

Figure 9. Statistics for the two ac-s measured a_{dg}.

Model-data comparison

A further comparison was made between the estimated a_{dg} by the quasi-analytical algorithm (QAA) [*Lee et al.*, 2002] and the ac-s measurements (Fig. 10). The in situ measured R_{rs} spectra were fed into the QAA algorithm. The measured a_{dg} was the average of two sets of ac-s measurements within the first 15 m. The error statistics is further provided in Fig. 11. It is clear that good agreement between the model and the data was achieved with the baseline+ method, at least for wavelengths of 412 nm, 443 nm and 490 nm for these clear waters.

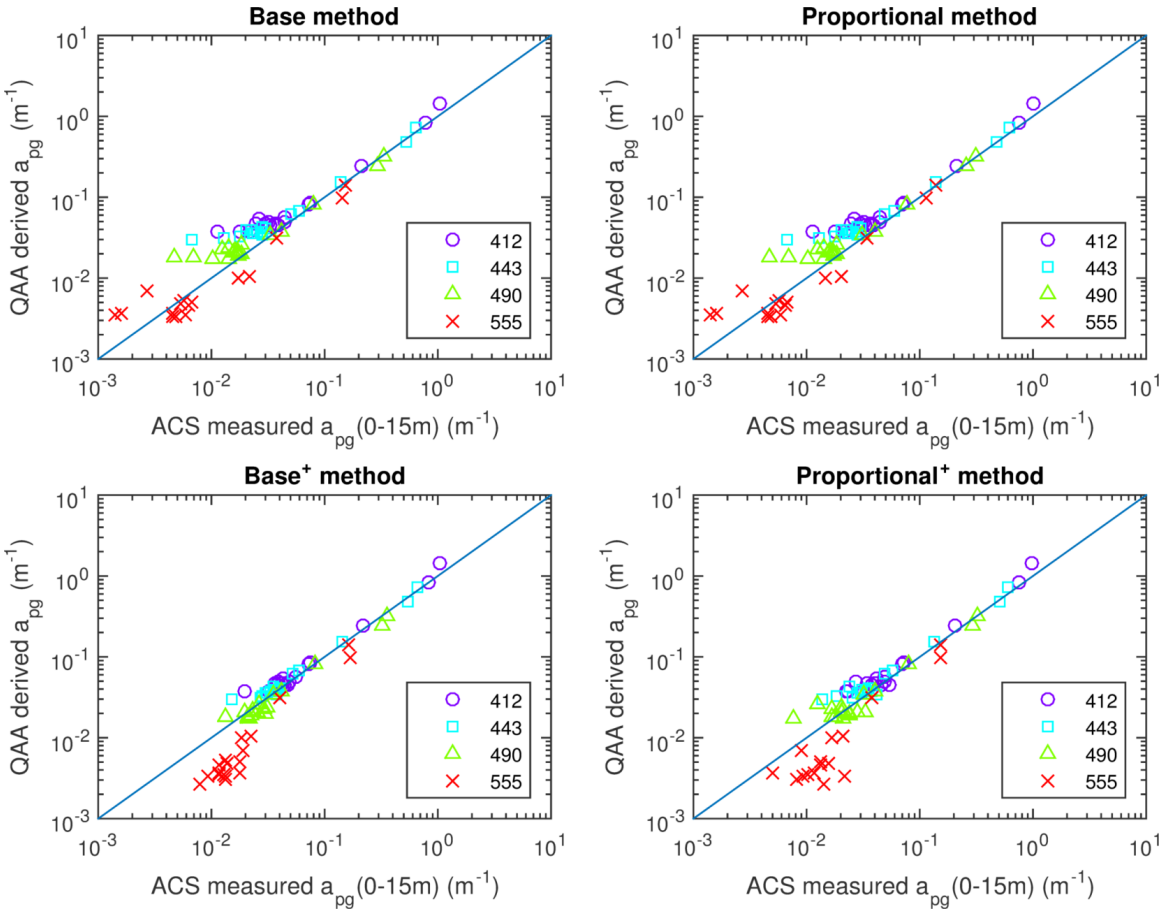

Figure 10. Comparison of the ac-s measurements and QAA estimations.

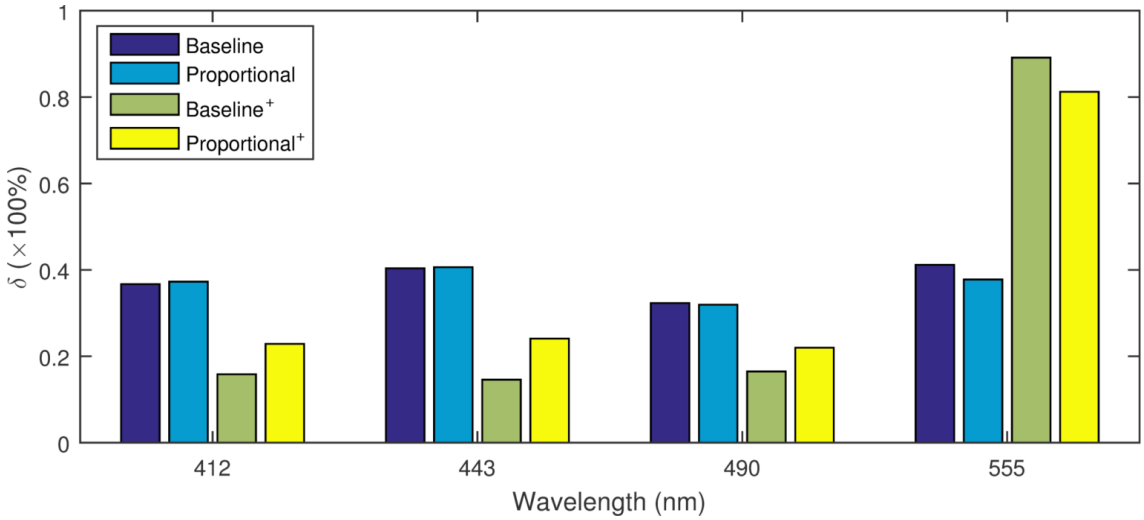

Figure 11. Error statistics between the ac-s measured a_{dg} and QAA estimated a_{dg}.

Abundance of phytoplankton cells

The IFCB continuously took high-resolution images of nano- and micro-phytoplankton (Fig. 12) from the flow-through system on board NOAA ship *Nancy Foster*. Phytoplankton cells larger than ~10 μm were identified and imaged every 21 min from 2 December 2015 to 13 December 2015 (Fig. 13).

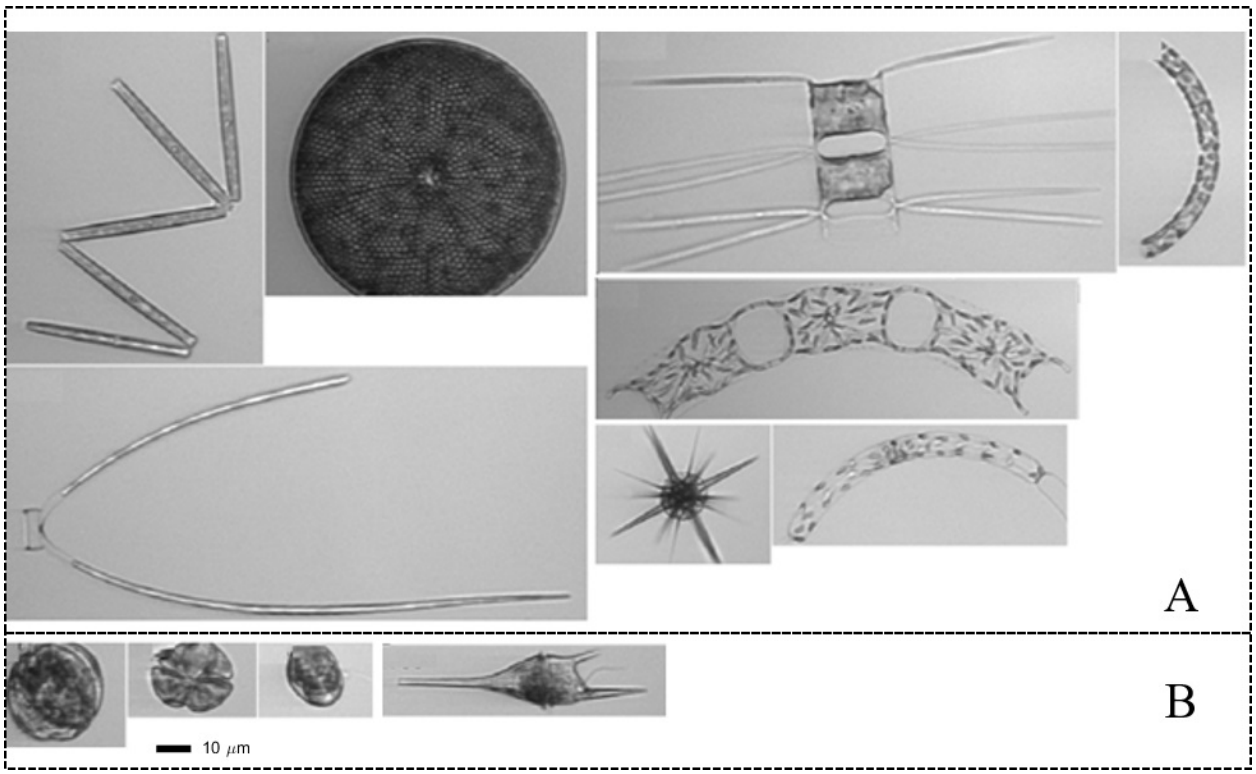

Figure 12. Sample images taken by IFCB from the 2015 cruise. The camera inside the IFCB was triggered by chlorophyll fluorescence to capture the phytoplankton cells flowing through the cytometry. Several species of diatoms (A) and dinoflagellates (B) captured by the camera are shown here.

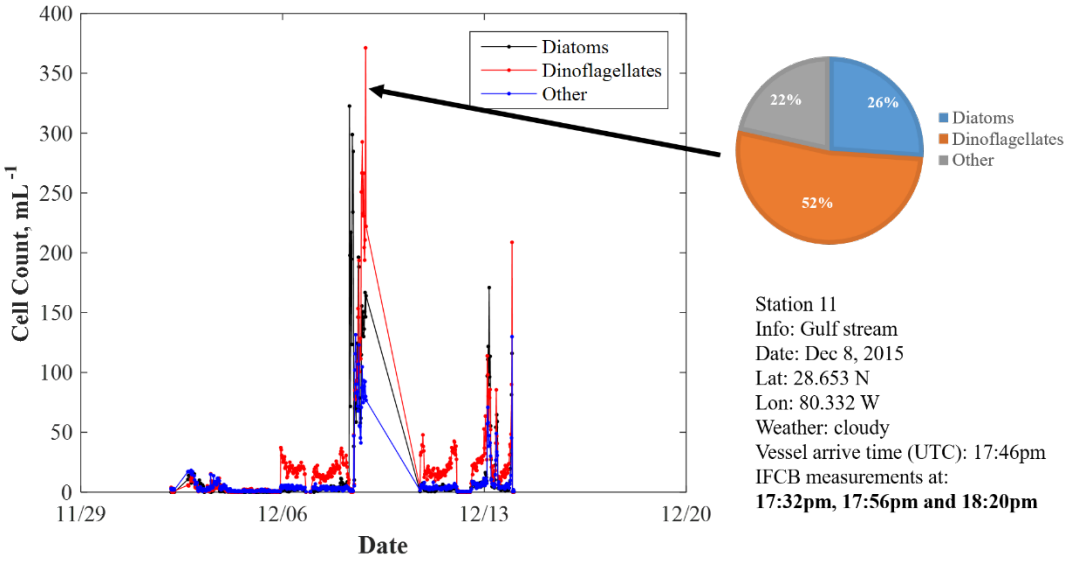

Figure 13. Time series of cell numbers of diatoms and dinoflagellates per mL from 2 December 2015 to 13 December 2015 (left panel). On the right panel, one station on the edge of the Gulf Stream was selected for a close look (the station 11 on the cruise record). The vessel arrived at the station around 17:46 UTC and stayed for 45 mins for optical measurements. During this time interval, three water samples were measured by IFCB (beginning at 17:32, 17:56 and 18:20 UTC separately). For this station, dinoflagellates are dominant (52% cell contribution) and diatoms are the second most abundant group with a 26% contribution to the phytoplankton composition.

Summary

More detailed findings on the remote sensing reflectance measurements, IOP measurement uncertainty, and the phytoplankton structure, abundance and particle size distribution will be reported once the full analyses are complete.

7.4 USF Optical Oceanography Laboratory – Chuanmin Hu, Charles Kovach, Jennifer Cannizzaro, and David English

Spectral absorption and pigment determinations

Understanding the variability in chlorophyll-specific phytoplankton absorption spectra, $a^*_{ph}(\lambda)$, is essential for primary production modeling, calculation of underwater light field characteristics, and development of remote sensing algorithms for estimating Chl-*a* concentrations. The spectral absorption of particles suspended in the water can be assessed by filtering a water sample through a glass fiber filter and quantifying the spectral transmission of the filter relative to a wetted blank. The subsequent extraction of the pigments from the particles captured by the filter, followed by re-measurement of both filters, allows for the total particulate absorption to be separated into living (or pigmented) and non-living (or detrital) components [*Kishino et al.*, 1985]. The extraction of pigments from the particles also enables Chl-*a* to be determined fluorometrically [*Holm-Hansen and Riemann*, 1978; *Welschmeyer*, 1994]. The filtrate from particulate filtration undergoes additional filtration using a Nuclepore 0.2 µm membrane filter. A spectrophotometer subsequently measures the absorption spectra of this filtrate to determine the CDOM absorption spectra, $a_g(\lambda)$, for the water sample.

At each station, Niskin bottles were used to collect water samples from just below the water's surface and from a second depth lower in the photic zone. The samples were used for assessment of the chlorophyll-a concentration, as well as the particulate, $a_p(\lambda)$, and detrital, $a_d(\lambda)$, absorption spectra. Duplicate samples were collected at selected stations. Aliquots were filtered using low vacuum pressure (<10 cm Hg) to

concentrate the particles for pigment and absorption determination onto a glass fiber GF/F (Whatman) filter. These filters were placed into containers and quickly frozen using liquid nitrogen. Samples were frozen and kept stored at -80˚ C until analysis. The filtrate from particulate filtration underwent additional filtration using a 0.2 µm filter, and a portion of the subsequent filtrate was placed in 250 mL glass bottles and kept refrigerated (~4° C) until analysis.

Chl-*a* and particulate absorption data were computed for the 6 L water samples collected during the cruise (Table 3). The water samples were taken from coastal and open-ocean waters, with the least Chl-*a* (0.10 mg m^{-3}) found at a depth of 16 m at station 25, and the greatest concentration of Chl-*a* (3.3 mg m^{-3}) was found at a depth of 2 m at station 12. Examples of the $a_p(\lambda)$, $a_d(\lambda)$ and $a_g(\lambda)$are shown in Fig. 14.

Table 3. Collection of water samples from depths >10 m and near the surface. Eleven additional samples were collected for flow-through system validation. ^{D}: Duplicate filter pad samples collected. A total of 58 water samples were collected and analyzed from the CTD stations. In addition, 11 flow-through samples were collected at 10 locations to calibrate the flow-through data.

	CTD Station:	1	2	4	5	6	7	8	9	10	12	13	15	16	18	19	20	21	23	24	25	26	27
Sample Depth	Surface (~2m)	X^D	X^D	X^D	X	X	X	X	X	X	X^D	X	X	X	X	X	X	X	X	X	X	X	X
	Deep (~10-40m)		X^D	X^D	X	X	X	X	X	X	X^D	X	X	X	X	X	X	X	X	X	X	X	X

In summary, the following parameters were determined from the water samples:

- $a_p(\lambda)$, $a_d(\lambda)$
- $a_{CDOM}(\lambda)$
- Chl-*a*

Of these, Chl-*a* was determined by both acidification technique and non-acidification technique, with the following results:

- Range: 0.10 mg m^{-3} to 3.3 mg m^{-3} (minimum → Cast 25 (16m); maximum → Station 12 (2 m)
- Mean: 0.61 ± 0.75 mg m^{-3}
- Median: 0.29 mg m^{-3}

The following provides a summary of the CDOM absorption measurements:

- Range: 0.027 m^{-1} to 1.33 m^{-1} (minimum → Cast 16 (2m); maximum → Flow-Through #10 (3 m)
- Mean: 0.108 ± 0.216 m^{-1}
- Median: 0.045 m^{-1}

Shipboard remote sensing reflectance

Spectral observations of surface waters have led to a better understanding of not only the absorption and transmission of light below that surface, but also of phytoplankton ecology and algal bloom dynamics. By analyzing the water-reflected radiance, researchers can infer information about the material in the near surface waters and improve algorithms for the analysis of airborne and satellite imagery. In situ measurements aid the interpretation and field validation of satellite imagery and can be used to assess plankton blooms, monitor sediment discharge, and develop climate models.

Above water $R_{rs}(\lambda)$ estimates were made using an ASD Inc. HandHeld2-Pro spectroradiometer. This instrument measures radiance at <3 nm spectral resolution for wavelengths from ~350 nm to >1000 nm. For each $R_{rs}(\lambda)$ measurement, multiple spectra were collected of the radiance reflected from the sky, water surface, and a gray plaque [*Carder and Steward*, 1985; *Mueller et al.*, 2003]. Sea surface measurements were made while viewing the water with a 30° to 40° zenith angle and at an azimuth angle between 90° to 135° relative to the sun. Sky measurements were made at a complimentary zenith angle for the sea surface measurement, at the same azimuth orientation. The HandHeld2-Pro was held >30 cm above a level reference plaque during the gray plaque measurement. The instrument's field of view was constrained to ~7.5°, and its integration time was kept constant throughout the series of gray, water, and sky measurements. Additional measurements of the NIST blue tile reflectance plaque were made at several stations.

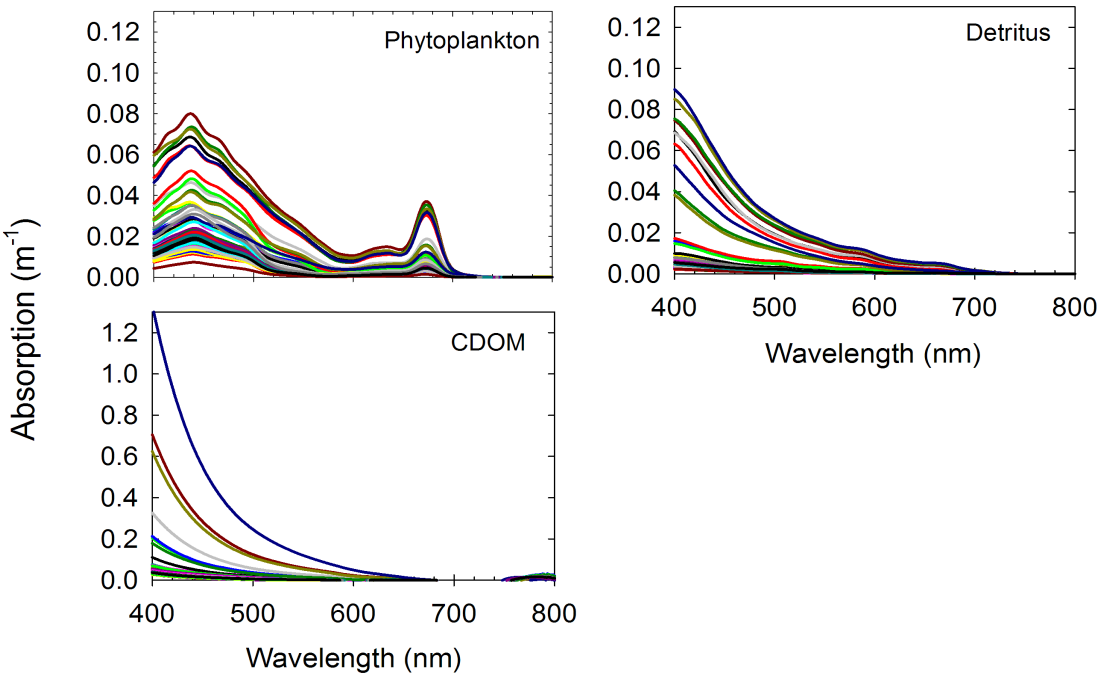

Figure 14. Particulate, detrital and CDOM absorption spectra derived from water samples collected on this cruise. Each spectrum (line color) represents a unique water sample.

$R_{rs}(\lambda)$ measurements were made at 15 stations, and preliminary $R_{rs}(\lambda)$ estimates have been derived. Only the initial measurements were made using the current USF Optical Oceanography Lab protocol, but the majority of the measurements were made by Sherwin Ladner using NRL protocols. Several preliminary $R_{rs}(\lambda)$ estimates for waters sampled during this cruise are shown in Fig. 15.

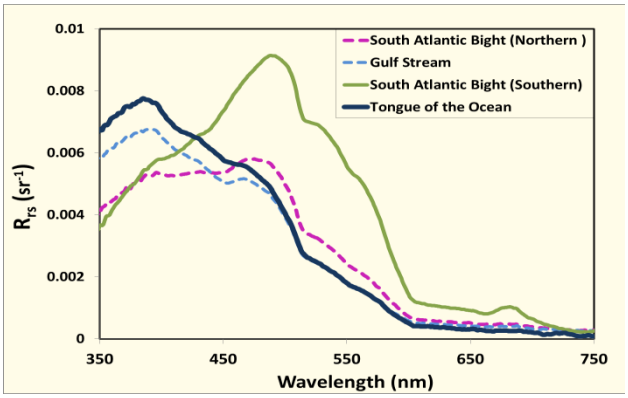

Figure 15. Examples of preliminary $R_{rs}(\lambda)$ estimates from the shipboard (above-water) remote sensing reflectance measurements.

Near-surface light field profiling

As an appropriately oriented pair of spectrometers falls through a water column, this system can measure the changes in the spectral distribution and magnitude of the ambient light field. Vertical profiles of upwelling radiance and downwelling irradiance allow computation of the in situ remote sensing reflectance as well as a spectral assessment of the available light within the water column. Extrapolation of the measurements made at multiple depths to the ocean's surface allows estimation of the remote sensing reflectance of the sea surface, and can provide validation data for ocean color satellites. Examples of the information that are produced from light field profiles include estimates of light attenuation, remote sensing reflectance, energy fluxes, and light available for photosynthesis.

Vertical profiles of the light available in the euphotic zone were collected using a Satlantic HyperPro-II, an integrated spectrometer system designed to measure ocean color as it descends through the euphotic zone. It concurrently measures depth, temperature, conductivity, backscattering of red light, and fluorescence from chlorophyll and dissolved material. The unit is equipped with two hyperspectral radiometers, one facing upward and the other downward. The sensors incorporated into this instrument system include pressure, temperature, conductivity, and tilt sensors, in addition to a WETLabs ECO-Puck Triplet and an above-water hyperspectral radiometer.

USF's Satlantic HyperPro- II system was deployed at most of the sampling stations using the manufacturer's recommended protocol [*Satlantic*, 2003; 2004] under the supervision of NOAA/STAR personnel. However, the instrument's in-water $E_d(\lambda)$ sensor failed early in the cruise. While the sensor failure prevented Satlantic's Prosoft software from processing the data normally, we have been able to extract and convert the $L_u(\lambda)$ data from the HyperPro- II. The light field and reflectance estimates for this cruise that were derived using the HyperPro's $E_d(\lambda)$ will be flagged as suspect because of the sensor's problem.

Direct solar irradiance measurement

The direct solar irradiance was measured at several stations using a Microtops II sunphotometer from Solar Light Co. Measurements from this hand held instrument can be used to estimate aerosol optical thickness for the sampling area. Though this particular instrument was intended to serve as backup instrumentation for other groups, measurements were made using the manufacturer's recommended protocol [*Solar_Light_Company_Inc*, 2003], but have not been analyzed.

Evaluation of VIIRS performance using field data

While some of the data are still being analyzed, preliminary results were obtained by comparing field-measured Chl-*a* and VIIRS-derived Chl-*a*. VIIRS data are from the most recent NOAA MSL12 science quality processing. Figure 16 shows the comparison results. Note that due to the prevailing cloud cover

during the cruise, only a few same day match-ups are available. In order to increase the number of match-ups, this analysis compares VIIRS data up to ±5 d from station observations.

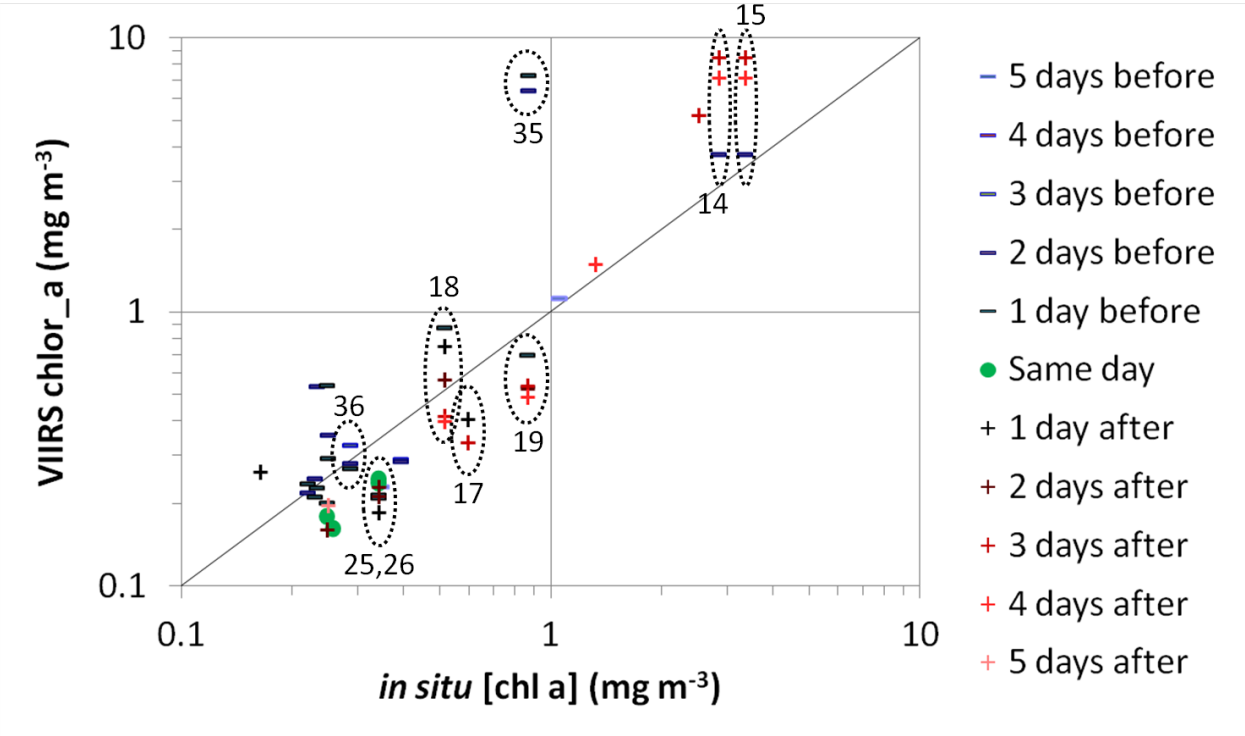

Figure 16. Comparison between field-measured and VIIRS-derived surface Chl-*a* for the December 2015 *Nancy Foster* cruise.

7.5 CCNY – Alex Gilerson, Carlos Carrizo, Ahmed El-Habashi, Robert Foster, Matteo Ottaviani and Sam Ahmed

Three instruments were used by CCNY group for above water observations: GER, SpectraVista, NY, ASD Handheld2, Boulder, CO and HyperSAS-POL, Satlantic, Nova Scotia, modified by CCNY.

1. The GER 1500, Field Portable Spectroradiometer, is a hand-held spectroradiometer designed to provide fast spectral measurements covering the UV, Visible and NIR wavelengths from 350 nm to 1050 nm at 3 nm full width half maximum (FWHM) resolution. It uses a diffraction grating with a silicon diode array that has 512 discrete detectors and provides the capacity of reading 512 spectral bands. A total of 482 spectral scans can be stored within its memory. Subsequent download and analysis is done using a personal computer with a standard RS232 serial port and the GER 1500 licensed operating software. The GER 1500 is equipped and operated with a standard lens with 4° nominal FOV for above water observations. The GER 1500 is used in the field to calculate $R_{rs}(\lambda)$ by measuring the total radiance (L_t) above the sea surface, the sky radiance (L_s), and the downwelling radiance (L_d).

The instrument has undergone radiometric and wavelength calibration in the optics mode (with the lens) at the manufacturer before the cruise but due to the nature of the measurement, calibration is not necessary.

In order to acquire L_t the instrument was placed at the azimuth angle ~90° from the sun and 40° viewing angle from the nadir and made 4 consecutive measurements. L_s was measured by pointing the instrument

at the sky at the same azimuth angle and 40° viewing angle from the zenith with 4 consecutive measurements. L_d data were obtained by pointing the instrument at the Spectralon reference plaque; also four consecutive measurements were made. Typically, a calibrated white reference plaque was used as the standard. In addition, at some stations a gray plaque (from other groups) was used as well. The NIST blue tile comparison was conducted at 4 stations (Stations 9, 16, 21 and 24). All measurements were executed in TAR (target) mode. Downwelling irradiance is determined as

$$E_d = A\pi L_d \quad (5)$$

where A = 0.99 and is the reflectance factor (8/h) of the white target according to manufacturer calibration for the entire spectral range (Labsphere). R_{rs} is calculated by

$$R_{rs} = (L_t - \rho L_s)/E_d \quad (6)$$

where ρ is the sea surface reflectance factor. Values of ρ = 0.021 to 0.028 were considered and will be given together with the processed data. For each station, the averages of all individual scans for L_t, L_s and L_d were taken into account and used in R_{rs} calculations. Since all measurements were carried out in relatively clear coastal waters R_{rs} (750) was subtracted for the entire R_{rs} spectrum to eliminate sunglint effects [*Mobley*, 1999]. Integration time is self-adjusted by the instrument and was typically 160 ms for water observations. All L_t, L_s and L_d sensors were calibrated at CCNY with NIST traceable radiance source. E_d sensors were calibrated at Satlantic before the cruise and at the NOAA optical laboratory after the cruise.

2. The ASD Handheld2 instrument is the same as used by other groups. Measurement and processing methodologies were similar to those described for the GER. The substantial difference being that an "optimization" procedure is required before each set of measurements which adapts the integration time for the illumination condition so that the instrument does not saturate. The integration time varied for water observations in the range 6 ms to 4000 ms. The ASD is equipped and operated with a standard lens with an 8° nominal FOV for above water observations. The ASD instrument was used at 15 stations. The instrument was purchased in 2013 when it was calibrated for the lens mode.

3. In 2014, the HyperSAS-POL instrument from the Long Island Sound Coastal Observatory platform underwent significant modifications to enable its deployment aboard a research vessel. These changes included: (1) alteration of the instrument platform for attachment to the forward mast of a research vessel; (2) development of the software, electronics and communication systems for continuous (underway) positioning of the HyperSAS-POL at 90° or 135° from the Sun (depending on ship orientation) for the sun glint minimization; (3) installation of additional radiometric sensors for polarimetric observations of the sky and (4) incorporation of a tilt sensor for exact knowledge of sensor geometry with respect to the ocean. This configuration and accompanying processing procedures were in place for the VIIRS Cal/Val cruise in November 2014 and remained the same for December 2015 cruise.

Photos of the HyperSAS-POL on the forward mast of the ship are shown in Fig. 17. The instrument contains 3 Hyper OCR sensors (Satlantic) with 3° FOV looking at the water with ~40° viewing angle from nadir (1 sensor is unpolarized, 1 sensor has horizontal polarization and 1 sensor has 45° polarization) and 3 similar sensors for the sky observations. One E_d sensor was positioned in the unobstructed area on the railing of the ship. The second E_d sensor was installed coincident to E_d sensors from other groups on top of a telescoping pole that was mounted to the deck of the ship. In the unpolarized mode the R_{rs} spectra were determined in the manner similar to the one described above for GER instrument with E_d used instead of from equation 5. The polarized mode processing is very complex and currently under study. Integration time is self-adjusted by the instrument and was 2000 ms for water

observations. Data were collected every 2 s during daytime. Multiple R_{rs} spectra collected for each station were averaged.

Comparison of spectra measured by HyperSAS and GER with VIIRS satellite data are shown for Station 03 (coastal) in Fig. 18 and Station 27 (clear water) in Fig. 19 demonstrating promising potential of the HyperSAS instrument for accurate above water observations. Satellite data are from MSL12 science quality processed by NOAA/STAR. True color images are at the bottom of the figures. Sky images are from the camera installed on the HyperSAS. In addition, aerosol optical thickness was measured by Microtops sunphotometer (Solar Light, PA) at 5 wavelengths: 380 nm, 500 nm, 675 nm, 870 nm and 1020 nm.

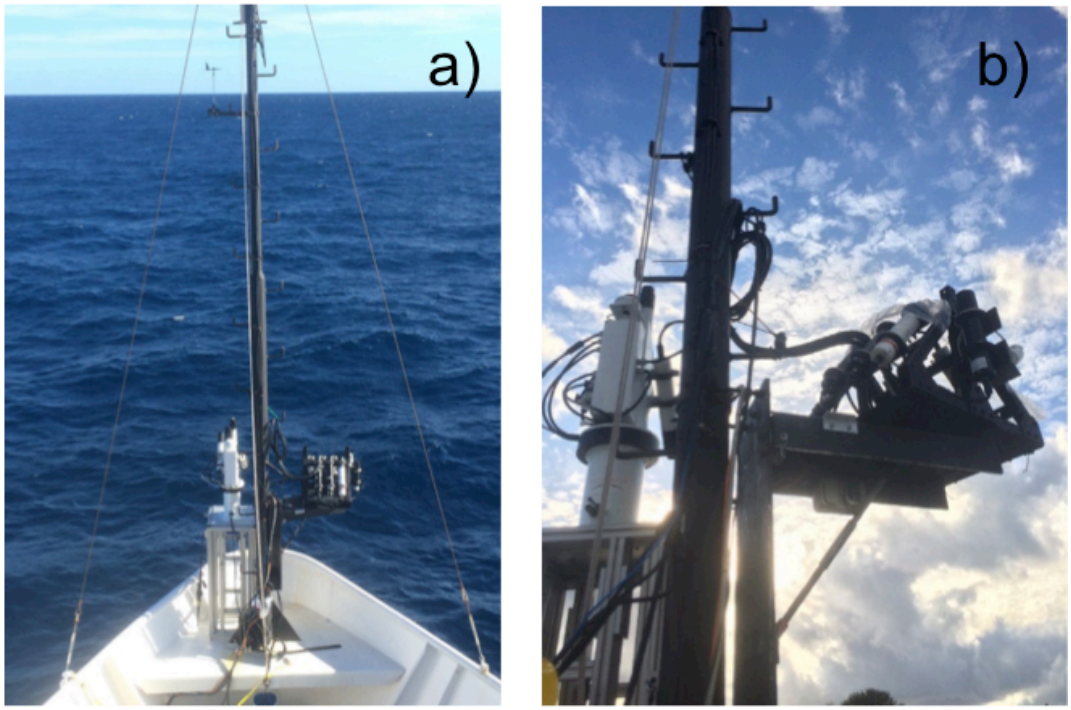

Figure 17. HyperSAS-POL on the mast at the bow of the ship.

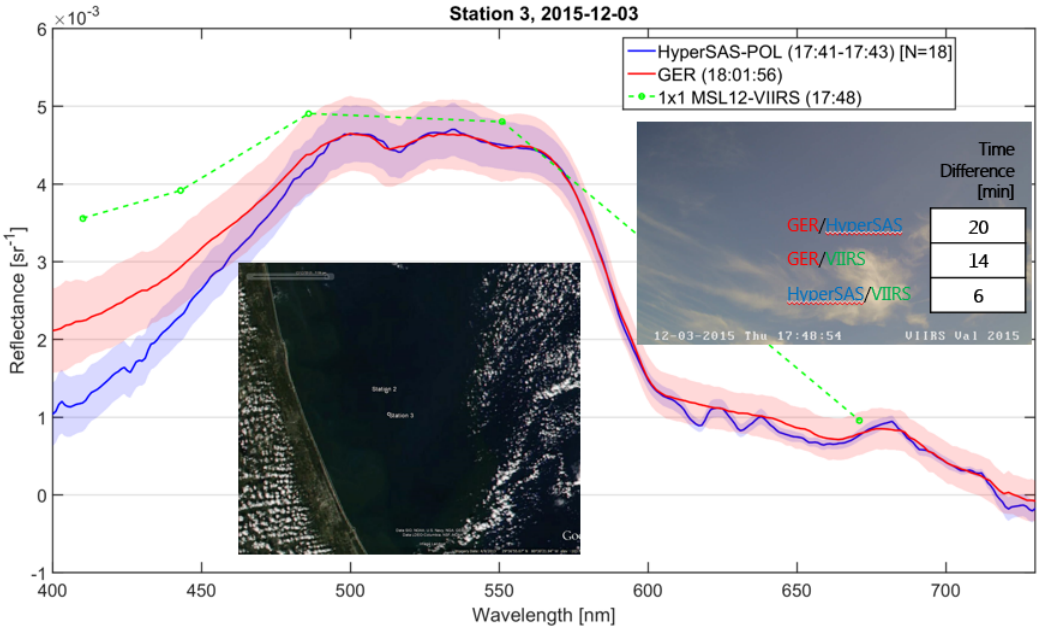

Figure 18. Comparison of measured spectra by the bow-mounted HyperSAS-POL and the handheld GER instruments with satellite data for Station 3 in coastal waters. Left inset shows true color imagery of sky/cloud conditions. Right inset gives time differences between measurements.

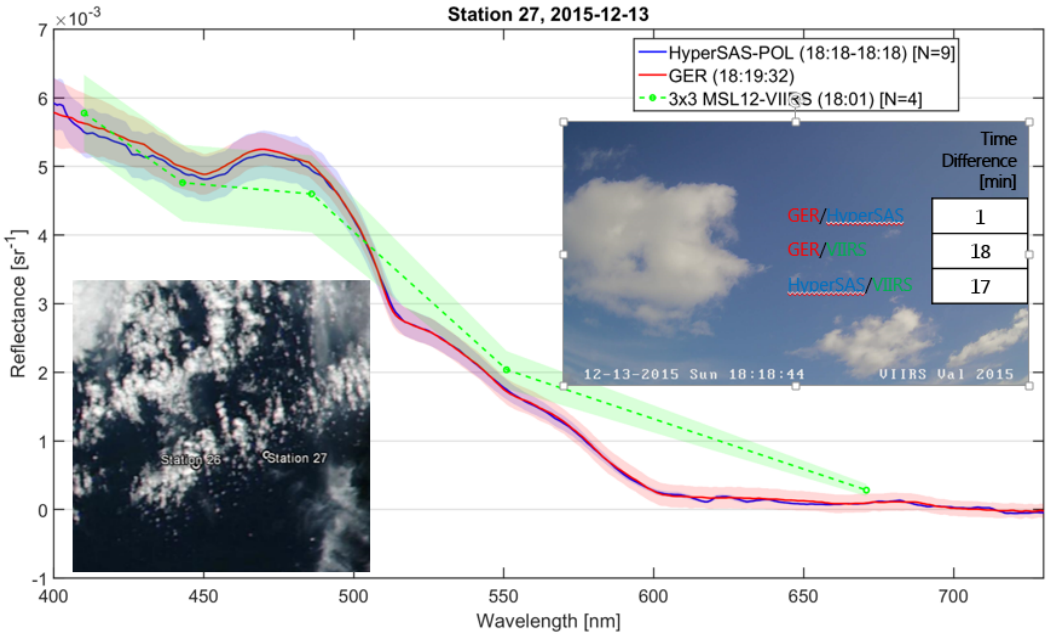

Figure 19. As for Fig. 18 but for Station 27 in the open ocean.

7.6 Stennis Cal Val Team – Robert Arnone, Sherwin Ladner, Wesley Goode, Ryan Vandermeulen (USM, NRL, NASA/SSAI)

Stennis participation and measurements on the VIIRS Cal Val cruise included coordination with NOAA for adaptively daily planning of the cruise track and sampling locations in the Tongue of the Ocean (Bahamas) and Gulf Stream which included optimizing stations for cloud cover and sea conditions. Measurements included: 1) underway IOPs; 2) above water and NIST blue tile radiance with ASD at optimal station locations; and 3) water leaving radiance with a floating Satlantic HyperPro. Goals included testing methods to develop protocols for consistent in situ optical ocean measurements from different instruments, which can be used for satellite calibration and validation. Certain goals selected a set protocol to be used by all parties (USM, NRL, NOAA/STAR, USF, UMB) allowing for consistent in situ optical ocean measurements from different (ASD, Spectral Evolution, GER, etc.) instruments used for satellite calibration and validation. By using the similar collection techniques and protocols, the observed differences between instruments were examined to investigate the causes of these differences. These measurements and the methods used for collection and data processing are documented below.

1) Inherent Optical Properties collected using underway flow-through system

IOPs were measured continuously on the cruise using two WetLabs hyperspectral *a* and *c* instruments (ac-s) connected to the ship's flow-through system. One ac-s measured the non-filtered water and the other measured filtered water (e.g., to determine CDOM). These measurements address cruise objectives to:

a. characterize the spatial variability of water's optical properties along the cruise track and how the variability impacts the uncertainty of in situ measurements at each station, which were used for VIIRS calibration and validation,
b. determine the water total and dissolved absorption (a_t, a_g) properties at specific wavelengths and validate the IOP measurements derived from the VIIRS ocean color satellite and determine the optical water mass characteristics using $b(\lambda)$ and $a(\lambda)$ to identify response of ocean color,
c. define Gulf Stream and frontal boundaries (coastal and Gulf Stream) using optical properties. The collected IOP data sets will be used to: 1) validate VIIRS ocean color products and 2) define ocean processes and define water masses.

The hyperspectral ac-s instruments measured $c(\lambda)$ and $a(\lambda)$. across the complete spectrum from 400 nm to 800 nm. The $b(\lambda)$ can be determined from the difference, i.e., $b = c - a$. [*Zaneveld et al.*, 1994; *Leymarie et al.*, 2010].

The IOP instruments were interfaced with the ship's flow-through system which pumped water from a water depth of ~3 m. Concurrent flow-through measurements of position, temperature, and salinity will be used for calibration of the ac-9 and ac-s systems. This is important to correctly address the scattering correction that must be applied [*Zaneveld et al.*, 1994; *WETLabs*, 2011].

The WetLabs ac protocols for data collection and processing were used and are considered standard throughout the ocean community. The non-filtered ac-s was used to measure the "total" IOPs, which includes both the particulate and the dissolved properties of the waters sampled. The filtered ac-s used water passed through a Cole Palmer 0.2 µm pore size filter to remove the particles so that the IOPs from the dissolved fraction were determined. The filtered ac-s is used to determine the $a(\lambda)$ and $b(\lambda)$ associated with CDOM (i.e., gelbstoff). The difference between the unfiltered and filtered instruments provides the $a(\lambda)$ and $b(\lambda)$ directly associated with particles [*Twardowski et al.*, 1999; *Twardowski and Donaghay*, 2001]:

$$a_p(\lambda) = a_g(\lambda)(filtered) - a_{pg}(\lambda)(non-filtered) \qquad (7)$$

where absorption constituents from particles (a_p) can be determined from the difference of total absorption (a_{pg}; non-filtered) and absorption of gelbstoff (a_g; filtered).

Figure 20. IOP setup shows water bath setup using the two ac-s instruments, which were located inside the PVC containers immersed in a temperature regulated water bath.

To ensure stability and reliability, both ac-s instruments were placed in a temperature regulated water bath to dissipate the instruments' heat and maintain a constant temperature (Fig. 20). This is critical because temperature instabilities impact the scattering and absorption measurements. The instruments had warm up time at the set temperature to allow them to stabilize and measure consistently. This was confirmed in the calibration results yielding consistent values.

The ac-s instruments were interfaced with a WET Labs DH4 data logger with additional inputs from the backscattering sensor (b_b(550) contributed by the NASA/GSFC group and also the ship's flow-through system. The ship's flow-through data inputs included position, time, date, heading, water temperature, salinity, and fluorescence. These inputs were required for the standard protocol corrections during the post processing of the ac-s data.

The DH4 host software was used to combine and store these data inputs and provided a display capability in real-time using the WetView software application. The $a(\lambda)$, $b(\lambda)$ and $c_t(\lambda)$ were displayed in real time to evaluate the ac-s and b_b data and to ensure the systems were operating correctly and producing reliable and consistent data. The data sample rate of the ac-s's was 6 Hz for the duration of the cruise. This equates to a spatial resolution of ~10 m at ship velocity of 5 knots. Data files from the DH4 were saved hourly for the entire cruise.

The ac-s instruments were calibrated 3 times: once prior to the cruise and twice during the cruise. Calibration of the ac meters included running nano-pure water through the systems using a gravity feed after the instruments were allowed to stabilize for some time period (~5 min to 10 min). The calibration procedure included obtaining the clear water calibration before and after cleaning the absorption and scattering tubes. An update to instrument device files was applied in real-time if it was deemed that new corrections were necessary to assure good quality measurements.

Post processing of the non-filtered ac-s data followed the "WET Labs, 2011" protocols. The filtered ac-s data were processed using a scattering correction [*Zaneveld et al.*, 1994], removal of a_g and addition of

the pure water absorption (a_w) [*Pope and Fry*, 1997]. Additionally, the a_w corrections for temperature and salinity were applied using the ship's flow-through data following [*Pegau et al.*, 1997; *Sullivan et al.*, 2006]. This is required to account for the large changes between coastal and open ocean waters.

The standard order of our post processing steps is the following:

- Apply temperature and salinity corrections to in situ ac data for *a* and *c* using the coincident ship flow-through data;
- Apply temperature correction to a_w and *c* calibration data;
- Subtract the pure water calibration data from the in situ data;
- Using a standard deviation filter, remove the spikes in the data due to bubbles, etc., and then interpolate;
- If the filtered ac-s meter (CDOM) exists, compute $a_p = a_t - a_g$;
- Apply the scatter correction [*Zaneveld et al.*, 1994] to a_p;
- If the filtered ac-s meter (CDOM) exists, add scatter corrected a_p back to a_g to yield $a_{t\text{-}w}$;
- Add spectral pure water absorption coefficients [*Pope and Fry*, 1997] to $a_{t\text{-}w}$ to yield a_t;
- Compute spectral scattering $b = c_t - a_t$;
- Compute spectral omega = b/c.

The ac-s flow-through data will be used to identify the spatial coherence of the IOPs and to identify water mass changes while on stations and underway. These data will be merged with the ship flow-through data using the WET Labs Archive Processing software to combine datasets. This merged dataset will be used to characterize the spatial variability of water optical properties. The flow-through data will also be used to determine the variability of the IOPs with respect to the changing water masses due to advection and ship displacement observed at each of the 27 stations. Continuous monitoring of the IOPs while on stations from start to end can account for the changing water masses during shipboard data collection due to ship drift. This can be significant especially during stations at frontal boundaries with high variability. We will examine how the IOPs changed throughout the duration of the stations to help define how the IOP variability contributes to the uncertainty in the L_w measurements from the HyperPro and the ASD, and also allow for better match-ups between radiometric, IOP and satellite measurements.

The flow-through system will provide an extensive data set demonstrating the large variety of the water masses and ocean processes that were identified on the cruise track. The flow-through IOP products of $a_t(\lambda)$ and $c(\lambda)$ for the spectral VIIRS channels will be used to validate the VIIRS IOP products derived using the QAA. Match-ups between ship collected and VIIRS derived IOPs will provide validation and uncertainty in different water masses including: 1) coastal US waters, 2) Tongue of the Ocean in the Bahamas, 3) Gulf Stream, 4) Gulf Stream shingles, 5) offshore oligotrophic waters and 6) frontal waters.

Additionally, the high spatial resolution of the flow-through system can be used to validate the spatial variability within the VIIRS 750 m pixel by defining the mean and variability of the IOP measurements within the VIIRS pixel.

2) Above water radiometry - ASD Measurements

The Above Water Group (AWG) collected data jointly at 20 stations. Measurements were made concurrently using 8 above-water radiometers: 5 ASDs (USM, NRL, NOAA/STAR, USF and CCNY), 1 GER (CCNY) and 2 Spectral Evolutions (OSU, UMB). At each station the AWG met on the 01 deck and made coincident measurements of the water reflectance using a gray plaque (NRL) and similar procedures, which were documented.

The AWG also collected measurements at the 02 deck and the stern at some stations. The collection of data at different deck heights (i.e., distance above the water affects the water spot size) and FOVs (1°, 7°, 8° and 10°) was to examine how these variables affected the values of the R_{rs} retrieved (Fig. 21). On the *Nancy Foster*, the stern is 1.5 m, 01 deck is 5 m and the 02 deck is 8 m above the water surface. A protocol for determining which deck of the ship to collect above the water measurements has yet to be established. Preliminary results showed some differences in the R_{rs} at different spot sizes and with different instruments during different solar azimuth angles.

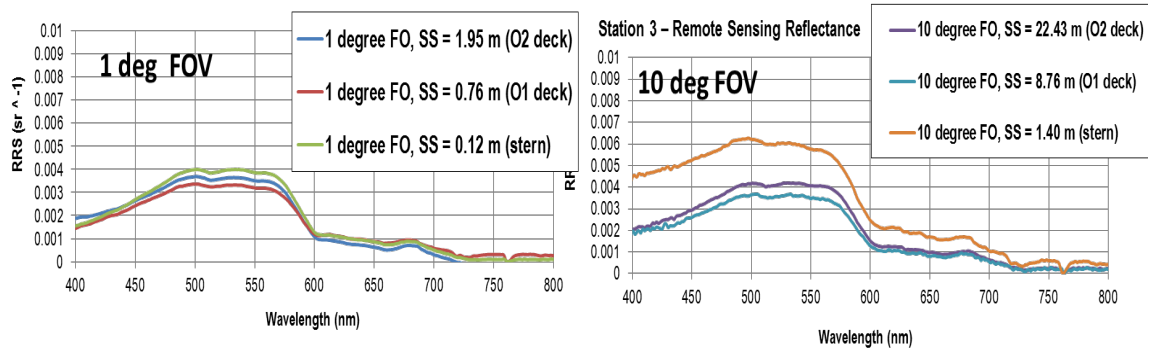

Figure 21. R_{rs} from one handheld instrument at 3 distances above the water for (left) 1° FOV and (right) 10° FOV. SS is spot size.

These instruments enable the derivation of above-water R_{rs} using un-calibrated spectroradiometers in radiance mode and a diffuse reflectance standard (gray plaque). The reflectance plaque is a 10% gray plaque with a known bi-directional reflectance function (BRDF), and is assumed to be a semi-Lambertian surface.

For all stations the AWG used the NRL gray reference plaque. In a few cases when sky conditions were clear, the AWG used their own individual plaques to compare to the standard protocol to look at uncertainty in processing. This was done using same protocol in reference to collection angles and location on ship. In addition to these, the AWG collected several stations using the blue tile with the same protocols (shooting the sky and blue tile only) to help define inter-sensor uncertainties.

The processing of the above water data was performed by NRL for stations collected using the NRL gray plaque with same protocols to look at inter-sensor uncertainty. Processing was done by each of the groups for stations in which each group used their own gray plaque to look at not only the inter-sensor uncertainty but also the uncertainty in each groups processing techniques.

Figure 22. Ryan Vandermeulen and Robert Arnone (USM) aboard the NOAA Ship *Nancy Foster*, taking above-water radiometric measurements of a gray plaque using an ASD.

The field collection protocols are described as follows.
Using a fore-optic attachment, five consecutive radiometric spectrum (S) measurements were taken of each of the following targets: Gray plaque (S_g), water (S_{sfc}), and sky (S_{sky}). Prior to measuring each individual target, the ASD instrument was manually re-optimized (i.e., integration time of the sensor was changed based on relative brightness of the target and new dark counts were taken to correct for instrument offset). Integration times ranged from 68 ms to 4352 ms. Most measurements were taken from the stern of the ship. The exact location of sampling (port vs. starboard) was dependent on the orientation of the ship relative to the sun to eliminate shadowing from the vessel. The optical sensor zenith angles for the water (θ_{sfc}), gray plaque (θ_g), and sky (θ_{sky}) measurements were 135°, 135° and 45°, respectively. The relative azimuth angle of the sensor to the sun ($\Delta\phi$) was > 90°, but may have been adjusted up to 135° depending on sea foam resulting from the ship's wash. The gray plaque has a known BRDF and is used to normalize the un-calibrated radiance measurements for E_s. Figure 22 demonstrates data collection with handheld instrument.

The processing protocols for deriving R_{rs} from above water radiometry follow method 2 of Chapter 3 of Mueller et al. [2003]. Reflectance, the sensor response signal, S, is obtained from averaging n readings (in this case n=5) from each target and normalized to the same integration time (1 s).

$$S = \frac{\int_{i=0}^{n} CI_{N/I_i}}{n} \qquad (8)$$

Here, C represents the dark-corrected output values from the instrument, I_i is the integration time used for that reading, I_N is the normalized integration time (standard N = 1sec), and n is the number of readings (3, 5, or 9 in practice depending on instrument protocol).

Following chapter 2 of the Optics Protocols [*Mueller et al.*, 2003], one can express the water-leaving radiance, L_w, and incident spectral irradiance, E_S, in terms:

$$L_w = F_L\left[S_{sfc} - \rho S_{sky}\right], E_S = \frac{\pi F_L S_g}{R_g} \qquad (9)$$

where, F_L is the unknown instrument radiance response calibration factor (which will cancel when finding R_{rs}) and R_g is the gray plaque's bi-directional reflectance function. The R_{rs} can be computed from the un-calibrated data using the following equation (correcting sky using Fresnel reflectance ρ of 0.021):

$$R_{rs}(\lambda) = \left(\frac{S_{sfc}(\lambda) - \rho S_{sky}(\lambda)}{\pi S_g(\lambda)}\right) R_g(\lambda) \qquad (10)$$

The computed R_{rs} should be "black" at about 750 nm. If the result is not zero, then it is assumed that the reflected skylight term (S_{sky}) was not estimated correctly. Following the "quick and easy" algorithm of Carder and Steward [1985], it is further assumed that any error in the skylight reflection term is white (not wavelength dependent) and one may simply subtract the computed $R_{rs}(750)$ from the entire spectrum. In practice, this may lead to negative reflectance values R_{rs} near 750 nm. Therefore, the processing subtracts the smallest R_{rs} in the range from 700 nm to 825 nm.

$$R_{rs}(\lambda) = R_{rs}(\lambda) - MIN\left(R_{rs}(700\ to\ 825)\right) \qquad (11)$$

To compare the in situ reflectance with satellite-derived reflectance, the mean reflectance is computed using the relative spectral response tables for each band of the satellite (VIIRS) data.

The Stennis team collected ASD spectroradiometer data at all 20 stations. These data were processed using NRL processing.

NIST Blue Tile: AWG- Above Water Group

To assess the differences among instruments at determining R_{rs}, the relative reflectance of the NIST blue tile was measured by the four ASDs, the GER and the Spectral Evolution identified above. The groups all used the same protocols (number of files collected, number of dark currents, angles, etc.) described above to measure the relative reflectance of the target, using the tile in place of the surface measurement. Blue tile comparisons were performed at four different times during the cruise under varying cloud cover conditions (0% to 40%). The blue tile measurements for the different instruments used the same gray plaque (NRL) and were processed using the NRL processing. Preliminary results suggest that sensor variability of the blue tile measurements vary with solar azimuth (Fig. 23).

Slightly modified equations were used to derive the relative reflectance of the blue tile (R_{tile}). For the blue tile measurements, the derived reflectance is simply expressed as the ratio of the radiance (or net signal) for the test target (S_{tile}) to the standard gray target:

$$R_{tile}(\lambda) = R_g(\lambda)\frac{S_{tile}(\lambda)}{S_{ref}(\lambda)}. \qquad (12)$$

There were up to seven sensors collecting data at each station from seven participating institutions (USM and NRL of the Stennis group, USF, CCNY and NOAA/STAR, OSU, UMB).

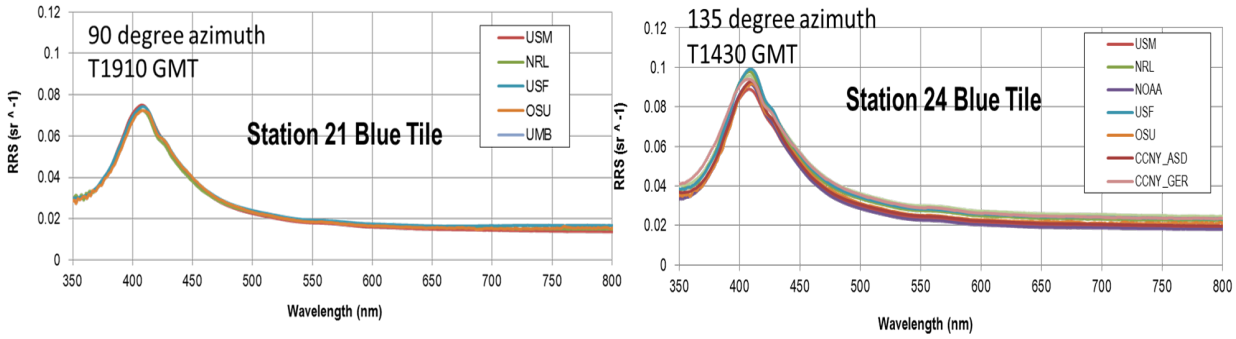

Figure 23. Blue tile R_{rs} calibration above water for Station 21 (right) and Station 24 (left). Note that all instruments agree very well and that each group used same protocols while collecting.

In addition to in situ collections, a blue tile laboratory experiment was attempted while at sea on the *Foster*. The objective was to evaluate the seven sensors capability to measure the blue tile using a constant LED light source with all sensors directed at the exact same look angle. Results of the lab study indicated that the light source did not have sufficient blue light levels, so the experiment did not work.

3) Floating HyperPro measurements

The Floating HyperPro is a hyperspectral profiling radiometer that simultaneously measures above-water E_d and in-water L_u on a fixed floating platform and downwelling E_s on the ship to determine R_{rs} and the nL_w for validation of the VIIRS nL_w. The Stennis team had 2 floating HyperPro's (USM and NRL) on the cruise and collected measurements at 21 stations. The spectral range of both E_s and L_u sensors is from 350 nm to 800 nm with 10 nm FWHM ± 0.3 nm resolution. These instruments were used with a molded floatation collar, enabling in-water surface measurements to be taken over time just below the sea surface. The downwelling E_d sensor uses a cosine collector and is approximately 30 cm above the water surface. The L_u sensor is mounted approximately 30 cm below the water surface. The E_s sensor was an cosine collector mounted on the 01 deck with the other HyperProSASs and was used for the downwelling computation of R_{rs} to omit the uncertainty in the E_d (on the floating instrument) due to tilting caused from sea state and tension on the line.

The USM HyperPro was calibrated by NOAA/STAR in October 2015. The NRL HyperPro was calibrated by NOAA/STAR in December 2015. The resulting instrument responsivities were similar to the Satlantic responsivities and no change was applied to the calibration coefficients.

The Floating HyperPro, equipped with a flotation collar, was deployed over the stern of the vessel (Fig. 24). The tether was let out a sufficient distance from the boat (20 m to 30 m), allowing the instrument to float away from the boat. This ensured there was no contamination from vessel-generated bubbles and ship shadowing or any other potential disturbances. Once the instrument was a sufficient distance from the vessel, data was recorded for 20 min to 30 min. Post processing of this dataset was done using Satlantic's Prosoft v8.1.1. During post-processing, the data are averaged over the deployment interval and a tilt greater than 2° was omitted.

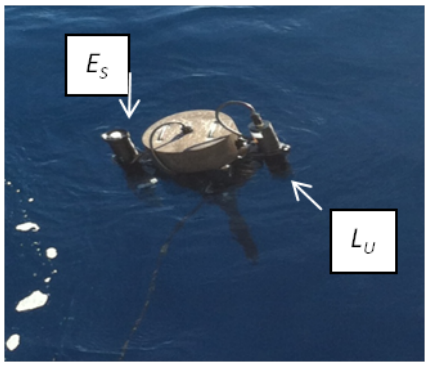

Figure 24. Deployment of the floating HyperPro Package

The processing protocols for deriving R_{rs} from in water radiometry follow Chapter 2 of Mueller et al. [2003]. L_w is computed as for Eq. 9 above, but where $\rho = 0.025$ is the Fresnel reflectance of the air sea interface, and $n = 1.34$ is the refractive index of seawater. R_{rs} is computed as for Eq. 10 above.

Floating HyperPro data were collected at 20 stations. A preliminary analysis revealed that nine stations had limited or absent cloud cover where a direct comparison with VIIRS-retrieved R_{rs} is possible. The HyperPro data were processed using Satlantic Prosoft v8.1 with set protocols within the software to level 4. Data filtering over the time period of collection removed data spikes when the sensor had tilting greater that 2°. These protocols for processing the floating HyperPro for deriving nL_w and R_{rs} are being tested and evaluated using different methods with Prosoft and comparison with the profiling HyperPro data and ASD.

7.7 OSU – Nicholas Tufillaro, Jasmine Nahorniak, and Curtiss O. Davis

The OSU section includes sub-sections describing instruments, deployment protocols, processing protocols and data information, including data description, example data and data access. Additional information can be found by following OSU hyperlinks provided as referenced within the sub-sections.

Instruments:
OSU operated a Satlantic Free Falling Optical Profiler II (i.e., HyperPro; http://satlantic.com/profiler) for in water radiance measurements, as well as a handheld Spectral Evolution Field Spectrometer, PSR-1100-F (http://www.spectralevolution.com/lightweight_portable_battery_operated_spectrometer.html) for above water radiance and reflectivity measurements (Fig. 25). The Optical Profiler is also equipped with a Wetlabs ECO-Puck with scattering at 470 nm and 700 nm, and chlorophyll fluorescence at 470 nm and 695 nm (http://wetlabs.com/eco-puck).

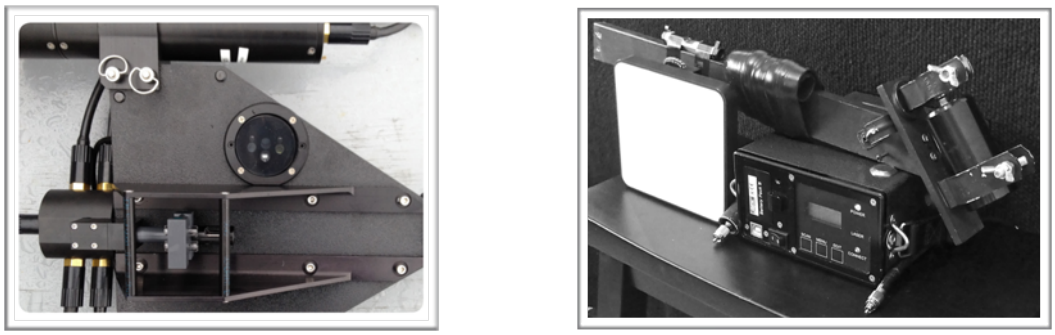

Figure 25. (Left) Satlantic Free Falling Optical Profiler II (aka 'HyperPro') with Wetlabs ECO-Puck Triple (Right) Spectral Evolution PSR-1000-F Field Spectrometer with 8° FOV fore optics, white reference card, and mount.

Protocols: Deployment

The HyperPro was deployed off the stern of the NOAA Ship *Nancy Foster* in a coordinated fashion with three other profiling radiometers (NOAA/STAR, USF and NASA/GSFC). Typical deployments were timed to be coincident with VIIRS overpasses and used the multicast 'yoyo' protocol with three sets of five repetitions each (up and down the water column five times), if sky conditions permitted. The deployments were supervised by Mike Ondrusek (NOAA/STAR). For reference, the normal OSU HyperPro deployment protocols can be found here: http://meris.coas.oregonstate.edu/tmp/OSU_NOAA_CRUISE_REPORT_2015_12/OSU_2_REPORT_APPENDIX_A_HyperProDeploymentProtocols_PDF.pdf.

The OSU Spectral Evolution Field spectrometer above water radiometry measurements protocols are documented here: http://meris.coas.oregonstate.edu/tmp/OSU_NOAA_CRUISE_REPORT_2015_12/OSU_3_REPORT_APPENDIX_B_Methods%20for%20measuring%20Rrs_2016-02-16_90%20deg8FOV_WORD.doc. Briefly, an 8° FOV fore optic is connected by a 1 m fiber optic cable to the spectrometer, and the fore optic is extended from the side of the ship with a level stick, which is held horizontally with the probe pointing down at a 40° angle from nadir for the Spectralon plaque and water measurements and then rotated 180° on its long axis so that the probe is pointing 140° from nadir for the sky measurement. Measurements were made 3 m to 5 m above the sea surface (depending on the deck) and 0.1 m to 0.15 m above the plaque. Each recorded measurement is an average of 10 consecutive measurements (performed internally by the instrument), and then ten measurements each were collected for the reference card, the water, and the sky for a total of 30 measurements. Additionally, measurements were coordinated for comparison with handheld spectrometers (e.g., ASD) deployed by other teams on the cruise and with additional calibration sources (lamp) and reference cards (NRL gray plaque, NIST blue tile).

Protocols: Processing

The HyperPro processing uses Satlantic's ProSoft program to produce nL_w and R_{rs}, as well as additional products. Details for the OSU ProSoft settings used and quality control procedures are found in "OMEL HyperPro Processing Instructions" here: http://meris.coas.oregonstate.edu/tmp/OSU_NOAA_CRUISE_REPORT_2015_12/OSU_4_REPORT_APPENDIX_C_HyperPro_Processing_Instructions_v8.1.3_20150831_PDF.pdf.

The SE PSR-1100-F Spectroradiometer measures light at 1.5 nm sampling and 3.2 nm spectral resolution over the 320 nm to 1100 nm spectral range. However, due to the difficulty in calibrating the 99% Spectralon plaque below 360 nm and the low signal-to-noise ratio received from the water above 850 nm, we generally only output spectra in the 360 nm to 850 nm range. R_{rs} is estimated from the above-water data using the formula:

$$R_{rs} = (S_{w+s} - S_{sky})\, m))/(\, \pi\, S_p/\, refl) \qquad (13)$$

where S_{w+s} is the measured signal from the water and includes both L_w and R_{sky}. S_{sky} is the measured signal from the sky, S_p is the average measured signal from the white Spectralon Plaque, and *refl* is the reflectivity of the plaque (approximately 99%; actual measured spectral values used in the calculation). The factor π converts the reflected radiance values to irradiance for this Lambertian diffuser. The measured sky radiance is multiplied by *m* which is the proportionality factor that relates the radiance measured when the detector views the sky to the reflected sky radiance measured when the detector views the sea surface. The value of *m* is dependent on wind speed and direction, detector FOV and sky radiance distribution. Only in the case of a level sea surface and a uniform sky radiance distribution does *m* equal the average of the Fresnel reflectance over the detector FOV. For our measurement angles under nominal sky and wind conditions, we calculated *m* using data from Mobley [2015]. Note that these values are always significantly higher than the value 0.023 used for conditions of complete overcast. Finally, the Spectral Evolution data have an offset in the red that biases the nL_w low, therefore, as the last step of the computation the minimum value of the radiance in the red (601 nm to 850 nm) was subtracted to correct for this bias.

Data Description

OSU Cruise data and images can be accessed via FTP protocol from http://meris.coas.oregonstate.edu/tmp/chs/data/NOAA_VIIRS_Cruise_2015_12/. The OSU log file http://meris.coas.oregonstate.edu/tmp/OSU_NOAA_CRUISE_REPORT_2015_12/OSU_5_REPORT_APPENDIX_D_OSU_CRUISE_LOG_TXT.txt should be compared against the official station log produced by Bob Arnone, http://meris.coas.oregonstate.edu/tmp/OSU_NOAA_CRUISE_REPORT_2015_12/OSU_6_REPORT_APPENDIX_E_COPY_OF_OFFICIAL_CRUISE_LOG_NF_2015_1_XLXS.xlsx. Station information is also shown in Tables A1-A5, Appendix A. Station 1 was on Wednesday, 2 December 2015 and the last station, Station 27 was on Sunday, 13 December 2015. In addition to HyperPro casts and Spectral Evolution data collections, a lamp test of the above water radiometers was conducted in the ship's lab on Monday, 7 December 2015 using both the NIST blue tile and the NRL gray plaque. At several stations, the radiometers were also compared on the side or stern of ship with coordinated measurements using, again, the NIST blue tile and the NRL gray plaque. Specific match-ups with VIIRS are shown in bold rows in Table 4.

Table 4. Match-ups between OSU HyperPro data and VIIRS NOAA Star MSL12 products. Day is day of year; Lat is latitude in decimal degrees N; Lon is longitude in decimal degrees E, Time_Diff is time difference in minutes between satellite and in situ observations.

Day	Sta	Time	Lat	Lon	~Time_Diff	Match
339	V	1848				
	6	**1800**	**24.42319**	**-77.32309**	**-50**	**x**
	7	2100	24.38379	-77.28607	130	
340	V	1829				
	8	**1830**	**23.66923**	**-76.58686**	**1**	**x**
	9	2030	23.67043	-76.59076	120	
341						
342	V	1754				
	12	**1930**	**28.72759**	**-80.43781**	**95**	**x**
343	V	1916				
	13	1440	30.72109	-80.53379	-275	
	14	1800	30.92241	-80.60434	-75	
	15	**1930**	**30.98747**	**-80.53848**	**15**	**x**
344	V	1857				
	16	1440	31.15840	-77.675208	-260	
	17	1745	31.16818	-77.734846	-95	
	18	**1920**	**31.07281**	**-77.53271**	**20**	**x**
345	V	1838				
	19	1345	32.22296		-260	
	20	1630	32.49639	-77.854955	-125	
	21	**1900**	**32.63534**	**-77.424925**	**20**	**x**
	22	2100			200	
346	V	1819				
	23	1420	33.10018	-78.247406	-220	
	24	**1730**	**33.24041**	**-78.006083**	**-45**	**x**
	25	1945	33.07888	-78.211748	85	
347	V	1800				
	26	1516	32.16127	-79.316675	-165	
	27	**1820**	**32.19267**	**-79.093385**	**20**	**x**

VIIRS NOAA STAR MSL12
ftp://ftp.star.nesdis.noaa.gov/pub/socd/mecb/color/VIIRS_for_Mike/req_20160107/

Example Data

VIIRS spectra for match-ups are computed from 5 x 5 pixel averages starting with NOAA STAR Science Quality MSL12 data. Station 12 shows the best match is Tuesday, 8 December 2015 at ~ 19:30 UTC (Fig. 26). The inset on the upper right shows the pixels surrounding the sample site. Gray pixels indicate a failed retrieval, typically because of either clouds or atmospheric correction failures. Station 15 shows a poor fit in the red end of the spectrum, but the number of gray pixels also suggests that the retrieval is poor (Fig. 27, left). However Station 18 shows good conditions for retrievals, but the VIIRS spectrum still undershoots the in situ OSU HyperPro spectra (Fig. 27, right).

The sea and sky conditions for Station 12 are shown in Fig. 28. These images are routinely taken as part of the Spectral Evolution data collection. Fig. 29 shows a comparison of the spectra between VIIRS, the OSU HyperPro and the above water Spectral Evolution measurements.

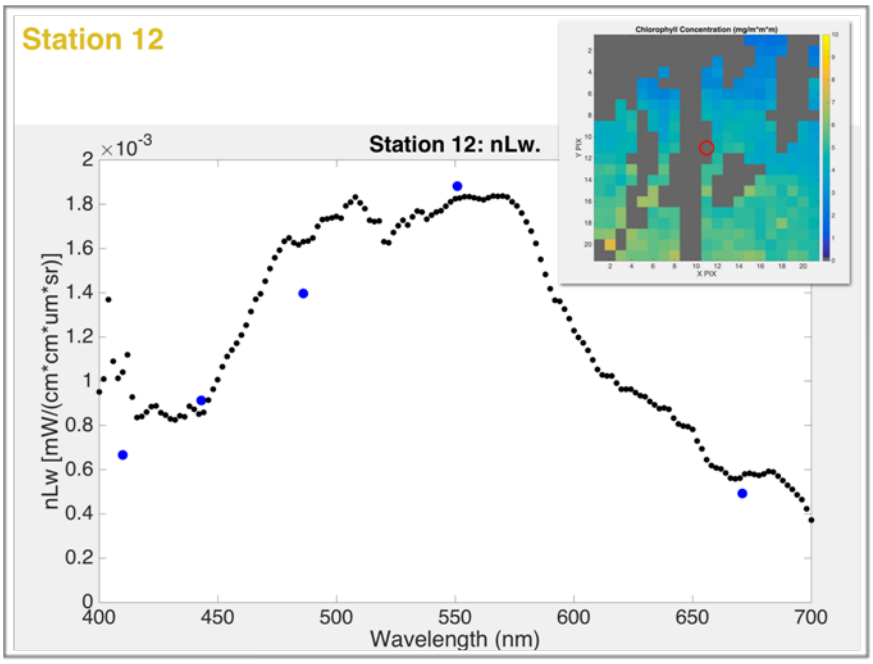

Figure 26. Station 12: $nL_w(\lambda)$. Black: OSU HyperPro. Blue: VIIRS NOAA MSL12. Inset (upper right) shows individual VIIRS pixels. VIIRS spectrum is computed from a 5 x 5 average and inset provides an indication number and quality of pixels used for spectral average.

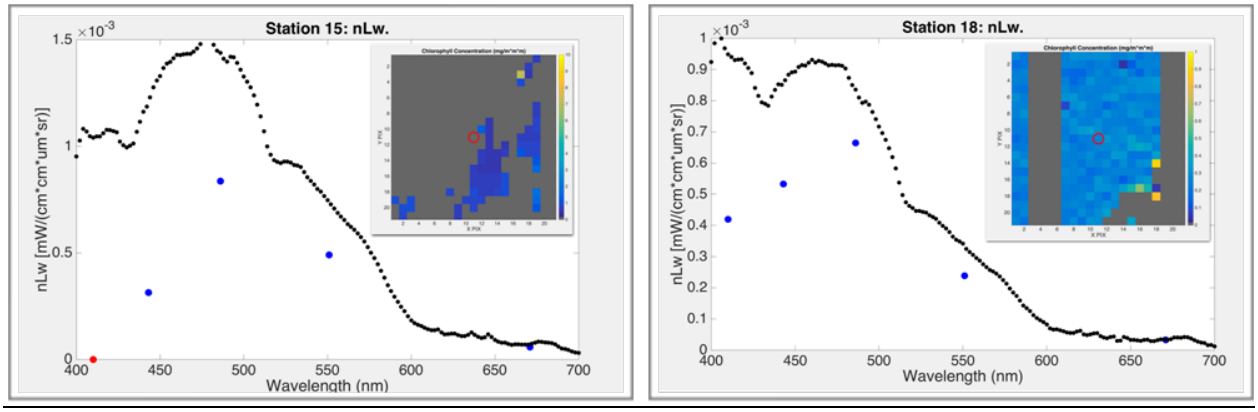

Figure 27. Station 15 (left) and Station 18 (right) $nL_w(\lambda)$. Black: OSU HyperPro; Blue: VIIRS NOAA STAR MSL12. The inset shows pixels surrounding sample site. Gray pixels are invalid retrievals and provide an indication of spectral quality.

Figure 28. Images of 'sea', 'shore', and 'sky' at Station 12, 2015-12-08 at ~ 14:30 EST.

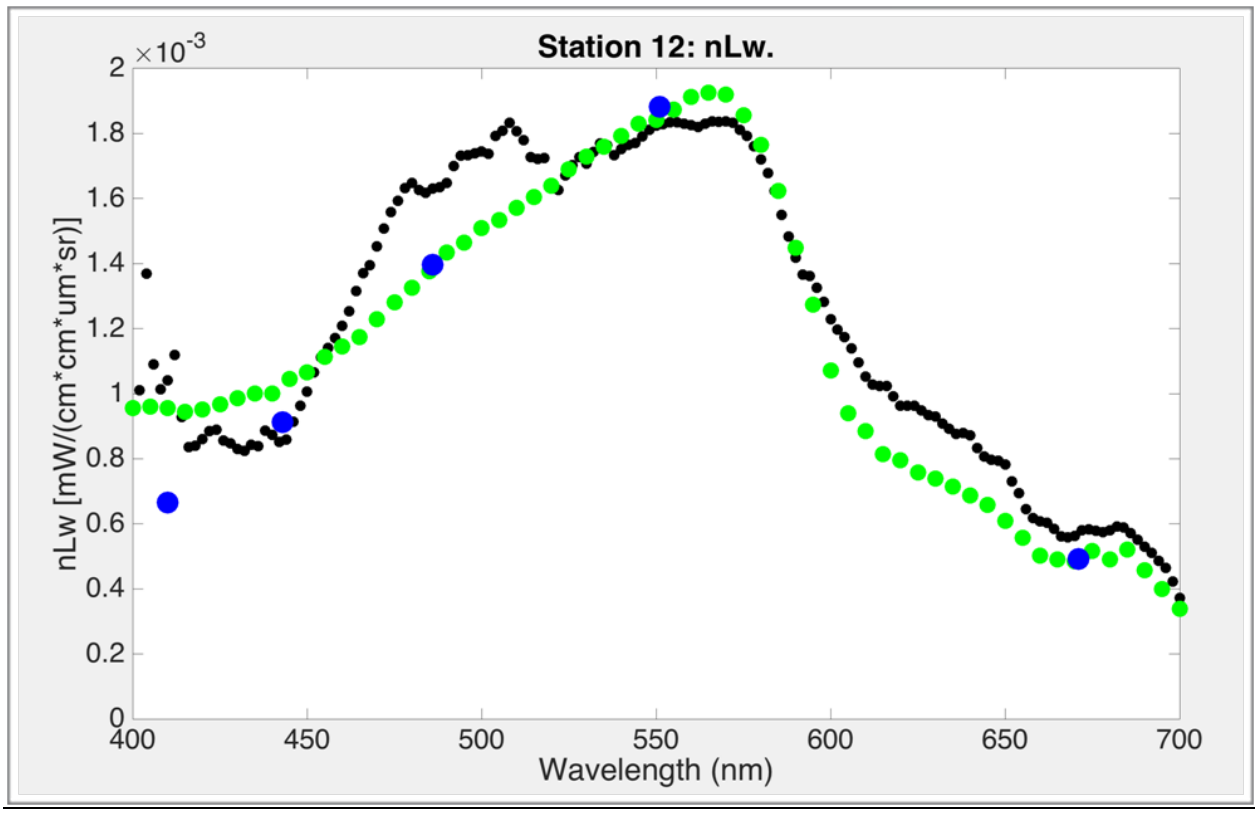

Figure 29. Station 12 spectral comparison. Blue: VIIRS NOAA STAR MSL12, Black: OSU HyperPro in water spectrometer. Green: OSU Spectral Evolution above water spectrometer.

Data Access

Details on navigating and reading the HyperPro data can be found in: http://meris.coas.oregonstate.edu/tmp/OSU_NOAA_CRUISE_REPORT_2015_12/OSU_4_REPORT_APPENDIX_C_HyperPro_Processing_Instructions_v8.1.3_20150831_PDF.pdf: . An example of the information provided is shown in Table 5. A compressed file with all the data from L1 to L4 is available by FTP from OSU for the cruise Stations 01 through 27.

The Spectral Evolution above water radiometry data is available as collection of Excel worksheets showing the estimation of R_{rs} starting from the above water radiance measurements. The spreadsheet contains target data with the OSU white card. In addition, the data was acquired for both the NRL gray

plaque and the NIST blue tile, usually as a part of comparisons of all the above water spectrometers. Table 6 shows dates and data file information for blue tile and gray plaque measurements:

Table 5. Example of data table showing where and how to navigate L4 HyperPro data.

Where can I find …	if I collected ….?	Location
Lw, Lwn	yoyo	SurfaceUpper/Ascii Files/*_MC_L4.dat subset/*_MC_surface_subset.txt (*subset of wavelengths only*)
bbp(470,z), bbp(700,z), fluor(z)	profile	Profiles/Ascii Files/*_L4.dat subset/*_profile_subset.txt
	yoyo	SurfaceFull/Ascii Files/*_MC_L4.dat
Rrs(0+)	yoyo	This parameter must be derived from the contents of SurfaceUpper/Ascii Files/*_MC_L4.dat using the equation: Rrs = Lw/AVG_ES

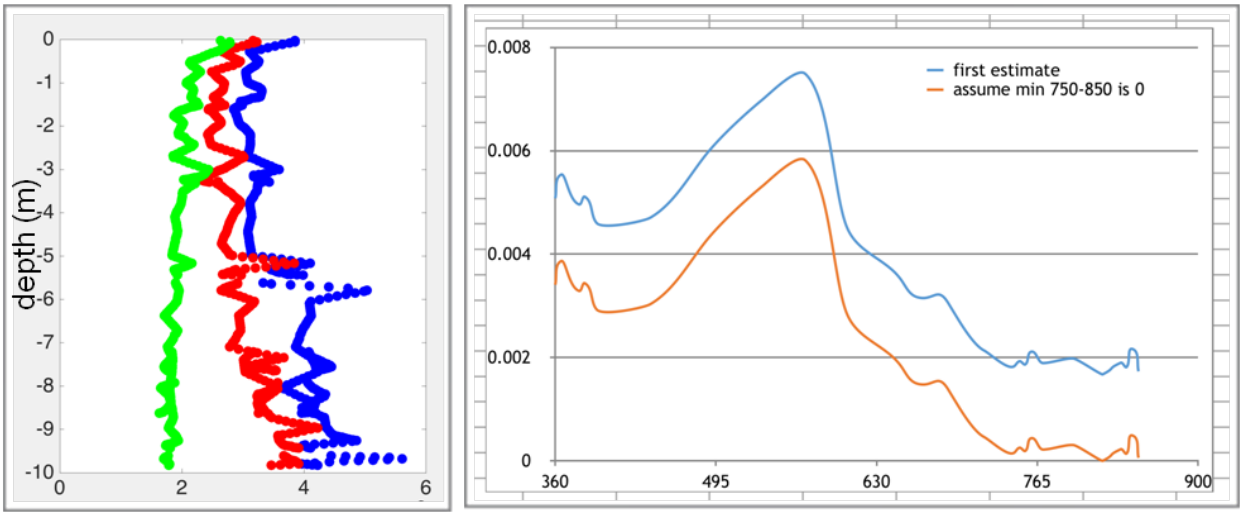

Figure 30. Station 12 (Left) ECO-Puck Sensors: Green: Chlorophyll fluorescence (mg m^{-3}), Blue: Blue backscatter (m^{-1} sr^{-1}), Red: Red backscatter (m^{-1} sr^{-1}). (Right) Estimate of R_{rs} from measurements of above water radiometry showing the computations for Station 12. Horizontal axis is wavelength (nm).

Table 6. Date and data file identifications for measurements of NIST blue tile and NRL gray plaque with the OSU handheld Spectral Evolution radiometer.

Date [yyyy-mm-dd]	Data Files	Comments (Compiled from OSU 'a_log.txt' file.)
NIST Blue Tile		
2015-12-07	06-10	Lab test
2015-12-10	56-65	Station 16, ~14:40 UTC
2015-12-01	136-140	Station 21, ~19:00 UTC, Sunny
2015-12-12	91-95	Station 24, ~ 17:50 UTC
NRL Gray plaque		
2015-12-05	61-89	Station 6, ~ 18;00 UTC
2015-12-06	01-16	Station 7, ~ 18:30 UTC, 5 gray, 5 sky, 5 water
2015-12-07	01-05	Lab Test
2015-12-08	31-35	Station 12
2015-12-09	01-05	Station 13, 01 Deck Port Side, ~ 15:15 UTC
2015-12-09	46-50	Station 14, 01 Deck Port Side, ~ 18:00 UTC
2015-12-09	91-95	Station 15, ~ 19:30 UTC
2015-12-10	01-05; 47-55	Station 16, ~ 14:40 UTC
2015-12-10	66-70	Station 17, ~ 17:45 UTC
2015-12-10	111-115	Station 18, ~ 19:20 UTC
2015-12-11	01-05	Station 19, ~ 13:45 UTC
2015-12-11	76-80	Station 20, ~ 16:30 UTC
2015-12-11	121-125	Station 21, ~ 19:00 UTC
2015-12-12	31-35	Station 23, ~ 14:20 UTC
2015-12-12	76-80	Station 24, ~ 17:50 UTC
2015-12-12	126-130	Station 25, ~ 19:45 UTC
2015-12-13	31-35	Station 26, ~ 15:16 UTC

7.8 LDEO – Joaquim I. Goes, Helga do Rosario Gomes and Kali McKee

Phytoplankton community composition and size structure and nutrients

Discrete Samples:

The LDEO group was not able to send a participant to join the cruise, however, Matteo Ottaviani of the CCNY group collected samples on our behalf. Aliquots of seawater samples were collected at each station. Where the CTD/Rosette cast was conducted, two depths were sampled, one near surface and the other deeper in the mixed layer (ranging from ~12 m to ~35 m) coincident with sampling for other chemical analyses. Occasionally, samples were collected from the ship's underway flow-through system to supplement CTD/Rosette sampling. Samples were collected and preserved according to protocols described below for the following post-cruise laboratory analyses:

i) Microscopic analysis of phytoplankton community composition and sizes;
ii) Counting, imaging and size estimations of phytoplankton and other detrital particles using a Fluid Imaging Technologies, Inc., FlowCam; and
iii) Inorganic nutrients (N, P and Si) by standard colorimetric assays.

i. Microscopy based phytoplankton identification and cell counts

For microscopic identification and enumeration of phytoplankton, samples were collected into 125 mL polyethylene terephthalate (PET) screw top bottles and fixed with 1% alkaline Lugol's iodine, preserved in 1.5% buffered formaldehyde solution and were stored under dark and cool conditions. Microscopic analysis is currently underway and includes overnight settling of 10 mL samples in an Ultermohl counting chamber and then counting the samples using a Nikon® inverted microscope at 200X and 400X magnifications. The smallest cells that can be enumerated by this method are >5 µm in diameter. Phytoplankton identifications are based on standard taxonomic keys [*Tomas*, 1997]. Cryptophytes are being identified by epifluorescence microscopy using their yellow-orange fluorescence signatures [*Booth*, 1993; *MacIssac and Stockner*, 1993; *Goes et al.*, 2014].

ii. FlowCam based phytoplankton identification, cell counts and cell sizes

In addition to the microscopic analysis of phytoplankton, two 25 mL aliquots of the preserved samples are being analyzed for phytoplankton community composition and size structure analysis using a FlowCam particle imaging system equipped with a 4X objective (UPlan FLN, Olympus®) and a 300 µm Field-of-View flow cell. Field-of-View flow cells ensure that the liquid passing through the flow cell is entirely encompassed within the camera's FOV. Phytoplankton cells within the preserved samples will be counted and imaged in auto-image mode with a peristaltic pump rate of approximately 0.32 mL min^{-1} to 0.44 mL min^{-1} as specified by the manufacturer. Cells will be classified to the genus-level using the Visual Spreadsheet program (v. 2.2.2, Fluid Imaging). The instrument provides the total number of particles imaged, together with the dimensions of each particle allowing estimations of phytoplankton community structure, particle size distribution of both phytoplankton and of detrital particles [*Jenkins et al.*, 2016].

iii. Inorganic nutrients (N, P and Si)

For nutrient analyses, 30 mL of seawater (from the CTD/Rosette discussed earlier and also shown in Table A3, Appendix A) were syringe-filtered with 0.22 µm pore size filters into new 50 mL Falcon centrifuge tubes and frozen at -80°C for later analyses back at the LDEO laboratory. Samples will be analyzed for inorganic nitrate, nitrite, phosphate, and silicate using a continuous segmented flow injection analyzer (Seal Analytical AA3 AutoAnalyzer) using protocols outlined in Knap et al. [1994].

7.9 NASA/GSFC – Scott Freeman, Joaquin Chaves and Antonio Mannino

The overarching goal of the NASA Goddard Field Support Group is ensuring and expanding the ability of the research community to generate complete sets of in situ optical and biogeochemical data for inclusion in Earth science climate data records and other supporting data records used for ocean color satellite vicarious calibration, data product validation, and bio-optical algorithm development. For all biogeochemical parameters described below, water from two hydrographic depths (mid depth and surface) from each CTD rosette cast was transferred from the Niskin bottles to 10 L carboys. The carboys were covered with black plastic bags to prevent high light exposure. HPLC pigments are used to characterize the phytoplankton community at each station and will be compared to the IFC and FlowCam data. Additionally, collection of organic carbon (POC, CDOM, DOC) provides a greater understanding of regional carbon sequestration and cycling.

Samples for phytoplankton pigments and other biogeochemical parameters were collected from water retrieved using the ship's CTD rosette. The 12-bottle rosette was lowered at each station to complete a hydrographic cast down to 200 m, or to just above the bottom, at shallower stations. During the upcast, six Niskin bottles were triggered at the chlorophyll maximum when this feature was evident on the rosette-mounted fluorometer, or at a depth reasonably within the first optical depth (12 m to 35 m), when it was absent. The remaining six bottles were triggered at the surface. Table 7 summarizes the number of samples collected for each parameter.

Phytoplankton Pigments
Duplicate samples from two depths, near-surface and at the chlorophyll maximum, were collected at each station for the analysis of phytoplankton pigments by HPLC. For each sample replicate a known volume of water was filtered under gentle vacuum (~17 kPa) onto a 25 mm diameter Whatman GF/F filter (nominal pore size ~0.7 μm). Samples were wrapped in aluminum foil, stored in liquid nitrogen and transported to NASA GSFC for analysis.

Spectral Absorption by Chromophoric Dissolved Organic Matter
One sample replicate was collected from each of the two sampled depths at each station for the determination of spectral absorption (a_g) by chromophoric dissolved organic matter (CDOM). Samples were filtered through 47mm diameter Whatman GF/F filter into pre-combusted, 250 mL amber glass bottles, and stored at 8°C. Samples were transported to GSFC for the determination of a_g.

Dissolved Organic Carbon
Two sample replicates were collected from each sampled depth at each station to measure the concentration of dissolved organic carbon (DOC). Samples were filtered through 47 mm diameter Whatman GF/F filter into pre-combusted, 40 mL amber glass vials, and stored frozen at -20°C. Samples were transported to GSFC for the determination of DOC.

Particle Organic Carbon
Two sample replicates were collected from each sampled depth at each station to measure the concentration of particulate organic carbon (POC). Each replicate sample was collected onto a 25 mm diameter Whatman GF/F filter under gentle vacuum (~17 kPa). Samples were wrapped in aluminum foil and stored in liquid nitrogen for transportation to GSFC for analysis.

Table 7. Samples for phytoplankton pigments and other biogeochemical parameters collected by the NASA/GSFC group participating in the 2015 VIIRS validation campaign.

Parameter	Number of sample replicates collected
Phytoplankton pigments	94
CDOM absorption	45
DOC	94
POC	171
Total	404

In-Water Optical Measurements (AOPs, IOPs)
The package to measure inherent optical properties (IOPs) was equipped with two attenuation and absorption spectrometers (ac-s, ac-9; WET Labs, Inc.). The ac-9 was equipped with a 0.2 μm pre-filter to allow the in situ measurement of a_g. The IOP package also included two scattering meters (BB-3, VSF-9; WET Labs, Inc.), and a Sea Bird SBE 49 CTD. The ac-s and ac-9 measure *a* and *c* (and *b* by difference) at 74 and 9 wavelengths, respectively, between 400 nm and 740 nm, while the BB-3 measures b_b at 3 wavelengths and 117°, 124°, and 151°. The VSF-9 measures scattering at 9 angles (62°, 76°, 80°, 90°, 110°, 120°, 140°, 160°, 170°) at 532 nm. A 31 Amp-hour Lithium-ion battery pack (Sartek, Inc.), housed in a Sexton, Inc. housing, was used for powering all instruments, and data was stored in a WET Labs DH-4 data handler. The package performed casts of up to 150 m at 22 of 26 stations during the campaign.

The IOP package was designed such that all instruments sample the same depth. The CTD and ac inlets are at the same level as the faces of the scattering instruments. However, with the flow-through ac-9 and ac-s, there is a delay between the water entering the flow tube and the measurement being made. In addition, water entering the ac-9 must also pass through a 0.2 μm filter. To account for this delay, a lag of 1.5 s is added to the ac-s data stream. Because of the strong correlation of absorption and water temperature at 715 nm, the temperature and a_{715} can be compared to find the appropriate delay. A MATLAB GUI was used to determine the delay.

The ac-9 and ac-s were calibrated twice during the cruise, on 6 December 2015 and 12 December 2015. Water for calibrations was produced onboard using a nano-pure water system. The scattering sensors were calibrated by James Sullivan at WET Labs in Rhode Island 20 October 2015. Dark current measurements were collected on 13 December 2015 with all pumps and instruments turned on.

In-water AOPs, both E_d and L_u, were measured using a Biospherical Instruments C-OPS system. E_s was measured with a matching reference radiometer. The three radiometers have a spectral range from 300 nm to 900 nm, with 19 center wavelengths each as listed below. The upwelling radiance radiometer substitutes a broad natural chlorophyll fluorescence sensor (27 nm FWHM, centered at 683 nm) for the 875 nm sensor. All other wavelengths are 10 nm FWHM. The radiometers feature three gain stages, which provide 9 decades of dynamic range [*Morrow et al.*, 2010].

List of 19 center wavelengths measured by NASA's C-OPS profiling radiometer (nm)

305	320	340	380	395	412	443	465	490	510
532	555	565	625	665	683	710	780	875	n/a

Before each deployment, dark current measurements at each of the three gain stages and a pressure tare were made by capping the sensors and running the dark current procedure through the μProfile software (C-OPS manual). The C-OPS system was deployed at each station, with over 200 profiles in total. Each radiometer was calibrated at NOAA/NESDIS, College Park before and after the cruise. The system was last calibrated at the manufacturer's facility in January 2015.

Above-water AOPs (E_s, L_{sky}, L_t) were measured using a Satlantic HyperSAS system. This system features a solar tracking mechanism, which relies on GPS and ship's compass data to rotate to the desired azimuth angle (90°), within the limits of viewing angle. Due to communications issues, the ship's compass data could not be used, and so the GPS heading data were used. These data are not as accurate because of magnetic influences from the ship's hull.

The radiometers were calibrated at Satlantic's calibration facilities after the cruise in February, 2016, and were also calibrated at NOAA/NESDIS, College Park both before and afterward. The hyperspectral radiometers have a spectral range of 305 nm to 1150 nm, and were calibrated for the full range.

7.10 NIST – B. Carol Johnson

NIST Blue Tile

The NIST blue tile is a reflectance target made from two pieces of 3.8 mm-thick, 16.51 cm square, F65 plate glass. The surface of one of the glass plates was roughened by sand blasting in the NIST Optical Shops to create a diffuse surface. Then the two plates were stacked together, with the diffuse surface on the top, and held in a 30.48 cm-square by 2 cm thick-black plastic mounting cell. The glass plates are mounted in a 7.6 cm-deep square area centered in the black plastic cell and held in place with two set screws that penetrate the mounting cell from one side. This arrangement results in the ground optical surface of the blue tile flush with the top of the black plate (Fig. 31). A wooden storage container with a cutout on the inside of the top lid holds the blue tile and prevents anything touching the optical surface

during storage or shipment. The bottom half of the storage container has two cutouts for ease of removal of the blue tile assembly from the storage container. Alignment indicators, labeled “point to Sun” and “90° azimuth” were placed on the surface of the mounting cell prior to the 2015 *Nancy Foster* cruise (blue tape in Fig. 31).

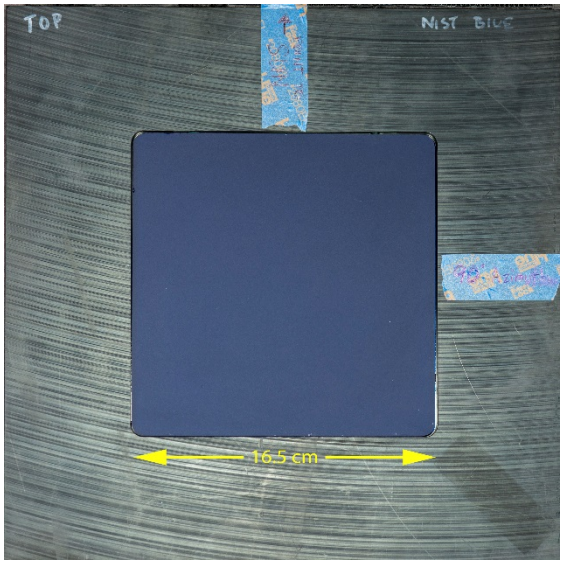

Figure 31. Photograph of the NIST blue tile in its black plastic mounting cell.

As described earlier, a portion of the activities during the December 2015 cruise involved derivation of remote sensing reflectance using in-air, hand-held, radiometers and a white or gray diffuse reflectance standard to establish traceability to the SI. This protocol is described in [*Mobley*, 1999; *Mueller et al.*, 2003; *Mobley*, 2015]. NIST first developed the blue tile in support of the Long Island Workshop that took place from small boat August 4 to 6, 2010 [*Johnson et al.*, 2012]. At that time, the tile was mounted on the top of a black anodized, 30.48 cm by 25.4 cm, aluminum optical breadboard. After remounting in the black plastic cell, it was deployed as an experimental validation standard in November 2014 [*Ondrusek et al.*, 2015] and December 2015, aboard the NOAA ship *Nancy Foster*.

The concept is simple: if the reflectance of the blue target is stable in time, all researchers should derive the same reflectance values for this faux water target when using their white or gray reflectance standard as the reference. With the reflectance scales of the various instruments thus compared to a common reference, the blue tile measurements could then be used to determine the sensitivity to other measurement conditions. Of course, an independent white or gray reflectance target could also be used for this purpose, but having a blue reflectance target for testing increases the parameter space to include the instrument sensitivity to stray light, which is exacerbated by differences between the spectral distribution of the calibration source (sunlight) and the unknown source (sky and water).

If both the reference reflectance standard and the blue tile are Lambertian diffusers, meaning the BRDF is a constant, independent of incident and scatter angles, and, in addition, spatially uniform in BRDF, non-polarizing, and exhibiting no inelastic scattering, *then* the reflected radiance $L_r(\lambda)$ is independent of the illumination conditions $E_i(\lambda)$ and [*Nicodemus et al.*, 1977]

$$L_r(\lambda) = f_{r,d}(\lambda) E_i(\lambda) \qquad (14)$$

Here $f_{r,d}$ is the BRDF, in inverse steradians, for this ideal sample. Note the sample may absorb a portion of the incident flux, that is, it is not lossless. Sequential measurements on the *Nancy Foster* of the reflectance standard and the blue tile using the hand-held, uncalibrated radiance radiometers give

$$f_{r,tile}(\lambda) = \frac{E_i(\lambda, t_{std})}{E_i(\lambda, t_{tile})} \frac{S_{r,tile}(\lambda, t_{tile})}{S_{r,std}(\lambda, t_{std})} f_{r,std}(\lambda) \qquad (15)$$

for the field measurements of the blue tile BRDF. Here S_r are net signals from the radiance radiometer and t_{std} and t_{tile} are the times corresponding to the measurements of the radiance of the white or gray plaque standard and the blue tile.

Following Nicodemus [*Nicodemus et al.*, 1977], BRDF is a function that geometrically characterizes the reflecting properties of a surface. Reflectance is the ratio of reflected spectral flux to the incident spectral flux. Reflectance factor is the ratio of the actual reflected flux to the flux that would be reflected by an ideal diffuse and lossless surface. If the sample is accurately described as having a constant BRDF, then the following holds (note all quantities are dimensionless):

- The bi-directional reflectance, e.g. 0° incident angle, 45° reflected angle, is $\rho_d(0;45;\lambda) = f_{r,d}(\lambda)\Omega_r$ where Ω_r is the projected solid angle subtended by the entrance pupil of the radiometer;
- The corresponding bi-directional reflectance factor is $R(0;45;\lambda) = \pi f_{r,d}(\lambda)$;
- The directional-hemispherical reflectance, e.g. 8° incident angle, collection over the entire hemisphere above the sample, is $\rho(8;\mathrm{h};\lambda) = \pi f_{r,d}(\lambda)$;
- The corresponding directional-hemispherical reflectance factor is $R(8;\mathrm{h};\lambda) = \pi f_{r,d}(\lambda)$.

The white or gray reflectance standards can be procured from companies such as Labsphere, Inc. (North Sutton, NH) or Avian Technologies LLC (New London, NH), who provide reflectance values, typically directional-hemispherical reflectance factors $R(8;\mathrm{h};\lambda)$, to customers for these standards. For the blue tile, preliminary measurements of $R(0;45;\lambda)$ by comparison to a NIST Spectralon (Labsphere white diffuser) standard were done prior to the 2010 Long Island Workshop. The NIST blue tile was measured for $R(0;45;\lambda)$ by the NIST Spectral tri-function automated reference reflectometer (STARR) [*Proctor and Barnes*, 1996] in October 2014 and February 2015; these measurements showed the reflectance of the blue tile was stable in time. The uncertainties in these bi-directional reflectance factors were between 5% and 8.6% ($k = 2$) between 280 nm to 440 nm. The peak reflectance was observed at 415 nm, see Fig. 32. The STARR measurements are in-plane. Because the plastic mounting cell was too large to be mounted in the STARR facility, the two glass pieces were removed and measured for $R(0;45;\lambda)$ with nothing behind the back surface.

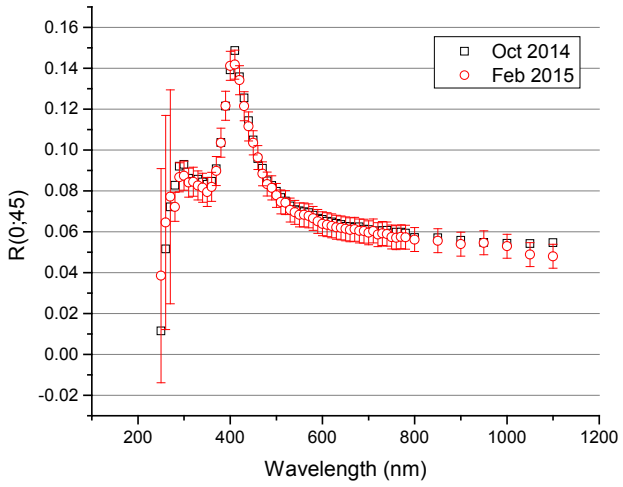

Figure 32. NIST STARR bi-directional reflectance values for the blue glass assembly.

Because the blue tile is used outdoors under conditions of hemispherical illumination, it is important to quantify the BRDF for out-of-plane angles. Georgi Georgiev of NASA/GSFC performed a series of measurements of the blue tile mounted in the black plastic cell in November 2015 using the Diffuser Calibration Laboratory described in [*Schiff et al.*, 1993; *Georgiev and Butler*, 2008]. The BRDF was measured at 350 nm, 410 nm, and 900 nm at 0° angle of incidence with θ_r = 15°, 30°, 45°, and 60° and ϕ_r = 0° to 315° in 45° steps. The BRDF was also measured at 410 nm for θ_i = 30°, 45°, and 60°, ϕ_i = 0° for θ_r = 15°, 30°, 45°, and 60°, ϕ_r = 0° to 180° in 90° steps. The standard uncertainty in BRDF values for white, high reflectance samples such as 99% Spectralon is 1%. Figure 33 illustrates variation in bi-directional reflectance factor for a scatter azimuth of 90° (ϕ_r = 90°) from the plane of incidence as a function of incident and reflected (view) zenith angles.

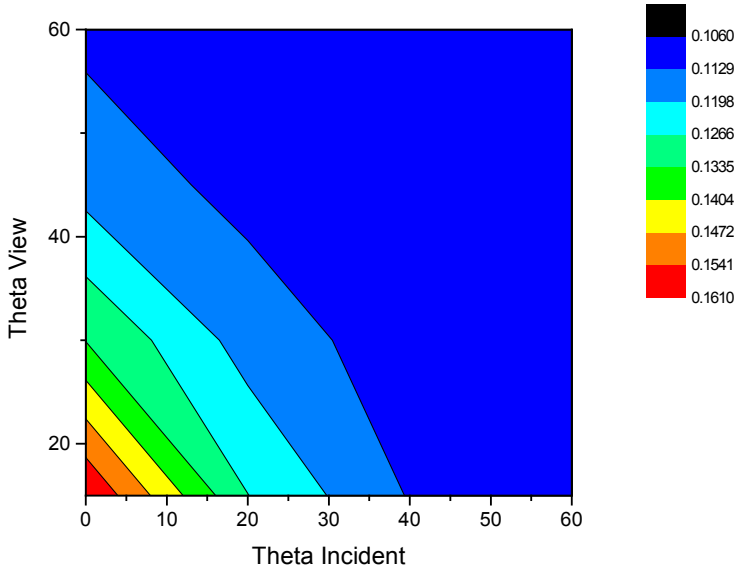

Figure 33. Blue tile bi-directional reflectance factor dependence on incident and reflected zenith angles at 90° to the plane of incidence and at 410 nm.

From Fig. 33, we see the blue tile is not Lambertian – the maximum variation is 50% for this subset of the data. Also, the in-plane results reveal a significant specular reflection. However, for the solar zenith angles during the cruise December 2015, and a view angle of 40° to 60°, the variation in bi-directional reflectance is reduced. Spectralon is also not Lambertian; in-plane measurements of the BRDF for four incident angles (0° to 60°) and a range of view angles (0° to ±60°) showed variations of up to 25% at large angles of incidence [*Early et al.*, 2000]. It has also been established for Spectralon that $R(0;45;\lambda) \cong 1.028R(8;\mathrm{h};\lambda)$, see Appendix B in [*Johnson et al.*, 1996]; not equal as would be the case if Spectralon were an ideal Lambertian diffuser. The non-Lambertian behavior of the blue tile reduces its effectiveness as a test standard because of the sky contribution, and we expect to see the least variability in its derived reflectance for the cloud free stations, stable atmospheres, and no interference in the light field from adjacent objects such as the ship's structure. The sky contribution to the calibration step of measuring the Spectralon standard means that using a laboratory value for $R(0;45;\lambda)$ or $R(8;\mathrm{h};\lambda)$ is not capturing the actual situation, where the reflected radiance is the integral over the hemisphere of the actual BRDF times the incident radiance distribution:

$$L_{\mathrm{r}}(\theta_r,\phi_r;E_{\mathrm{i}}) = \int_{\omega_r}\int_{2\pi} f_{\mathrm{r}}(\theta_i,\phi_i;\theta_r,\phi_r)dE_{\mathrm{i}}(\theta_i,\phi_i) = \int_{\omega_r}\int_{2\pi} f_{\mathrm{r}}(\theta_i,\phi_i;\theta_r,\phi_r)L_{\mathrm{i}}(\theta_i,\phi_i)\cos(\theta_i)d\omega_i \,. \quad (16)$$

Measurements of the blue tile and Spectralon targets not used for the reflectance calibration will be analyzed using Eq. 15, although the availability of contemporaneous E_i data is to be determined. The reflectance for the Spectralon standard will be the same as that which the corresponding researcher used for their remote sensing reflectance determinations. Comparisons will be made among the different instruments and stations as well as to the laboratory measurements. The NIST BRDF measurements will be repeated with the blue glass mounted in a smaller black plastic cell, in order to compare more accurately with the NASA/GSFC results.

8. Conclusion

The 2015 dedicated VIIRS Cal/Val cruise aboard the NOAA Ship *Nancy Foster* was successful in making many in situ measurements corresponding with VIIRS satellite data retrievals. Valid match-ups with VIIRS were found for 10 stations covering 4 separate days. Rain and cloudy conditions precluded satellite match-ups in the Tongue of the Ocean. However, several in situ measurements were made there and these observations will be useful in characterizing optical properties in these waters as well as for algorithm development. Instrumentation included profiling, floating and above-water radiometers for AOP measurements from several perspectives. IOP measurements were also made with multiple optical instruments deployed in several modes (e.g., profiling, flow-through, etc.). Furthermore, water samples were collected for later processing to provide measurements of additional ocean properties such as Chl-*a*, phytoplankton characteristics, nutrients, organic carbon constituents and SPM. Uncertainties in the in situ and satellite validation measurements will be estimated by utilizing pre- and post-cruise calibrations of instruments, simultaneous measurements of parameters utilizing multiple techniques and instruments and evaluation of data processing techniques. Oceanic processes will be investigated using multiple platform techniques, which include near-real time satellite measurements, in situ flow-through, profiling, and above water data. As during the 2014 cruise, the 2015 cruise track crossed several Gulf Stream fronts. These strong spatial gradients will be studied using in situ data and compared to VIIRS data to assess the ability of the VIIRS sensor to capture the scales and magnitude of the naturally occurring variability. In summary, a wealth of high quality in situ data was collected and is being analyzed to provide a comprehensive evaluation of VIIRS performance, validation techniques, and various ocean color applications.

9. Acknowledgments

All data collected on this cruise will be publically available through NOAA CoastWatch/OceanWatch repository and will be formally archived with NOAA/NCEI according to their guidelines. Data users are strongly encouraged to communicate with cruise investigators for appropriate collaborations and/or citations. Funding for this project was provided as follows: NOAA OMAO for ship time and crew support; JPSS VIIRS Ocean Color Cal/Val funding supported some science group participation. Investigator groups external to the JPSS VIIRS Ocean Color Cal/Val provided their own support. We are grateful to Georgi Georgiev of NASA/GSFC and Catherine Cooksey of NIST for BRDF measurements of the blue tile. We thank the crew of the NOAA Ship *Nancy Foster* for their support in making data collection possible. We thank two reviewers from NIST for their comments and edits. The views, opinions, and findings contained in this report are those of the authors and should not be construed as an official NOAA or US Government position, policy, or decision.

10. References Cited

Arnone, R.A., D.A. Wiesenburg and K.D. Saunders (1990), The origin and characteristics of the Algerian Current, *J. Geophys. Res.-Oceans*, *95*(C2), 1587-1598, doi: 10.1029/JC095iC02p01587.

Booth, B.C. (1993), *Estimating cell concentration and biomass of autotrophic plankton using microscopy.*, Lewis Publishers, Boca Raton, Florida, USA.

Carder, K.L. and R.G. Steward (1985), A remote-sensing reflectance model of a red-tide dinoflagellate off West Florida, *Limnology and Oceanography*, *30*(2), 286-298.

Clark, D.K., H.R. Gordon, K.J. Voss, Y. Ge, W. Broenkow and C. Trees (1997), Validation of atmospheric correction over the oceans, *Journal of Geophysical Research-Atmospheres*, *102*(D14), 17209-17217, doi: 10.1029/96jd03345.

Dickey, T.D. (1991), The emergence of concurrent high-resolution physical and bio-optical measurements in the upper ocean and their applications, *Reviews of Geophysics*, *29*(3), 413, doi: 10.1029/91RG00578.

Early, E.A., P.Y. Barnes, B.C. Johnson, J.J. Butler, C.J. Bruegge, S.F. Biggar, P.R. Spyak and M. Pavlov (2000), Bidirectional reflectance round-robin in support of the Earth Observing System Program, *J. Atmos. and Oceanic Tech.*, *17*, 1077 - 1091.

EPA (1971), Methods for chemical analysis of water and wastes, EPA-NERL: 160.2, US Environmental Protection Agency.

Georgiev, G.T. and J.J. Butler (2008), Laboratory-based bidirectional reflectance distribution functions of radiometric tarps, *Applied Optics*, *47*(18), 3313 - 3323.

Gleason, A.C.R., K.J. Voss, H.R. Gordon, M. Twardowski, J. Sullivan, C. Trees, A. Weidemann, J.F. Berthon, D. Clark and Z.P. Lee (2012), Detailed validation of the bidirectional effect in various Case I and Case II waters, *Optics Express*, *20*(7), 7630-7645, doi: 10.1364/oe.20.007630.

Goes, J.I., H.d.R. Gomes, A.M. Chekalyuk, E.J. Carpenter, J.P. Montoya, V.J. Coles, P.L. Yager, W.M. Berelson, D.G. Capone, R.A. Foster, D.K. Steinberg, A. Subramaniam and M.A. Hafez (2014), Influence of the Amazon River discharge on the biogeography of phytoplankton communities in the western tropical north Atlantic, *Progress In Oceanography*, *120*(0), 29-40, doi: 10.1016/j.pocean.2013.07.010.

Gordon, H.R. (2010), Some reflections on thirty-five years of ocean-color remote sensing, in *Oceanography from Space: Revisited*, Edited by Barale, V., Gower, J.F.R. and Alberotanza, L., pp. 289-305, Springer Netherlands.

Gordon, H.R. and M. Wang (1994), Retrieval of water-leaving radiance and aerosol optical thickness over the oceans with SeaWiFS: A preliminary algorithm, *Appl. Opt.*, *33*, 443–452.

Gordon, H.R., D.K. Clark, J.L. Mueller and W.A. Hovis (1980), Phytoplankton Pigments from the Nimbus-7 Coastal Zone Color Scanner: Comparisons with Surface Measurements, *Science*, *210*(4465), 63-66, doi: 10.2307/1684604.

Gould, R.W., R.A. Arnone and M. Sydor (2001), Absorption, scattering; and remote-sensing reflectance relationships in coastal waters: Testing a new inversion algorithm, *J. Coast. Res.*, *17*(2), 328-341.

GUM (1995), Evaluation of measurement data - Guide to the expression of uncertainty in measurement.(ed.), http://www.bipm.org/en/publications/guides/gum.html.

Holm-Hansen, O. and B. Riemann (1978), Chlorophyll a determination: improvements in methodology, *Oikos*, *30*, 438-447.

Hovis, W.A., D.K. Clark, F. Anderson, R.W. Austin, W.H. Wilson, E.T. Baker, D. Ball, H.R. Gordon, J.L. Mueller, S.Z. El-Sayed, B. Sturm, R.C. Wrigley and C.S. Yentsch (1980), Nimbus-7 Coastal Zone Color Scanner: System Description and Initial Imagery, *Science*, *210*(4465), 60-63, doi: 10.2307/1684603.

Hu, C., Z. Lee and B. Franz (2012), Chlorophyll a algorithms for oligotrophic oceans: A novel approach based on three-band reflectance difference, *J. Geophys. Res.-Oceans*, *117*, doi: 10.1029/2011jc007395.

Hunter, C. (2006), Particulate organic carbon, nitrogen and total suspended matter. Methodologies, protocols and analyses used in the development of ocean color product algorithms., Technical Publication 06–1(ed.), Moss Landing Marine Laboratories.

IOCCG (2010), Atmospheric correction for remotely-sensed ocean-colour products. Wang, M. (ed.), *Reports and monographs of the International Ocean-Colour Coordinating Group,* No. 10, International Ocean-Colour Coordinating Group, Dartmouth, Canada.

Jenkins, C.A., J.I. Goes, K. McKee, H. Gomes, R. do, R. Arnone, M. Wang, M. Ondrusek, P.V. Nagamani, T.P. Latha, K.H. Rao and V.K. Dadhwal (2016), High-resolution shipboard measurements of phytoplankton: a way forward for enhancing the utility of satellite SST and chlorophyll for mapping microscale features and frontal zones in coastal waters., (ed.), *Proceedings of SPIE Asia-Pacific Remote Sensing* International Society for Optics and Photonics, 7 May 2016.

Johnson, B.C., G.S. Fargion, R.D. Saunders and M. Ondrusek (2012), Comparisons of reflectance targets at the Above Water Radiometry Workshop on Long Island Sound, August 4 - 6, 2010, in *2010 American Geophysical Union Fall Meeting*, edited, pp. A33M-0330, San Francisco, CA.

Johnson, B.C., J. Rice, H. Yoon and A. Parr (2014), Principles of optical radiometry, in *Optical radiometry for ocean climate measurements*, edited by Zibordi, G., Donlon, C. and Parr, A., pp. 13-67, Academic Press, Waltham, MA.

Johnson, B.C., S.S. Bruce, E.A. Early, J.M. Houston, T.R. O'Brian, A. Thompson, S.B. Hooker and J.L. Mueller (1996), *The Fourth SeaWiFS Intercalibration Round-Robin Experiment (SIRREX-4), May 1995*, 65 pp., NASA Goddard Space Flight Center, Greenbelt, Maryland.

Kishino, M., M. Takahashi, N. Okami and S. Ichimura (1985), Estimation of the spectral absorption coefficients of phytoplankton in the sea, *Bulletin of Marine Science*, *37*(2), 634-642.

Knap, A., A. Michaels, A. Close, H. Ducklow and A. Dickson (1994), Protocols for the Joint Global Ocean Flux Study (JGOFS) Core Measurements. JGOFS Report,(ed.) 170 pp.

Lee, Z.P., K.L. Carder and R.A. Arnone (2002), Deriving inherent optical properties from water color: a multiband quasi-analytical algorithm for optically deep waters, *Applied Optics*, *41*(27), 5755-5772, doi: 10.1364/ao.41.005755.

Lee, Z.P., N. Pahlevan, Y.-H. Ahn, S. Greb and D. O'Donnell (2013), Robust approach to directly measuring water-leaving radiance in the field, *Applied Optics*, *52*(8), 1693-1701.

Lee, Z.P., K.L. Carder, R.G. Steward, T.G. Peacock, C.O. Davis and J.L. Mueller (1997), *Remote-sensing reflectance and inherent optical properties of oceanic waters derived from above-water measurements*, 160-166 pp., Spie - Int Soc Optical Engineering, Bellingham, doi: 10.1117/12.266436.

Leymarie, E., D. Doxaran and M. Babin (2010), Uncertainties associated to measurements of inherent optical properties in natural waters, *Applied Optics*, *49*(28), 5415-5436, doi: 10.1364/ao.49.005415.

MacIssac, E.A. and J.G. Stockner (1993), Enumeration of phototrophic picoplankton by autofluorescence microscopy., in *Handbook of Methodology in Aquatic Microbial Ecology*, Edited by Kemp.P.F., Sherr, B.F., Sherr, E.B. and J., C.J., pp. 187-197, Lewis Publishers, Boca Raton, Florida, USA.

Mobley, C.D. (1999), Estimation of the remote-sensing reflectance from above-surface measurements, *Applied Optics*, *38*(36), 7442-7455, doi: 10.1364/ao.38.007442.

Mobley, C.D. (2015), Polarized reflectance and transmittance properties of windblown sea surfaces, *Applied Optics*, *54*(15), 4828-4849, doi: 10.1364/ao.54.004828.

Morel, A., D. Antoine and B. Gentili (2002), Bidirectional reflectance of oceanic waters: accounting for Raman emission and varying particle scattering phase function, *Applied Optics*, *41*(30), 6289-6306, doi: 10.1364/ao.41.006289.

Morrow, J.H., C.R. Booth, R.N. Lind and S.B. Hooker (2010), The Compact Optical Profiling System (C-OPS). Advances in Measuring the Apparent Optical Properties (AOPs) of Optically Complex Waters, NASA Tech. Memo. 2010–215856, Morrow, J.H., Hooker, S.B., Booth, C.R., Bernhard,

G., Lind, R.N. and J.W., B. (ed.) 42–50 pp, NASA Goddard Space Flight Center, Greenbelt, Maryland.
Mueller, J.L., C.O. Davis, R. Arnone, R. Frouin, K. Carder, Z.P. Lee, R.G. Steward, S.B. Hooker, C.D. Mobley and S. McLean (2003), Above-water radiance and remote sensing reflectance measurement and analysis protocols, in *Ocean Optics Protocols For Satellite Ocean Color Sensor Validation, Revison 4, Volume III: Radiometric Measurements and Data Analysis Protocols*, Edited by Mueller, J.L., Fargion, G.S. and Mcclain, C., pp. 21 - 31, Goddard Space Flight Center, National Aeronautics and Space Administration, Greenbelt, Maryland.
Neckel, H. and D. Labs (1984), The solar radiation between 3300-A and 12500-A, *Solar Physics*, *90*(2), 205-258.
Nicodemus, F.E., J.C. Richmond, J.J. Hsia, I.W. Ginsberg and T. Limperis (1977), *Geometrical Considerations and Nomenclature for Reflectance*, 34 plus appendices pp., Washington, D. C. 20402.
O'Reilly, J.E., S. Maritorena, B.G. Mitchell, D.A. Siegel, K.L. Carder, S.A. Garver, M. Kahru and C. McClain (1998), Ocean color chlorophyll algorithms for SeaWiFS, *Journal of Geophysical Research-Oceans*, *103*(C11), 24937-24953, doi: 10.1029/98jc02160.
Ondrusek, M., E. Stengel, C.S. Kinkade, R.L. Vogel, P. Keegstra, C. Hunter and C. Kim (2012), The development of a new optical total suspended matter algorithm for the Chesapeake Bay, *Remote Sensing of Environment*, *119*, 243-254, doi: 10.1016/j.rse.2011.12.018.
Ondrusek, M., E. Stengel, V.P. Lance, M. Wang, K. Voss, G. Zibordi, M. Talone, Z. Lee, J. Wei, J. Lin, et al. (2015), NOAA Technical Report NESDIS 146: Report for Dedicated JPSS VIIRS Ocean Color Calibration/Validation Cruise, US Department of Commerce, 60 pp., doi: 10.7289/V52B8W0Z.
Pegau, W.S., D. Gray and J.R.V. Zaneveld (1997), Absorption and attenuation of visible and near-infrared light in water: dependence on temperature and salinity, *Applied Optics*, *36*(24), 6035-6046, doi: 10.1364/ao.36.006035.
Pope, R.M. and E.S. Fry (1997), Absorption spectrum (380-700 nm) of pure water .2. Integrating cavity measurements, *Applied Optics*, *36*(33), 8710-8723, doi: 10.1364/ao.36.008710.
Proctor, J.E. and P.Y. Barnes (1996), NIST high accuracy reference reflectometer-spectrophotometer, *Journal of Research of the National Institute of Standards and Technology*, *101*(5), 619 - 627.
Röttgers, R., D. McKee and S.B. Woźniak (2013), Evaluation of scatter corrections for ac-9 absorption measurements in coastal waters, *Methods in Oceanography*, *7*, 21-39, doi: http://dx.doi.org/10.1016/j.mio.2013.11.001.
Satlantic (2003), Operation Manual for Profiler II.(ed.), Satlantic Incorporated, Halifax, Nova Scotia.
Satlantic (2004), SatView Data Logging / Display Program Users Guide; Version 2.8.(ed.), Satlantic Incorporated, Halifax, Nova Scotia.
Schiff, T.F., M.W. Knighton, D.J. Wilson, F.M. Cady, J.C. Stover and J.J. Butler (1993), Design review of a high accuracy UV to near IR scatterometer, *Calibration of Passive Remote Observing Optical and Microwave Instrumentation*, *1995*, 121 - 130.
Solar_Light_Company_Inc (2003), Microtops II Sunphotometer user's guide, vers. 5.5.(ed.), Philadelphia, PA.
Son, S. and M.H. Wang (2015), Diffuse attenuation coefficient of the photosynthetically available radiation K-d(PAR) for global open ocean and coastal waters, *Remote Sensing of Environment*, *159*, 250-258, doi: 10.1016/j.rse.2014.12.011.
Sosik, H.M. and R.J. Olson (2007), Automated taxonomic classification of phytoplankton sampled with imaging-in-flow cytometry, *Limnology and Oceanography: Methods*, *5*(6), 204-216.
Sullivan, J.M., M.S. Twardowski, J.R.V. Zaneveld, C.M. Moore, A.H. Barnard, P.L. Donaghay and B. Rhoades (2006), Hyperspectral temperature and salt dependencies of absorption by water and heavy water in the 400-750 nm spectral range, *Applied Optics*, *45*(21), 5294-5309.
Tomas, C.R. (1997), *Identifying marine phytoplankton*, Academic press.

Twardowski, M.S. and P.L. Donaghay (2001), Separating in situ and terrigenous sources of absorption by dissolved materials in coastal waters, *J. Geophys. Res.-Oceans*, *106*(C2), 2545-2560, doi: 10.1029/1999jc000039.

Twardowski, M.S., J.M. Sullivan, P.L. Donaghay and J.R.V. Zaneveld (1999), Microscale quantification of the absorption by dissolved and particulate material in coastal waters with an ac-9, *J. Atmos. Oceanic Technol.*, *16*, 691–707.

Voss, K.J. and G. Zibordi (1989), Radiometric and geometric calibration of a spectral electro-optic "fisheye' camera radiance distribution system, *J. Atmosph. and Ocean. Techn.*, *6*, 652-662.

Voss, K.J. and A. Morel (2005), Bidirectional reflectance function for oceanic waters with varying chlorophyll concentrations: Measurements versus predictions, *Limnology and Oceanography*, *50*(2), 698-705.

Voss, K.J. and A.L. Chapin (2005), Upwelling radiance distribution camera system, NURADS, *Optics Express*, *13*(11), 4250-4262, doi: 10.1364/opex.13.004250.

Voss, K.J., A. Morel and D. Antoine (2007), Detailed validation of the bidirectional effect in various Case 1 waters for application to ocean color imagery, *Biogeosciences*, *4*(5), 781-789.

Wang, M. (2007), Remote sensing of the ocean contributions from ultraviolet to near-infrared using the shortwave infrared bands: simulations, *Applied Optics*, *46*(9), 1535-1547, doi: 10.1364/ao.46.001535.

Wang, M., S. Son and L.W. Harding (2009), Retrieval of diffuse attenuation coefficient in the Chesapeake Bay and turbid ocean regions for satellite ocean color applications, *Journal of Geophysical Research: Oceans*, *114*(C10), C10011, doi: 10.1029/2009jc005286.

Wang, M., X. Liu, L. Tan, L. Jiang, S. Son, W. Shi, K. Rausch and K. Voss (2013), Impact of VIIRS SDR performance on ocean color products, *J. Geophys. Res. Atmos.*, *118*, 10347–10360, doi: doi:10.1002/jgrd.50793.

Wang, M., X. Liu, L. Jiang, S. Son, J. Sun, W. Shi, L. Tan, P. Naik, K. Mikelsons, X. Wang and V. Lance (2014), Evaluation of VIIRS Ocean Color Products, *Proc. SPIE 9261*, *92610E*, doi: 10.1117/12.2069251.

Welschmeyer, N.A. (1994), Fluorometric analysis of chlorophyll a in the presence of chlorophyll b and pheopigments, *Limnology and Oceanography*, *39*(8), 1985-1992.

WETLabs (2011), ac meter protocol document. ac meter protocol (acprot); Revision Q 20 April 2011(ed.).

Zaneveld, J.R.V., J.C. Kitchen and C.C. Moore (1994), Scattering error correction of reflecting-tube absorption meters, (ed.), *Proceedings*, doi: 10.1117/12.190095.

Zibordi, G. and K.J. Voss (2014), In situ Optical Radiometry in the Visible and Near Infrared, *Experimental Methods in the Physical Sciences*, *47*, 247-304.

Appendix A – Station Information Tables

Table A1. Times, locations, drift.

NF-15-13 Stations	Date in 2015	Julian Day	Station Start Time [UTC hh:mm]	Start Latitude [decimal degrees]	Start Longitude [decimal degrees]	Station End Time [UTC hh:mm]	End Latitude [decimal degrees]	End Longitude [decimal degrees]	Approximate Station Drift [nautical miles]
1	2-Dec	336	19:23	32.5352	-79.8974	21:10	32.5352	79.8974	1.2
2	3-Dec	337	15:00	29.6935	-80.7437	n/a	n/a	n/a	n/a
3	3-Dec	337	17:53	29.5922	-80.7308	n/a	n/a	n/a	n/a
4	4-Dec	338	20:21	26.3792	-78.5291	21:48	n/a	n/a	n/a
5	5-Dec	339	14:03	24.4237	-77.4508	16:25	24.4210	77.4661	<1
6	5-Dec	339	17:35	24.4867	-77.3204	19:27	24.4841	77.3310	<1
7	5-Dec	339	20:30	24.3761	-77.2800	22:30	24.3833	77.2876	<1
8	6-Dec	340	17:48	23.6568	-76.5817	19:25	23.6698	76.5885	<1
9	6-Dec	340	20:04	23.7108	-76.6029	21:50	23.7216	76.6056	<1
10	7-Dec	341	20:55	26.4005	-78.5107	22:10	26.4074	78.5166	<1
11	8-Dec	342	17:48	28.6532	-80.3323	18:10	n/a	n/a	<1
12	8-Dec	342	18:55	28.7256	-80.4422	22:00	n/a	n/a	> 1.5 to South
13	9-Dec	343	13:55	30.7233	-80.5351	15:15	30.7710	80.5341	<1
14	9-Dec	343	17:00	30.9184	-80.6023	18:35	30.9202	80.6024	<1
15	9-Dec	343	19:18	30.9877	-80.5386	20:40	30.9949	80.5459	<1
16	10-Dec	344	13:00	31.1231	-77.6733	n/a	31.1175	77.9961	1
17	10-Dec	344	16:52	31.1643	-77.7388	17:49	31.1718	77.7339	Returned
18	10-Dec	344	19:06	31.0734	-77.5326	21:00	n/a	n/a	n/a
19	11-Dec	345	13:00	32.2048	-77.7976	14:35	32.2254	77.7723	n/a
20	11-Dec	345	16:06	32.4855	-77.8772	17:30	32.5125	77.8272	1.9
21	11-Dec	345	18:39	32.6256	-77.8846	20:30	32.6492	77.8338	n/a
22	11-Dec	345	21:10	32.6809	-77.8318	21:30	n/a	n/a	n/a
23	12-Dec	346	13:21	33.1013	-78.2607	14:20	33.1060	78.2246	3
24	12-Dec	346	16:41	33.2427	-78.0205	17:59	33.2423	78.0196	n/a
25	12-Dec	346	19:36	33.0739	-78.2113	2100	33.0790	78.2141	0.5
26	13-Dec	347	14:28	32.1560	-79.3214	16:08	32.1736	79.3101	1.3 to North
27	13-Dec	347		32.1848	-79.0819	18:35	32.1946	79.0946	Finished

Table A2. Clouds, wind, sea state, water depth, log comments.

NF-15-13 Stations	Date in 2015	Sky Cover [% clouds and condition]	Wind Direction [degrees]	Wind Speed [kt]*	Sea State [feet]*	Water Depth [m]	Comments
1	2-Dec	65	190	10	1-2	13	Coastal; Charleston SC; 0.44 nm from S1, off Charleston, SC entrance - 8 nm; Overnight transet to station 3 and return to station 2 at 0800
2	3-Dec	25	180	10	2-3	33	Coastal Florida; Off St Augustine Florida 20 nm
3	3-Dec	30	180	12	3	33	Short Florida; some VIIRS overpass; off St Augustine Florida 20 nm; 5nm from previous Station
4	4-Dec	100	30	6	1	750	Freeport cloudy; no VIIRS; after Gulf Stream; south of Freeport , Bahamas 8 nm
5	5-Dec	20	N	5 to 6	1	1750	Tongue; no VIIRS
6	5-Dec	50	N	5 to 6	1	1468	Tongue; no VIIRS coverage; Near Morgan City !!; Tongue of Ocean- Middle on east side
7	5-Dec	20 to 30	N	5	1	1500	Tongue; no VIIRS coverage; Tongue of Ocean - central - off Green Cay 8 nm; plan was next day shallow stations - rain had to head south
8	6-Dec	70	60	10	1	1500	Tongue; Near Morgan City !!\Very Southern Tongue of Ocean ; next station is close; IMAGERY on Dec 6 is clouds
9	6-Dec	40	65	10	1	1500	Tongue; Southern Tongue of Ocean on east side; next heading northern Freeport - clouds
10	7-Dec	100	202	3	1	750	Freeport ; Next heading to west to Gulf Stream; ASD,GER, SE- Lab Experiment
11	8-Dec	20	NE	10	3-4	50+	Left for hole; clouds can in and headed west; off cape canaveral
12	8-Dec	40	NE	10	2	35	5 nm north; OK, clouds , repeated; will head north tonight
13	9-Dec	10	NE	10	2	40	Jacksonville
14	9-Dec	25	NE	10	2	40	NE -Jacksonville; is 5 nm from St 13; took off NE for hole
15	9-Dec	40	343	7.5	2	31	5 nm away; stated crossing the Stream; East -to night crossing of Gulf Stream
16	10-Dec		n/a				Drfted 3 nm south east; very Clear water
17	10-Dec	0	313	6.7	3	950	Heading west for hour
18	10-Dec	0% ; (40% at horizon)	316	7	2	1000	Very Clear water Station east of Gulf Stream
19	11-Dec	50; patchy	274	7.9	2	not recorded	
20	11-Dec	0	294	8.3	2	1000	
21	11-Dec	0	296	7.1	2	1000	
22	11-Dec	0	280	7.1	2	1000	Sun 20 deg
23	12-Dec	0	315	7	2	50	Lauched Drifter; followed drifter
24	12-Dec	0	318	8.9	2	40	
25	12-Dec	30	316	5	2	n/a	Return to drifter; Back to drifter; 2.95 from St. 23
26	13-Dec	60; patchy	155	16	3	55	Shelf front
27	13-Dec	60; patchy	149	17.6	3	110	Offshore -shelf; Sea raising 4 hours from Charleston light

*These values are reported here in units as they were recorded on the ship rather than converting them to SI units.

Table A3. Rosette/CTD time, location, bottle depths, parameters sampled. FT, flow-through samples.

NF-15-13 Stations	Ship Rosette Start Time - CTD, Chlorophyll Fluorometer, O2 [UTC; hh:mm]	Ship Rosette Start Latitude [decimal degrees]	Ship Rosette Start Longitude [decimal degrees]	Ship Rosette Nominal Bottle Depths [m]	Nutrients [m] (LDEO)	HPLC Pigment; POC; CDOM; DOC [m] (NASA/ GSFC)	Extracted fluorometric Chl-*a* (2 methods); Filter Pad Absorption [m] (USF)	SPM [m] (NOAA/ STAR)
1	19:59	32.536	-79.896	12.5, 1.7	12.5, 1.7	12.5, 1.7	12.5, 1.7	12.5, 1.7
2	16:16	29.687	-80.754	15, 2	15, 2	15, 2	15, 2	15, 2
3	n/a	n/a	n/a	n/a	n/a	n/a	n/a	n/a
4	21:02	26.373	-78.527	20, 2	20, 2	20, 2	20, 2	20, 2
5	14:03	24.424	-77.451	20, 2	20, 2	20, 2	20, 2	20, 2
6	18:29	24.495	-77.326	20, 2	20, 2	20, 2	20, 2	20, 2
7	22:13	24.383	-77.288	25, 2	25, 2	25, 2	25, 2	25, 2
8	18:48	23.670	-76.589	37, 2	37, 2	37, 2	37, 2	37, 2
9	21:40	23.721	-76.607	22, 2	22, 2	22, 2	22, 2	22, 2
10	20:58	26.400	-79.344	12, 2	12, 2	12, 2	12, 2	12, 2
11	n/a	n/a	n/a	n/a	n/a	n/a	n/a	n/a
12	20:10	28.720	-80.434	14, 2	14, 2	14, 2	14, 2	14, 2
13	13:55	30.724	-80.535	14, 2	14, 2	14, 2	14, 2	14, 2
14	n/a	n/a	n/a	n/a	n/a	FT (no POC)	FT	n/a
15	20:36	30.995	-80.546	14, 2	14, 2	14, 2	14, 2	14, 2
16	13:28	31.126	-77.676	30, 2	30, 2	30, 2	30, 2	30, 2
17	n/a	n/a	n/a	n/a	n/a	FT	FT	n/a
18	20:30	31.073	-77.533	35, 2	30, 2	30, 2	35, 2	35, 2
19	13:15	32.209	-77.792	30, 2	30, 2	30, 2	30, 2	30, 2
20	16:07	32.488	-77.875	30, 2	30, 2	30, 2	30, 2	30, 2
21	20:27	32.640	-77.862	31,2	31,2	31,2	31,2	31,2
22	20:27	n/a	n/a	n/a	n/a	FT (no POC)	FT	n/a
23	13:24	33.101	-78.261	14, 2	14, 2	14, 2	14, 2	14, 2
24	16:54	33.241	-78.016	14, 2	14, 2	14, 2	14, 2	14, 2
25	20:30	33.079	-78.214	16, 2	16, 2	16, 2	16, 2	16, 2
26	15:04	32.160	-79.319	21, 2	21, 2	21, 2	21, 2	21, 2
27	17:19	32.185	-79.082	35, 2	35, 2	35, 2	35, 2	35, 2

Table A4. Times and locations for profiling IOP packages, profiling HyperPros, floating HyperPros and Secchi depth.

NF-15-13 Stations	IOP Profiling Package Start Time (UTC hh:mm) NASA	IOP Profiling Package Start Time (UTC hh:mm) UMB	HyperPro Profiling (4 instruments, simul-taneouly) Start Time [UTC hh:mm][3]	HyperPro Profiling Start Latitude [decimal degrees]	HyperPro Profiling Start Longitude [decimal degrees]	HyperPro Floating (3 packages) Start Times [UTC hh:mm in order UMB, NRL, USM]	HyperPro Floating Latitude [decimal degrees]	HyperPro Floating Longitude [decimal degrees]	Secchi Depth (Time same as Floaters) [m]
1	n/a	20:40	20:35	32.5397	-79.8876	19:56, 19:53, 18:53	32.5397	-79.8876	n/a
2	n/a	16:40	15:32	29.6882	-80.7558	16:00, n/a, 16:00	29.6882	-80.7558	n/a
3	n/a	n/a	18:02	29.5933	-80.7308	n/a	n/a	n/a	n/a
4	21:30	22:00	20:33	26.3763	-78.5276	n/a	n/a	n/a	n/a
5	14:15	n/a	15:21	24.4222	-77.4582	16:00, 15:54, 15:54	24.4222	-77.4582	n/a
6	19:10 - 19:27	n/a	17:33	24.4860	-77.3201	18:04, 18:08, 18:08	24.4949	-77.3272	n/a
7	21:16	n/a	20:32	24.3765	-77.2801	21:00, 20:55, 20:54	24.3735	-77.2794	15.5
8	19:15	19:25	18:02	23.6613	-76.5826	n/a, 18:30, 18:31	23.6581	-76.5819	18
9	21:00	21:22	20:14	23.7142	-76.6021	20:45, 20:43, 20:43	23.7131	-76.6021	15
10	21:30	21:52		26.4003	-78.5102	n/a	n/a	n/a	15.5
11	n/a	n/a	17:48	28.6535	-80.3319	n/a	n/a	n/a	n/a
12	20:20	20:30	19:06 and 21:14	28.7267 (1); 28.7142 (2)	80.4408 (1); 80.4330 (2)	19:30, 19:28, 19:28	28.726	-80.4418	3.5
13	14:05	14:35	15:01	30.7212	-80.5352	14:15, 14:38, 14:38	30.7197	-80.5331	10.5
14	18:25	n/a	17:46	30.9211	-80.6039	18:18, 18:09, 18:10	30.9192	-80.6032	9
15	19:25	19:32	19:56	30.9895	-80.5408	19:20, 20:21, 20:21	30.9875	-80.5385	10
16	13:57	13:57	15:09	31.1186	-77.6647	n/a, 14:38, 14:38	31.126	-77.6765	n/a
17	17:00	17:00	17:25	31.1672	-77.7395	n/a	n/a	n/a	n/a
18	20:15	20:15	19:13	31.0731	-77.5328	19:40, 19:45, 19:44	31.0727	-77.5328	17
19	13:40	13:40	14:18	32.2333	-77.7701	13:50, 13:33, 13:44	32.2222	-77.7759	n/a

NF-15-13 Stations	IOP Profiling Package Start Time (UTC hh:mm) NASA	IOP Profiling Package Start Time (UTC hh:mm) UMB	HyperPro Profiling (4 instruments, simul-taneouly) Start Time [UTC hh:mm][3]	HyperPro Profiling Start Latitude [decimal degrees]	HyperPro Profiling Start Longitude [decimal degrees]	HyperPro Floating (3 packages) Start Times [UTC hh:mm in order UMB, NRL, USM]	HyperPro Floating Latitude [decimal degrees]	HyperPro Floating Longitude [decimal degrees]	Secchi Depth (Time same as Floaters) [m]
20	16:35	16:35	17:26	32.5096	-77.8302	17:00, 16:58, 16:59	32.497	-77.851	17
21	19:43	19:43	18:51	32.6267	-77.8829	19:05, 19:16, 19:17	32.6323	-77.8765	17
22	21:40	21:40	21:06	32.6788	-77.8348	n/a	n/a	n/a	17
23	13:45		14:47	33.0981	-78.2427	13:45, 14:07, 14:07	33.0999	-78.247	17
24	16:49	16:49	17:46	33.2424	-78.0052	17:20, 17:16, 17:19	33.2425	-78.0199	18
25	21:00	21:00	19:49	33.0773	-78.2115	20:00, 20:10, 20:10	33.0742	-78.2117	18
26	14:28	14:28	15:50	32.1687	-79.3130	15:33, 15:12, 15:11	32.1624	-79.3156	13
27	17:41	17:41	18:04	32.1876	-79.0926	18:20, 18:22, 18:22	32.186	-79.0872	15

Table A5. Times for NURADS, handheld above water radiometers and Microtops; operations of HyperSASs; and VIIRS overpass times and match-up assessments.

NF-15-13 Stations	NURADS Time [UTC hh:mm]	Handheld Above Water Radiometers (8 instruments ~simultaneous) [UTC hh:mm][4]	Microtops [UTC hh:mm][5]	HyperSAS-POL (continuous) CUNY	HyperSAS (continuous) NASA	VIIRS Overpass Time [Start time of granule, UTC hh:mm]	Good VIIRS Match-up
1	n/a	20:35 (only UMB Spectral Evolution)		on	on	18:07	no
2	n/a	15:22 3 Decks NRL and USF ASD; 16:35 Rear Decks OSU Sp. Ev.; 15:47 UMB Sp. Ev.	15:50 UMB	on	on	17:48	no
3	n/a	17:53 3 decks for USM, NRL, USF CCNY ASDs and for CCNY GER; 17:55 2nd deck for UMB Sp. Ev.	17:56 USF; 17:50 UMB	on	on	17:48	yes
4	n/a	n/a		on	on	17:27 and 19:08	no
5	n/a	n/a		on	on	18:48	no
6	n/a	18:30		on	on	18:48	no
7	n/a	n/a		on	on	18:48	no
8	n/a	18:50 except n/a for UMB Sp. Ev.		on	on	18:29	no
9	n/a	21:40 including Blue Tile		on	on	18:29	no
10	n/a	n/a		on	on	18:12	no
11	n/a	n/a		on	on	17:54 bottom edge	no
12	19:30	19:47	NRL, time unavailable	on	on	17:54 bottom edge	***
13	14:15	15:11		on	on	17:35 + 19:16; edges overlap	no
14	n/a	18:00		on	on	17:35 + 19:16; edges overlap	no
15	n/a	19:31	19:31 UMB	on	on	17:35 + 19:16; edges overlap	no
16	n/a	15:10; 15:20 to 15:35 Blue Tile		on	on	18:57	no
17	n/a	17:04	17:04 UMB	on	on	18:57	yes
18	19:40	19:05	19:05 UMB	on	on	18:57	yes
19	n/a	14:20		on	on	18:38	yes
20	17:00	16:43	16:05 USF, CCNY, UMB	on	on	18:38	yes
21	19:05	18:40 including Blue Tile		on	off	18:38	yes
22	n/a	n/a		on	off	18:38	yes
23	13:45	14:39		on	off	18:19	yes
24	17:20	17:45 including Blue Tile		on	off	18:19	yes
25	20:00	19:44		on	off	18:19	yes
26	15:33	15:40		on	off	18:19	no
27	n/a	18:05	18:05 UMB	on	off	18:19	no

*5 ASDs: USM serial number (s/n#) 1338; NRL s/n# 1707; NOAA s/n#1847; USF s/n# 1007; CCNY s/n# 1075; 2 Spectral Evolutions (Sp. Ev.): OSU and UMB; 1 GER: CCNY
**4 Microtops: CCNY, NRL, UMB, USF
***nearby @ 11:14 UTC, 28.7132° latitude, -80.4330° longitude

Table A6. Flow-through log and observations.

NF-15-13 Stations	Ship Flow-through Temperature [°C]	Ship Flow-through Salinity [psu]	Ship Flow-through Fluorescence for Chl / UV [volts]	IOP Flow-through ac-s Filtered and Unfiltered (Stennis) [m^{-1}]	Flow-through b_b (Stennis) [m^{-1}]	IFCB (UMB)	PAR- 2
1	18.6	33.20	0.25	yes	yes	yes	yes
2	22.2	35.10	2.5	yes	yes	yes	yes
3	22.2	35.10	2.5	yes	yes	yes	yes
4	26.8	36.34	2.4 /0.903	yes	yes	yes	yes
5	27.4	35.76	1.69/0.98	*a*(413) 0.033 /0 .071 *c*(534) 0.112 / *c*(531) 0.013	b_b(532) 0.0017	yes	yes
6	27.7	36.78	1.159 /0 .9047	*a*(413) 0.033 *a*(412) 0.64 *c*(531) 0 .012 0.104 @17:44 UC	b_b(532) 0.0019	yes	yes
7	27.6	36.76	1.856 /0 .427; scan 27209	*a*(412) 0.60 *a*(413) 0.030 *c*(534) 0.122 *c*(531) 0 .013	b_b(532) 0.0020	yes	yes
8	28.0	36.98	1.42/0.952	*a*(413)-0.03 a412 0.052 *c*(534) 0.102 *c*(531) 0.015	b_b(532) 0.0019	yes	yes
9	28.0	36.95	1.26/0.92	*a*(412) 0.040 *a*(413) 0.036 *c*(534) 0.103 *c*(531) 0.0136	b_b(532) 0.0020	yes	yes
10	26.9	36.48	2.47/0.9035	*a*(413) 0.038 *a*(412) 0.068 *c*(531) 0.018 *c*(534) 0.116	b_b(532) 0.0019	yes	n/a
11	21.6	34.15	3.394/0.00557	*a*(412) 0.485 *a*(413) 0.246 *c*(534) 0.708 *c*(531) 0.056	b_b(532) 0.0303	yes	n/a
12	20.8	32.37	7.045/0 .00135	*a*(412) 1.088 *a*(413) 0.554 *c*(534) 1.695 *c*(531) 0.111	b_b(532) 0.0427	yes	n/a
13	23.4	36.02	0.003/1.056	*a*(412) 0.134 *a*(413) 0.031 *c*(534) 0.258 *c*(531) 0.017	b_b(532) 0.0029	yes	n/a
14	20.5	35.57	0.0258 / 1.4407	*a*(412) 0.208 *a*(413) 0.085 *c*(534) 0.358 *c*(531) 0.027	0.0035	yes	n/a
15	21.2	36.03	0.00355 1.0866	*a*(412) 0.156 *a*(413) 0.043 *c*(534) 0.313. *c*(531) 0.202	0.0033	yes	n/a
16	26.4	36.42	0.3223 0.915	*a*(412) 0.075 *c*(534) 0.099	0.0005	yes	n/a
17	26.5	36.41	0.282 /0 .891	*a*(412) 0.069 *c*(532) 0.118; *a*(412) 0.072 *c*(534) 0.139	0.00045	yes	n/a
18	26.5	36.34	0.424 /0 .8913	*a*(412) 0.072 *c*(534) 0.139	0.00045	yes	n/a
19	26.7	36.31	0.40048 0.9035	*a*(412) 0.069 *c*(532) 0.084	n/a	yes	n/a
20	27.0	36.13	0.30647 0.9157	*a*(412) 0.061 *a*(534) 0.071 *c*(412) 0.119 *c*(532) 0.070	n/a	yes	n/a
21	30.0	36.19	0.43 /0 .87912	*a*(412) 0.076 *a*(534) 0.039 *c*(412) 0.152 *c*(532) 0.109	n/a	yes	n/a
22	26.9	36.16	0.3944 / 0 .9034	*a*(412) 0.070 *a*(534) 0.039 *c*(412) 0.151 *c*(532) 0.099	n/a	yes	n/a
23	24.7	36.17.95	0.412 /0 .976	*a*(412) 0.085 *a*(532) 0.048 *c*(412) 0.176 *c*(531) 0.127	n/a	yes	n/a
24	24.4	36.22	0.40537 / 1.0234	*a*(412) 0.074 *a*(532) 0.045 *c*(412) 0.161 *c*(531) 0.116	n/a	yes	n/a
25	25.1	36.18	0.45909/0 .94017	*a*(412) 0.078 *a*(532) 0.045 *c*(413) 0.157 *c*(531) 0.117	n/a	yes	n/a
26	26.3	36.05	0.5457 /0 .927	*a*(412) 0.074 *a*(532) 0.110 *c*(413) 0.163 *c*(533) 0.102	n/a	yes	n/a
27	26.3	36.07	0.539 /0 .9035	*a*(412) 0.072 *a*(532) 0.047 *c*(413) 0.157 *c*(532) 0.122	n/a	n/a	n/a

Appendix B – Abbreviations, Units and Acronyms

Table B1. Notations, descriptions and units if applicable.

Abbreviation	Description	Typical Units (if applicable)
a	Absorption coefficient	m^{-1}
a_{CDOM}	Absorption coefficient due to CDOM	m^{-1}
a_d	Absorption coefficient of detrital matter	m^{-1}
a_g	Absorption coefficient due to gelbstoff (detrital matter)	m^{-1}
AOPs	Apparent optical properties	
a_p	Absorption due to particles	m^{-1}
a_{pg}	Absorption due to particles plus gelbstoff (detrital matter)	m^{-1}
a_{ph}	Phytoplankton pigment absorption coefficient	m^{-1}
a^*_{ph}	Chlorophyll-specific phytoplankton absorption coefficient	$m^2\ mg^{-1}$
a_t	Total absorption (all components)	m^{-1}
$a_{t\text{-}w}$	Total absorption minus pure water absorption	
b	Scattering (in any/all directions)	m^{-1}
b_b	Backscattering (scattering in the backwards direction)	m^{-1}
BRDF	Bi-directional reflectance distribution function	
b	Scattering coefficient	m^{-1}
c	Attenuation coefficient	m^{-1}
Cal/Val	Calibration and Validation	
CCNY	City College of New York	
CDOM	Chromophoric dissolved organic material	ppb
CEOS	Committee on Earth Observation Satellites	
c_g	Attenuation coefficient due to gelbsoff (detrital matter)	
Chl-*a*	Chlorophyll *a* concentration	$mg\ m^{-3}$
c_t	Total attenuation coefficient	m^{-1}
CZCS	Coastal Zone Color Scanner instrument aboard the NIMBUS-7 satellite	
DOC	Dissolved Organic Carbon	$mmol\ C\ m^{-3}$
E_d	Downwelling irradiance	$mW\ cm^{-2}\ \mu m^{-1}$
EDIS	Environmental Data Information Service	
EDR	Environmental Data Record	
EDS	Environmental Data Service	
EPA	US Environmental Protection Agency	
E_s	Downwelling irradiance just above water surface	
ESSA	Environmental Science Services Administration	
EST	Eastern Standard Time	
FAFOV	Full Angle Field of View	
FEL	Lamp type designation assigned by the American National Standards Institute (not an acronym)	
F_L	Unknown spectral response calibration factor	
F_0	Mean extraterrestrial solar irradiance	$mW\ cm^{-2}\ \mu m^{-1}$
FOV	Field of view	
FWHM	Full width half maximum	
GCOM-C	Global Climate Observation Mission-Climate	
HPLC	High Pressure Liquid Chromatography	
IFCB	Imaging Flow CytoBot instrument (see Table B2)	
I_f	Immersion factor accounting for the change in responsivity of the sensor when immersed in water with respect to air	
I_i	integration time used for that reading	s
I_N	normalized integration time	s
INSITU-OCR	International Network for Sensor Inter-comparison and Uncertainty assessment for Ocean Color Radiometry	
IOCCG	International Ocean Colour Coordinating Group	
IOPs	Inherent optical properties	
JPSS	Joint Polar Satellite System (program)	
JPSS-1; JPSS-2	Joint Polar Satellite System -1 -2 (future satellite missions)	
K_d	Downwelling diffuse attenuation coefficient	m^{-1}
K_{Lu}	Upwelling radiance diffuse attenuation coefficient	m^{-1}
L	Radiance	$mW\ cm^{-2}\ \mu m^{-1}\ sr^{-1}$
L_d	Downwelling radiance	$mW\ cm^{-2}\ \mu m^{-1}\ sr^{-1}$
LDEO	Lamont-Doherty Earth Observatory at Columbia University	
LISCO	Long Island Sound Coastal Observatory	
L_{ref}	Radiance of reference	$mW\ cm^{-2}\ \mu m^{-1}\ sr^{-1}$
L_{sky}	Radiance of sky	$mW\ cm^{-2}\ \mu m^{-1}\ sr^{-1}$
L_t	Total radiance	$mW\ cm^{-2}\ \mu m^{-1}\ sr^{-1}$
L_u	Upwelling radiance	$mW\ cm^{-2}\ \mu m^{-1}\ sr^{-1}$
$L_u(0^-, \lambda)$	Spectral upwelling radiance just below water surface	$mW\ cm^{-2}\ \mu m^{-1}\ sr^{-1}$

Abbreviation	Description	Typical Units (if applicable)
L_w	Water-leaving radiance	mW cm^{-2} μm^{-1} sr^{-1}
MIN	Minimum	
MOBY	Marine Optical BuoY	
MSL12	Multi-Sensor Level-1 to Level-2 processing system	
n	number of readings	
n/a	Not available	
NASA	National Aeronautics and Space Agency	
NASA/GSFC	NASA/Goddard Space Flight Center	
NCEI	National Centers for Environmental Information	
NESC	National Environmental Satellite Center	
NESDIS	National Environmental Satellite, Data, and Information Service	
NESS	National Environmental Satellite Service	
NIR	Near infrared	
NIST	National Institute of Standards and Technology	
nL_w	Normalized water-leaving radiance	mW cm^{-2} μm^{-1} sr^{-1}
NOAA	National Oceanic and Atmospheric Administration	
NOAA/STAR	NOAA/Center for Science tech, algorithm, research	
NRL	Naval Research Laboratory	
NURADS	New Upwelling Radiance Distribution camera System	
n_w	Refractive index of seawater	
OCR-VC	Ocean Colour Radiometry Virtual Constellation	
OLCI	Ocean and Land Colour Instrument	
OMAO	Office of Marine and Air Operations	
OSU	Oregon State University	
PAR	Photosynthetically Active Radiation	
PI	Principal Investigator	
POC	Particulate Organic Carbon	mmol C m^{-3}
PON	Particulate Organic Nitrogen	mmol N m^{-3}
PSU	Practical salinity unit	
R_g	Bi-directional reflectance of gray plaque	
R_{rs}	Remote sensing reflectance	sr^{-1}
R_{tile}	Relative reflectance of the NIST blue tile	
s	Seconds	
s/n	Serial number	
S	Radiometric spectrum measurement	
SABOR	Ship-Aircraft Bio-Optical Research	
SeaWiFs	Sea-viewing Wide Field-of-view Sensor	
S_g	Radiometric spectrum measurement of gray plaque	
SGLI	Second Generation Global Imager	
SNPP	Suomi National Polar-orbiting Partnership	
S_{sfc}	Radiometric spectrum measurement of surface water	
S_{sky}	Radiometric spectrum measurement of sky	
SST	Sea surface temperature	°C
STARR	NIST Spectral tri-function automated reference reflectometer	
S_{tile}	Radiometric spectrum measurement of the NIST blue tile	
SPM	Suspended Particulate Material	mg L^{-1}
t	Time	s
U. Miami	University of Miami	
UMB	University of Massachusetts – Boston	
USF	University of South Florida	
USM	University of Southern Mississippi	
UTC	Coordinated Universal Time	
UV	Ultraviolet	
VIIRS	Visible Infrared Imaging Radiometer Suite	
$\Delta\phi$	Relative azimuth between the sun and the instrument viewing direction	°
λ	Wavelength	nm
ϕ_i	Scatter azimuth, incident	°
ϕ_r	Scatter azimuth, reflective	°
φ	Relative azimuth of the sensor to the sun	°
ρ	Reflectance	
$\rho(\lambda, \theta)$	Fresnel reflectance factor of seawater	
θ	Angle	°
θ_g	Sensor zenith angle for gray plaque	°
θ_i	Sensor zenith angle, incident	°
θ_r	Sensor zenith angle, reflective	°
θ_{sfc}	Sensor zenith angle for water surface	°
θ_{sky}	Sensor zenith angle for sky	°

Table B2. Instrument shorthand, description and manufacturer with modifications when applicable.

Instrument Shorthand	Full Identification/Purpose	Manufacturer or Citation
ac-9	In situ spectrophotometer - 9 channel resolution	WET Labs
ac-s	In situ spectrophotometer – high spectral resolution	WET Labs
ADCP	Acoustic Doppler Current Profiler	Teledyne RD Instruments
ASD	Analytical Spectral Device; HandHeld2-Pro visible and near infrared spectrophotometer	PANalytical
BB-3	Backscatter – 3 channels	
BB7FL2	Backscatter – 7 channels, Fluorescence – 2 channels	WET Labs
C-OPS	compact hyperspectral optical profiling system	Biospherical Instruments, Inc.
CTD	Conductivity, Temperature, Depth	Generic, various manufacturers
ECO-Puck Triplet Fluorometer	Fluorescence at 3 channels for determining chlorophyll, CDOM and phycoerythrin	WET Labs
ECO-Puck Triplet Scatterometer	Scatter – 3 channels (443, 550, 860)	WET Labs
GER	Field portable spectroradiometer	Spectra Vista Corporation
FlowCam	Dynamic imaging particle analysis for species composition and size measurements	Fluid Imaging Technologies, Inc.
HyperOCI	Hyperspectral irradiance sensor	Satlantic LP
HyperOCR	Hyperspectral radiance sensor	Satlantic LP
HyperPro, HyperPro-II	Free-falling hyperspectral optical profiler	Satlantic LP
HyperSAS	Above water optical system	Satlantic LP
HyperSAS-POL	Above water optical system with sky polarimeter	Satlantic LP with modifications by CCNY
HyperTSRB	Hyperspectral radiometer configured to float on the sea surface	Satlantic LP
Imaging Flow CytoBot (IFCB)	Automated microscopic imaging instrument	McLane Research Labs
Microtops	Handheld sun photometer (atmospheric aerosols and optical depth)	Solar Light Company
NURADS	Upwelling Radiance Distribution Camera System	Voss and Chapin, 2005
Sartorius CPA 2250	Balance	Sartorius
RISBA	Radiometer Incorporating the Sky Blocking Approach	Lee et al. 2013
SBE 49	Conductivity, Temperature, Depth	SeaBird Scientific
VSF-9	Volume scattering function – 9 channels	WET Labs
SR1900 (Spectral Evolution)	Spectroradiometer, handheld	Spectral Evolution, Inc.